

Unitary and Nonunitary A - D - E minimal models: Coset graph fusion algebras, defects, entropies, SREEs and dilogarithm identities

Paul A. Pearce^{a,b,c}, Jared Heymann^a, Thomas Quella^a

^a*School of Mathematics and Statistics, University of Melbourne
Parkville, Victoria 3010, Australia*

^b*School of Mathematics and Physics, University of Queensland
St Lucia, Brisbane, Queensland 4072, Australia*

^c*High Energy Physics Research Unit, Faculty of Science
Chulalongkorn University, Bangkok 10330, Thailand*

papearce@unimelb.edu.au jared.heyman@student.unimelb.edu.au
Thomas.Quella@unimelb.edu.au

Abstract

We consider unitary and nonunitary (A, G) coset minimal models on the cylinder with $G = A, D, E$. Elementary topological defects are implemented as non-contractible Verlinde, Pasquier and Ocneanu lines around the cylinder. The decomposition of compound defects, formed by fusing elementary defects together, is described by the Verlinde, Pasquier and Ocneanu graph fusion algebras. The action of the compound defects on the left- or right-vacuum boundary state builds the known conformal cylinder boundary conditions. Fusing these defects, in the presence of vacuum boundary conditions, reproduces the known general formulas for the conformal cylinder partition functions. We define the coset graph $A \otimes G/\mathbb{Z}_2$, argue that it is a universal object and show that it encodes (i) the coset graph fusion algebra, (ii) the Affleck-Ludwig boundary g -factors, (iii) the defect g -factors given by quantum dimensions and (iv) the relative Symmetry Resolved Entanglement Entropies (SREEs). Additionally, it is shown that the boundary and defect g -factors are related to the asymptotic counting of fusion paths on the coset graph. On the lattice, the defects are constructed as Yang-Baxter integrable seams including special braid and graph automorphism transfer matrices. Remarkably, many of the boundary CFT structures, such as fusion matrices, modular matrices, quantum dimensions and defects, appear at the level of lattice Yang-Baxter integrable A - D - E Restricted Solid-On-Solid (RSOS) models and these structures and their properties carry over to the CFT in the continuum scaling limit. Importantly, in the continuum scaling limit, the lattice transfer matrix T - and Y -system functional equations carry over to produce the coset graph fusion algebra for the defect lines. Moreover, the effective central charges and conformal weights are expressed in terms of dilogarithms of the braid and bulk asymptotics of the Y -system expressed in terms of the quantum dimensions.

Contents

1	Introduction	3
2	Data of A-D-E Minimal CFTs	4
2.1	A - D - E Lie algebra data	4
2.2	Central charges, conformal weights and characters	5
2.3	Classification of conformal partition functions and nimreps	6
2.4	Modular matrices and modular transformations	8
2.5	Coset graph fusion algebras and polynomial rings	8
2.6	Defect lines and their properties	10
2.7	Boundary and defect g -factors and coset quantum dimensions	11
2.8	Asymptotic counting of coset fusion paths	13
2.9	Relative symmetry resolved entanglement entropies	13
3	Prototypical CFTs	14
3.1	Prototypical unitary CFTs	14
3.1.1	Critical Ising model $\mathcal{M}(3, 4) = (A_2, A_3)$	14
3.1.2	Tricritical Ising model $\mathcal{M}(4, 5) = (A_3, A_4)$	16
3.1.3	Critical 3-state Potts model (A_4, D_4)	17
3.1.4	Tricritical 3-state Potts model (A_6, D_4)	19
3.2	Prototypical nonunitary CFTs	21
3.2.1	Critical Lee-Yang model $\mathcal{M}(2, 5) = (A_1, A_4)$	21
3.2.2	Critical $\mathcal{M}(2, 7) = (A_1, A_6)$ model	22
3.2.3	Critical $\mathcal{M}(3, 5) = (A_2, A_4)$ model	23
3.2.4	Critical $\mathcal{M}(5, 7) = (A_4, A_6)$ model	24
3.2.5	Critical (A_4, E_6) model	26
4	A-D-E RSOS Lattice Models	28
4.1	A - D - E lattice models and their T - and Y -systems	28
4.2	Braid and bulk scaling limits of integrable seams	30
4.3	Dilogarithm identities	31
4.4	Construction of integrable seams on the lattice	33
4.5	Conformal defects as limits of integrable lattice seams	34
4.6	Boundary conditions on the lattice	36
4.7	Boundary conditions and fusion rules for double row transfer matrices	37
5	Conclusion	38
A	Coset graphs and coset nimreps	39
B	Yang-Baxter equation for critical A-D-E models	40

1 Introduction

Recent years have witnessed a paradigm shift in the understanding of symmetries of physical systems. At the heart of this development is the insight that global symmetries should be implemented through the action of topological defects [1–3]. This perspective has been particularly influential and powerful in 2D Conformal Field Theories (CFTs) which naturally arise as continuum limits of integrable and non-integrable classical and quantum lattice models [4–8] and where fusion categories provide a rigorous and well-developed mathematical framework for the study of their symmetries [9]. Yet, despite impressive progress there still exist a number of open problems concerning the relation between continuum CFTs and discrete lattice models. Here we explore the interplay between the symmetries and other properties encoded by Dynkin diagrams, and their generalizations, in the framework of *integrable* lattice models and their associated CFTs in the continuum scaling limit.

More specifically, in this paper, we work in the context of the unitary and nonunitary A - D - E minimal model CFTs $\mathcal{M}(m, m')$ [10–12]. These theories are rational CFTs [13, 14] with respect to the Virasoro algebra and admit a realization in terms of the Goddard-Kent-Olive (GKO) coset construction [11]. The modular invariant partition functions of these CFTs on the torus are classified by Cappelli, Itzykson and Zuber [16] in terms of the simply-laced A - D - E Lie algebras and their Dynkin graphs. The conformal partition functions on the cylinder, or equivalently the annulus, for specified boundary conditions are given in [14]. The twisted partition functions, resulting from the insertion of topological defect lines on the torus, were obtained by Petkova and Zuber [17, 18]. Recently, it was proposed [19, 20] that topological defect lines [21–24] for the A - D - E minimal CFTs on the torus satisfy the Ocneanu algebra [25]. Our primary interest here is to study the properties of defect lines of these theories in cylindrical geometry in the presence of boundaries. Our central premise is that the quantum dimensions and other properties of these theories are encoded through their associated universal *coset graphs* (as defined in Appendix A). This use of the word “coset” should not be confused with the distinct use of coset in the GKO construction. The properties of defects for CFTs with diagonal modular invariants are well understood [26] in terms of the Verlinde algebra [27] but, for theories with non-diagonal modular invariants, it is necessary to properly incorporate the Pasquier [28] and Ocneanu [25] graph fusion algebras.

The layout of the paper is as follows. After the introduction we collate, in Section 2, the basic Virasoro minimal model CFT data including (i) the central charges, conformal weights, characters and modular S matrices, (ii) the coset graph algebras and their graph fusion matrices (nimreps) along with the properties of topological defect lines and (iii) the quantum dimensions, boundary/defect g factors [29] and (iv) the relative Symmetry Resolved Entanglement Entropies (SREEs) [30–37]. In Section 3, we present many prototypical examples of unitary and nonunitary Virasoro minimal CFTs alongside their CFT data derived from the coset graph. In Section 4, we use Yang-Baxter integrability [38] to study the properties of the defect lines in these CFTs via the continuum scaling limit of integrable defect seams of the associated A - D - E Restricted Solid-On-Solid (RSOS) lattice models [39–45]. More specifically, we (i) construct integrable defect seams on the lattice, (ii) consider the associated T - and Y -systems of functional equations satisfied by the transfer matrices and integrable seams, (iii) obtain their braid and bulk limits in terms of quantum dimensions and (iv) exhibit expressions for the central charges and conformal weights in terms of the analytic continuation of dilogarithms with arguments given by the braid and bulk limits.

Lie Algebra	Graph G	m	$\text{Exp}(G)$	Type/ H	Γ
A_{m-1}		m	$1, 2, \dots, m-1$	I	\mathbb{Z}_2
D_{l+2} (l even)		$2l+2$	$1, 3, \dots, 2l+1, l+1$	I	\mathbb{Z}_2
D_{l+2} (l odd)		$2l+2$	$1, 3, \dots, 2l+1, l+1$	II/ A_{2l+1}	\mathbb{Z}_2
E_6		12	$1, 4, 5, 7, 8, 11$	I	\mathbb{Z}_2
E_7		18	$1, 5, 7, 9, 11, 13, 17$	II/ D_{10}	1
E_8		30	$1, 7, 11, 13, 17, 19, 23, 29$	I	1

Figure 1: Dynkin diagrams of the classical simply-laced A - D - E Lie algebras. The nodes associated with the identity and the fundamental are labelled by 1 and 2 respectively. We note that the fundamental is the unique neighbour of the identity. Also shown are the Coxeter numbers m , exponents $\text{Exp}(G)$, the type I or II, the so-called parent A - D - E graph $H \neq G$ and the diagram automorphism group Γ . It is the exponents of the parent graph H that appear in the modular invariant partition functions as in Table 1. The D_4 graph is exceptional having the noncommutative automorphism group \mathbb{S}_3 . The eigenvalues of G are $2 \cos \frac{\ell\pi}{m}$ with $\ell \in \text{Exp}(G)$. By abuse of notation, we use G to denote the graph, its adjacency matrix and its set of vertices with cardinality $|G|$ but the meaning should be clear from context.

2 Data of A - D - E Minimal CFTs

2.1 A - D - E Lie algebra data

The A - D - E minimal CFTs [12] are coset models built on a pair of Dynkin diagrams of simply-laced A - D - E Lie algebras with coprime Coxeter numbers (m, m') and data as shown in Figure 1. The models can be characterized by the pair (A, G) of A - D - E diagrams, or more precisely, by the coset graph $A \otimes G / \mathbb{Z}_2$. Within graph theory [46], coset graphs are constructed mathematically by combining the standard graph theory constructs of tensor products and quotients of graphs as described in Appendix A. The (A, A) series is associated with the minimal models $\mathcal{M}(m, m')$ of Belavin, Polyakov and Zamolodchikov [10]. More generally, these models are in fact unitary ($m' = m \pm 1$) or nonunitary ($m' \neq m \pm 1$) coset models [15, 12]. The unitary A - D - E minimal models are classified [16] into a critical and tricritical series

$$(A, G) = \begin{cases} (A_{m-2}, D_{(m+2)/2}), \\ (A_{10}, E_6), \\ (A_{16}, E_7), \\ (A_{28}, E_8), \end{cases} \quad (A, G) = \begin{cases} (A_m, D_{(m+2)/2}), & m = 6, 8, 10, \dots \\ (A_{12}, E_6), & m = 12 \\ (A_{18}, E_7), & m = 18 \\ (A_{30}, E_8), & m = 30 \end{cases} \quad (2.1)$$

where m is the Coxeter number of G . The coset theories (A, G) and (G, A) are equivalent so we only use the (A, G) pair. There is no distinction between the two A -types $(A_{m-1}, A_m) \equiv (A_m, A_{m-1})$. The critical Ising model is (A_3, A_4) and the tricritical Ising model is (A_4, A_5) . The critical 3-state Potts model is (A_4, D_4) and the tricritical 3-state Potts model is (A_6, D_4) . As shown in Table 1, the Coxeter exponents $\text{Exp}(A)$ and $\text{Exp}(H)$ appear in the modular invariant partition functions [16].

Defining quantum dimensions by $S_a = [a]_x = \frac{x^a - x^{-a}}{x - x^{-1}}$ with $x = e^{\pi i/m}$, the nondegenerate largest eigenvalue of the adjacency matrix G is $[2]_x = x + x^{-1} = 2 \cos \frac{\pi}{m}$ and the associated (unnormalized) Perron-Frobenius eigenvector ψ is

$$G\psi = [2]_x \psi, \quad \psi = (\psi_a)_{1 \leq a \leq |G|} = \begin{cases} ([1]_x, [2]_x, \dots, [l]_x), & G = T_l \\ ([1]_x, [2]_x, \dots, [l]_x), & G = A_l \\ ([1]_x, [2]_x, \dots, [l]_x, \frac{[l]_x}{[2]_x}, \frac{[l]_x}{[2]_x}), & G = D_{l+2} \\ ([1]_x, [2]_x, [3]_x, [2]_x, [1]_x, \frac{[3]_x}{[2]_x}), & G = E_6 \\ ([1]_x, [2]_x, [3]_x, [4]_x, \frac{[6]_x}{[2]_x}, \frac{[4]_x}{[3]_x}, \frac{[4]_x}{[2]_x}), & G = E_7 \\ ([1]_x, [2]_x, [3]_x, [4]_x, [5]_x, \frac{[7]_x}{[2]_x}, \frac{[5]_x}{[3]_x}, \frac{[5]_x}{[2]_x}), & G = E_8 \end{cases} \quad (2.2)$$

where $\psi_a = [a]_x = S_a$ for the A series and T_l , with $m = 2l + 1$, is the tadpole graph with l nodes. To normalize these vectors, we need their norms

$$\|\psi\| = \begin{cases} \frac{\sqrt{2L+1}}{2} \csc \frac{\pi}{2L+1}, \quad \sqrt{\frac{L+1}{2}} \csc \frac{\pi}{L+1}, \quad \sqrt{\frac{L-1}{2}} \csc \frac{\pi}{2L-2}, & G = T_L, A_L, D_L \\ \frac{\sqrt{3-\sqrt{3}}}{\sin \frac{\pi}{12}} = \sqrt{\frac{24}{3-\sqrt{3}}}, \quad \frac{\sqrt{9/2}}{\sin \frac{\pi}{18}}, \quad \frac{\sqrt{15-\sqrt{75+30\sqrt{5}}}}{2 \sin \frac{\pi}{30}}, & G = E_{6,7,8} \end{cases} \quad (2.3)$$

For unitary models $(m' - m = \pm 1)$, ψ is chosen to be the Perron-Frobenius eigenvector with eigenvalue $2 \cos \frac{\pi}{m}$. For nonunitary cases, ψ is chosen to be the eigenvector corresponding to the eigenvalue $2 \cos \lambda$ with $\lambda = \frac{(m'-m)\pi}{m'}$ and $m' - m \in \text{Exp}(G)$.

2.2 Central charges, conformal weights and characters

The central charges c , conformal weights Δ and Virasoro characters $\chi_{r,s}^{m,m'}(q)$ of the A - D - E minimal CFTs are

$$c = 1 - \frac{6(m'-m)^2}{mm'}, \quad \Delta = \Delta_{r,s}^{m,m'} = \frac{(rm' - sm)^2 - (m' - m)^2}{4mm'} \quad (2.4a)$$

$$\chi_{r,s}^{m,m'}(q) = \frac{q^{-c/24 + \Delta_{r,s}^{m,m'}}}{(q)_\infty} \sum_{k=-\infty}^{\infty} [q^{k(kmm' + rm' - sm)} - q^{(km+r)(km'+s)}], \quad (q)_\infty = \prod_{k=1}^{\infty} (1 - q^k) \quad (2.4b)$$

where q is the modular nome, (r, s) are the Kac labels and $(r, s) = (1, 1)$ is the vacuum. The Kac symmetry is given by $\Delta_{r,s}^{m,m'} = \Delta_{m-r, m'-s}^{m,m'}$ with $\chi_{r,s}^{m,m'}(q) = \chi_{m-r, m'-s}^{m,m'}(q)$. The effective central charges are

$$c_{\text{eff}} = c - 24\Delta_{\min} = 1 - \frac{6}{mm'}, \quad \Delta_{\min} = \min_{(r,s) \in \text{Kac}} \Delta_{r,s}^{m,m'} = \Delta_{r_0, s_0}^{m,m'} = \frac{1 - (m' - m)^2}{4mm'} \quad (2.5)$$

where $(r, s) = (r_0, s_0)$ is the groundstate. Specifically, since m and m' are coprime, (r_0, s_0) is given by the solution of the Diophantine equation

$$m'r_0 - ms_0 = 1 \quad (2.6)$$

which is guaranteed to be unique by the Bezout lemma [12]. For unitary models with $m' = m \pm 1$, $\Delta_{\min} = 0$ and $c = c_{\text{eff}}$ whereas, for nonunitary models, $\Delta_{\min} < 0$ and $c \neq c_{\text{eff}}$.

2.3 Classification of conformal partition functions and nimreps

Coset (A, G)	Modular Invariant Partition Function
$(A_{m-1}, A_{m'-1})$	$Z = \frac{1}{2} \sum_{r=1}^{m-1} \sum_{s=1}^{m'-1} \chi_{r,s} ^2$
$(A_{m-1}, D_{2\rho+2})$ $m'=4\rho+2 \geq 6$	$Z = \frac{1}{2} \sum_{r=1}^{m-1} \left\{ \sum_{\substack{s=1 \\ s \text{ odd}}}^{2\rho-1} \chi_{r,s} + \chi_{r,4\rho+2-s} ^2 + 2 \chi_{r,2\rho+1} ^2 \right\}$
$(A_{m-1}, D_{2\rho+1})$ $m'=4\rho \geq 8$	$Z = \frac{1}{2} \sum_{r=1}^{m-1} \left\{ \sum_{\substack{s=1 \\ s \text{ odd}}}^{4\rho-1} \chi_{r,s} ^2 + \chi_{r,2\rho} ^2 + \sum_{\substack{s=2 \\ s \text{ even}}}^{2\rho-2} (\chi_{r,s} \bar{\chi}_{r,4\rho-s} + \bar{\chi}_{r,s} \chi_{r,4\rho-s}) \right\}$
(A_{m-1}, E_6) $m'=12$	$Z = \frac{1}{2} \sum_{r=1}^{m-1} \left\{ \chi_{r,1} + \chi_{r,7} ^2 + \chi_{r,4} + \chi_{r,8} ^2 + \chi_{r,5} + \chi_{r,11} ^2 \right\}$
(A_{m-1}, E_7) $m'=18$	$Z = \frac{1}{2} \sum_{r=1}^{m-1} \left\{ \chi_{r,1} + \chi_{r,17} ^2 + \chi_{r,5} + \chi_{r,13} ^2 + \chi_{r,7} + \chi_{r,11} ^2 \right. \\ \left. + \chi_{r,9} ^2 + [(\chi_{r,3} + \chi_{r,15})\bar{\chi}_{r,9} + (\bar{\chi}_{r,3} + \bar{\chi}_{r,15})\chi_{r,9}] \right\}$
(A_{m-1}, E_8) $m'=30$	$Z = \frac{1}{2} \sum_{r=1}^{m-1} \left\{ \chi_{r,1} + \chi_{r,11} + \chi_{r,19} + \chi_{r,29} ^2 \right. \\ \left. + \chi_{r,7} + \chi_{r,13} + \chi_{r,17} + \chi_{r,23} ^2 \right\}$

Table 1: A - D - E classification of (A, G) minimal model modular invariant partition functions on the torus. The central charges are $c = 1 - \frac{6(m-m')^2}{mm'}$, $\chi_{r,s} = \chi_{r,s}(q)$ are Virasoro characters and bars denote complex conjugates. Here r, s are the Coxeter exponents of (A, G) and (m, m') are coprime. The coset theories (A, G) and (G, A) are equivalent. The unitary minimal models have $m' = m \pm 1$.

The A - D - E CFTs can be considered in different topologies but they are classified [16] by the modular invariant torus partition functions shown in Table 1. More generally, the twisted conformal partition functions on the torus are classified in terms of A - D - E Ocneanu graphs exhibited explicitly in [17]. Our main focus here will be on the cylinder which is equivalent by conformal transformation to the annulus. On the torus, the coset graph fusion algebra is replaced by the coset Ocneanu graph fusion algebra $A \otimes \text{Oc}(G)/\mathbb{Z}_2$ as in Appendix A.

To present the classification of the cylinder partition functions, we first need to define various graph fusion matrices. The fused adjacency matrices (intertwiners) n_s and graph fusion matrices \widehat{N}_a are defined by the finitely truncated recursions

$$n_1 = I, \quad n_2 = G, \quad n_s n_2 = n_{s-1} + n_{s+1}, \quad n_0 = n_{m'} = 0; \quad n_s = U_{n-1}(\frac{1}{2}G) \quad (2.7a)$$

$$\widehat{N}_1 = I, \quad \widehat{N}_2 = G, \quad G \widehat{N}_b = \sum_{c \in G} G_{bc} \widehat{N}_c, \quad a, b, c \in G \quad (2.7b)$$

where $U_n(x)$ are the Chebyshev polynomials of the second kind and the graph fusion matrices \widehat{N}_a only exist for graphs G of type I (see Figure 1). The $A_{m'-1}$ fusion matrices, denoted $n_i = N_i$, are the

Verlinde fusion matrices [27]. The various fusion matrices form nimreps (nonnegative integer matrix representations) of the commutative associative fusion algebras

$$n_i n_j = \sum_{k=1}^{m'-1} N_{ij}^k n_k, \quad \widehat{N}_a \widehat{N}_b = \sum_{c \in G} \widehat{N}_{ab}^c \widehat{N}_c, \quad n_s \widehat{N}_a = \sum_{b \in G} n_{sa}^b \widehat{N}_b \quad (2.8)$$

where the nonnegative integer structure constants are

$$N_{ij}^k = (N_i)_j^k, \quad \widehat{N}_{ab}^c = (\widehat{N}_a)_b^c, \quad n_{sa}^b = (n_s)_a^b \quad (2.9)$$

The nimreps are all symmetric matrices except for the case $G = D_{4l}$ for which $\widehat{N}_{4l} = \widehat{N}_{4l-1}^T \neq \widehat{N}_{4l}^T$. In these cases, there are some complex eigenvalues. If the \mathbb{Z}_2 automorphism σ is excluded for D_{2l} , then all the nimreps are normal, mutually commuting and simultaneously diagonalizable. Denoting the complex unitary matrices of (normalized) eigenvectors of N_2 , \widehat{N}_2 by S_i^ℓ (modular matrix), Ψ_a^ℓ respectively with $S_1^\ell, \Psi_1^\ell > 0$, the Verlinde and Verlinde-type formulas are

$$N_{ij}^k = \sum_{\ell=1}^{m'-1} \frac{S_i^\ell S_j^\ell \overline{S_k^\ell}}{S_1^\ell}, \quad \widehat{N}_{ab}^c = \sum_{\ell \in \text{Exp}(G)} \frac{\Psi_a^\ell \Psi_b^\ell \overline{\Psi_c^\ell}}{\Psi_1^\ell}, \quad n_{ia}^b = \sum_{\ell \in \text{Exp}(G)} \frac{S_i^\ell \Psi_a^\ell \overline{\Psi_b^\ell}}{S_1^\ell} \quad (2.10)$$

where bars denote complex conjugates.

The conformal cylinder partition functions [14] are given in terms of the graph fusion matrices N_i , n_s and \widehat{N}_a by

$$Z_{(r',b)|(r'',c)}^{m,m'}(q) = \begin{cases} \sum_{r=1}^{m-1} \sum_{a \in G} N_{rr'}^{r''} \widehat{N}_{ab}^c \hat{\chi}_{ra}(q), & G \text{ is type I} \\ \sum_{r=1}^{m-1} \sum_{s=1}^{m'-1} N_{rr'}^{r''} n_{sb}^c \chi_{rs}(q), & G \text{ is type I or II} \end{cases} \quad (2.11)$$

where the block characters, associated with extended chiral symmetry in type I cases, are

$$\hat{\chi}_{r,a} = \sum_{s=1}^{m'-1} n_{s1}^a \chi_{r,s}(q) \quad (2.12)$$

and the fundamental rectangular intertwiner C has entries

$$C_{sa} = n_{s1}^a \quad (2.13)$$

For type I theories, these two expressions agree since, by (2.9),

$$\sum_{a \in G} n_{s1}^a \widehat{N}_a = n_s \widehat{N}_1 = n_s \quad (2.14)$$

If G is of A -type, the fusion matrices n_s and \widehat{N}_a both reduce to the Verlinde matrices N_s . The origin of the form of the cylinder partition functions is explained, in terms of propagating defect lines, in Figure 2. In the $G = D_{4l}$ cases, it is understood [47] that the b on the RHS of (2.11) is replaced with b^* where the star involution is defined by $a^* = a$ for $a = 1, 2, \dots, 4l-2$, $(4l)^* = (4l-1)$ and $(4l-1)^* = (4l)$. In all other cases, the star conjugation reduces to the identity. We note that the \mathbb{Z}_2 graph automorphism is included as a generator of the graph fusion algebras in all cases except for the D_{2l} cases. In these cases, adding the \mathbb{Z}_2 graph automorphism to the graph fusion algebra results in a noncommutative algebra (see for example [20]).

2.4 Modular matrices and modular transformations

For general $(A_{m-1}, A_{m'-1})$ theories, the fusion rules and adjacency matrix \tilde{A} of the coset graph $(A_{m-1} \otimes A_{m'-1})/\mathbb{Z}_2$ are diagonalized by the modular \mathcal{S} -matrix

$$\mathcal{S}_{r,s,r',s'} := \mathcal{S}_{(r,s),(r',s')} = \sqrt{\frac{8}{mm'}} (-1)^{1+rs'+sr'} \sin \frac{\pi rr'm'}{m} \sin \frac{\pi ss'm}{m'}, \quad (r,s), (r',s') \in \mathbb{K} \quad (2.15)$$

This formula is invariant under the Kac table symmetry $(r,s) \equiv (m-r, m'-s)$. The set

$$\mathbb{K} = \{\text{either } (r,s) \text{ or } (m-r, m'-s) : 1 \leq r \leq m-1, 1 \leq s \leq m'-1\}, \quad |\mathbb{K}| = \frac{1}{2}(m-1)(m'-1) \quad (2.16)$$

consists of one representative from each equivalent pair $(r,s) \equiv (m-r, m'-s)$ of Kac labels. We regard this as an ordered set with an arbitrary but fixed choice for the ordering. Once the ordering of the elements in \mathbb{K} is fixed, the elements are labelled by $\mu = 1, 2, \dots, |\mathbb{K}|$. Depending on the parities of m, m' , it can be convenient to choose \mathbb{K} by the restriction $r+s$ even or $r \leq \frac{1}{2}(m-1)$ or $s \leq \frac{1}{2}(m'-1)$. The \mathcal{S} -matrix is a real orthogonal matrix satisfying $\mathcal{S}^2 = I$ and is unique up to a reordering of the elements of \mathbb{K} . The unique row/column with all positive entries coincides with the groundstate $(r,s) = (r_0, s_0)$. For unitary theories, the groundstate (r_0, s_0) coincides with the vacuum $(1,1)$ but this is not the case for nonunitary theories.

Under modular transformation \mathcal{S} , the characters transform as

$$\chi_{r,s}(q) = \sum_{(r',s') \in \mathbb{K}} \mathcal{S}_{(r,s),(r',s')} \chi_{r',s'}(\tilde{q}), \quad q = e^{2\pi i\tau}, \quad \tilde{q} = e^{-2\pi i/\tau}, \quad \text{Im}(\tau) > 0 \quad (2.17)$$

where τ is the modular parameter and \tilde{q} is the conjugate modular nome.

2.5 Coset graph fusion algebras and polynomial rings

Symbolically, the $sl(2)$ Verlinde fusion rules for A_{m-1} are

$$(r) \times (r') = \sum_{r''=1}^{m-1} N_{rr'}^{(m)r''} (r'') = \sum_{\substack{r''=|r-r'|+1 \\ r+r'+r''=1 \pmod{2}}}^{r_{\max}} (r''), \quad 1 \leq r, r' \leq m-1 \quad (2.18a)$$

If $r' = 1$, then $(r) \times (1) = (r)$ so (1) acts as the identity. If $r' = 2$ is the fundamental, then r'' are the neighbours of r on A_{m-1} , that is, $(r) \times (2) = (r-1) + (r+1)$ for $r \leq m-1$ and $(m-1) \times 2 = (m-2)$.

It follows that the Verlinde fusion rules for the A -type $\mathcal{M}(m, m') = A_{m-1} \otimes A_{m'-1}/\mathbb{Z}_2$ coset minimal models are given by the tensor product

$$(r,s) \times (r',s') = \sum_{r''=1}^{m-1} \sum_{s''=1}^{m'-1} N_{rr'}^{(m)r''} N_{ss'}^{(m')s''} (r'',s'') = \sum_{\substack{r''=|r-r'|+1 \\ r+r'+r''=1 \pmod{2}}}^{r_{\max}} \sum_{\substack{s''=|s-s'|+1 \\ s+s'+s''=1 \pmod{2}}}^{s_{\max}} (r'',s'') \quad (2.18b)$$

$$r_{\max} = \min[r+r'-1, 2m-r-r'-1], \quad s_{\max} = \min[s+s'-1, 2m'-s-s'-1] \quad (2.18c)$$

subject to application of the Kac equivalence $(r,s) \equiv (m-r, m'-s)$. For example, restricting \mathbb{K} so that $1 \leq s \leq 3$ for $\mathcal{M}(5,7)$ and applying the Kac equivalence by hand gives

$$\begin{aligned} (2,2') \times (3,3') &= (2 \times 3, 2' \times 3') = (2+4, 2'+4') = (2,2') + (2,4') + (4,2') + (4,4') \\ &\equiv (2,2') + (3,3') + (4,2') + (1,3') \end{aligned} \quad (2.19)$$

where, for clarity, the s labels in (r, s) are shown with a prime. The (r, s) nodes on the right side of (2.19) are the (diagonal) neighbours of $(3, 3')$ in the Kac table. Continuing this process by applying the coset fundamental $(r, s) = (2, 2)$ to consecutive neighbours (r, s) , with $r + s$ even and $1 \leq s \leq 3$, leads to the connected component coset graph \tilde{G} of Figure 12. Since $(3, 3')$ is a neighbour of itself, this leads to a loop at this node of \tilde{G} . All of the coset graph fusion algebras can be obtained in this manner giving the coset fusion rules

$$(\mu) \times (\mu') = \sum_{\mu''=1}^{|\mathbb{K}|} \tilde{N}_{\mu\mu'\mu''}(\mu''), \quad \mu, \mu' = 1, 2, \dots, |\mathbb{K}| \quad (2.20)$$

where $\tilde{N}_{\mu\mu'\mu''} = (\tilde{N}_{\underline{\mu}})_{\mu'\mu''}$ are the structure constants, \tilde{N}_{μ} are the fusion matrices, $\tilde{N}_1 = I$ and the fundamental $\tilde{N}_2 = \tilde{G}$ is the adjacency matrix of the coset graph. The fusion matrices are easily read off from the Cayley table as is illustrated for the trivial case of the critical Ising model A_3

$$\begin{pmatrix} 1 \times 1 & 1 \times 2 & 1 \times 3 \\ 2 \times 1 & 2 \times 2 & 2 \times 3 \\ 3 \times 1 & 3 \times 2 & 3 \times 3 \end{pmatrix} = \begin{pmatrix} 1 & 2 & 3 \\ 2 & 1+3 & 2 \\ 3 & 2 & 1 \end{pmatrix} = (1) \begin{pmatrix} 1 & 0 & 0 \\ 0 & 1 & 0 \\ 0 & 0 & 1 \end{pmatrix} + (2) \begin{pmatrix} 0 & 1 & 0 \\ 1 & 0 & 1 \\ 0 & 1 & 0 \end{pmatrix} + (3) \begin{pmatrix} 0 & 0 & 1 \\ 0 & 1 & 0 \\ 1 & 0 & 0 \end{pmatrix} = \sum_{\mu=1}^3 (\mu) \tilde{N}_{\mu} \quad (2.21)$$

The fusion matrices yield nonnegative integer matrix representations (nimreps) of the coset graph fusion algebra

$$\tilde{N}_{\mu} \tilde{N}_{\mu'} = \sum_{\mu''=1}^{|\mathbb{K}|} \tilde{N}_{\mu\mu'\mu''} \tilde{N}_{\mu''}, \quad \mu, \mu' = 1, 2, \dots, |\mathbb{K}| \quad (2.22)$$

The coset graph fusion algebras are satisfied by (i) the nimreps, (ii) the defect lines \mathcal{L}_{μ} and (iii) the defect eigenvalues (quantum dimensions \tilde{d}_{μ}) including the g -factors corresponding to the Perron-Frobenius eigenvalues. General expressions for the coset nimreps as tensor products are given in Appendix A.

The graph fusion matrices \tilde{N}_{μ} are nonnegative commuting normal matrices. They are therefore simultaneously diagonalizable with the spectral decomposition yielding a Verlinde-like formula. The Perron-Frobenius eigenvalues coincide with the quantum dimensions $\tilde{d}_{\mu} > 0$ leading to a 1-dimensional representation of the coset graph fusion algebra

$$\tilde{d}_{\mu} \tilde{d}_{\mu'} = \sum_{\mu''=1}^{|\mathbb{K}|} \tilde{N}_{\mu\mu'\mu''} \tilde{d}_{\mu''}, \quad \mu, \mu' = 1, 2, \dots, |\mathbb{K}| \quad (2.23)$$

Substituting $(\mu) \mapsto \tilde{d}_{\mu}$ into (2.20) gives the decomposition of a rank-1 matrix of products of quantum dimensions into a sum of the fusion matrices

$$\mathcal{D} = \begin{pmatrix} \tilde{d}_1^2 & \tilde{d}_1 \tilde{d}_2 & \cdots & \tilde{d}_1 \tilde{d}_n \\ \tilde{d}_2 \tilde{d}_1 & \tilde{d}_2^2 & \cdots & \tilde{d}_2 \tilde{d}_n \\ \vdots & \vdots & \ddots & \vdots \\ \tilde{d}_n \tilde{d}_1 & \tilde{d}_n \tilde{d}_2 & \cdots & \tilde{d}_n^2 \end{pmatrix} = \begin{pmatrix} \tilde{d}_1 \\ \tilde{d}_2 \\ \vdots \\ \tilde{d}_n \end{pmatrix} (\tilde{d}_1 \ \tilde{d}_2 \ \cdots \ \tilde{d}_n) = \sum_{\mu=1}^n \tilde{d}_{\mu} \tilde{N}_{\mu}, \quad n = |\mathbb{K}| \quad (2.24)$$

thus encoding the fusion rules with $\tilde{d}_1 = 1$. The total quantum dimension D [48, 49] is given by

$$D^2 = \text{Tr } \mathcal{D} = \sum_{\mu=1}^n \tilde{d}_{\mu}^2 \quad (2.25)$$

Algebraically, the coset graph fusion algebra of $\mathcal{M}(m, m')$ can also be realized [50, 51] as a polynomial ring in two indeterminates $\mathbb{Z}[x, y]$ quotiented by an ideal $\mathcal{I} = \langle p_1(x), p'_1(y), p_2(x, y) \rangle$

$$\mathbb{Z}[x, y] / \langle p_1(x), p'_1(y), p_2(x, y) \rangle \quad (2.26a)$$

$$p_1(x) = U_{m-1}\left(\frac{x}{2}\right), \quad p'_1(y) = U_{m'-1}\left(\frac{y}{2}\right), \quad p_2(x, y) = U_{m-2}\left(\frac{x}{2}\right) - U_{m'-2}\left(\frac{y}{2}\right) \quad (2.26b)$$

where $U_n(x)$ are Chebyshev polynomials of the second kind. The ideal \mathcal{I} can always be reduced further, so that it is generated by one or two polynomials, as seen in the examples in Section 3. The indeterminates are the fundamentals so the polynomials generating the ideal vanish when evaluated with $x \mapsto [2]_x = 2 \cos \frac{\pi}{m}$ and $y \mapsto [2]_y = 2 \cos \frac{\pi}{m'}$. Curiously, we observe that the coset graph fusion algebras of $\mathcal{M}(m, m')$ coincide with the coset graph fusion algebras of the projective Grothendieck representations for the logarithmic minimal models $\mathcal{LM}(m-2, m'-2)$ [52–54]. This means, for example, that the critical Ising model $\mathcal{M}(3, 4)$ and dense polymers $\mathcal{LM}(1, 2)$ and similarly the tricritical Ising model $\mathcal{M}(4, 5)$ and critical percolation $\mathcal{LM}(2, 3)$ are described by the same coset graph fusion algebras.

2.6 Defect lines and their properties

$$\begin{aligned} Z_{(r',b)|(r'',c)}^{m,m'}(q) &= \begin{array}{|c|} \hline (r',b) \quad (r'',c) \\ \hline \square \\ \hline \end{array} = \begin{array}{|c|} \hline (1,1) \quad \widehat{\mathcal{L}}_{(r',b)} \quad \widehat{\mathcal{L}}_{(r'',c)} \quad (1,1) \\ \hline \square \times \square \\ \hline \end{array} = \sum_{r=1}^{m-1} \sum_{a \in G} N_{rr'r''} \widehat{N}_{ab}^c \begin{array}{|c|} \hline (1,1) \quad \widehat{\mathcal{L}}_{(r,a)} \quad (1,1) \\ \hline \square \\ \hline \end{array} \\ &= \sum_{r=1}^{m-1} \sum_{a \in G} N_{rr'r''} \widehat{N}_{ab}^c \begin{array}{|c|} \hline (1,1) \quad (r,a) \\ \hline \square \\ \hline \end{array} = \sum_{r=1}^{m-1} \sum_{a \in G} N_{rr'r''} \widehat{N}_{ab}^c Z_{(1,1)|(r,a)}^{m,m'}(q), \quad G \text{ is type I} \\ \\ Z_{(r',b)|(r'',c)}^{m,m'}(q) &= \begin{array}{|c|} \hline (r',b) \quad (r'',c) \\ \hline \square \\ \hline \end{array} = \begin{array}{|c|} \hline (1,1) \quad \widehat{\mathcal{L}}_{(r',b)} \quad \widehat{\mathcal{L}}_{(r'',c)} \quad (1,1) \\ \hline \square \times \square \\ \hline \end{array} = \sum_{r=1}^{m-1} \sum_{s=1}^{m'-1} N_{rr'r''} n_{sb}^c \begin{array}{|c|} \hline (1,1) \quad \mathcal{L}_{(r,s)} \quad (1,1) \\ \hline \square \\ \hline \end{array} \\ &= \sum_{r=1}^{m-1} \sum_{s=1}^{m'-1} N_{rr'r''} n_{sb}^c \begin{array}{|c|} \hline (1,1) \quad (r,s) \\ \hline \square \\ \hline \end{array} = \sum_{r=1}^{m-1} \sum_{s=1}^{m'-1} N_{rr'r''} n_{sb}^c Z_{(1,1)|(r,s)}^{m,m'}(q), \quad G \text{ is type I/II} \\ \\ Z_{(1,1)|(r,a)}^{m,m'}(q) &= \hat{\chi}_{ra}(q), \quad Z_{(1,1)|(r,s)}^{m,m'}(q) = \chi_{rs}(q) \end{aligned}$$

Figure 2: The conformal cylinder partition functions (2.11) are generated by propagating the defect lines \mathcal{L}_μ (with $\mu = (r, a)$ or $\mu = (r, s)$) glued to the two boundaries to the center and fusing them. If G is of A -type, then n_{sb}^c reduces to the Verlinde structure constants $N_{ss's''}$ and the cylinder partition functions are then compatible with the Kac symmetry since $\mathcal{L}_{(r,s)} = \mathcal{L}_{(m-r, m'-s)}$. Similar arguments apply for more general topological defects.

The conformal defect lines are labelled by fusions μ which encode their internal structure (charges).

The defect lines are in fact operators. They satisfy the same fusion relations as their fusion labels and possess a number of properties. In particular, the defect lines \mathcal{L}_μ :

- (i) are topological in the sense that they freely propagate,
- (ii) are mutually commuting (Abelian) so they pass through one another,
- (iii) satisfy the Kac symmetry $\mathcal{L}_{(r,s)} = \mathcal{L}_{(m-r,m'-s)}$,
- (iv) factorize as $\mathcal{L}_{(r,s)} = \mathcal{L}_r \mathcal{L}_s$, $\mathcal{L}_{(r,a)} = \mathcal{L}_r \mathcal{L}_a$ with $\mathcal{L}_r = \mathcal{L}_{(r,1)}$, $\mathcal{L}_s = \mathcal{L}_{(1,s)}$ and $\mathcal{L}_a = \mathcal{L}_{(1,a)}$,
- (v) satisfy the coset graph fusion algebra (2.20),
- (vi) carry a defect entropy $S_{(r,a)}^{\text{defect}} = \log \hat{d}_{(r,a)}$ with $\hat{d}_{(r,a)} = \sum_{s=1}^{m'-1} n_{s1}^a \tilde{d}_{(r,s)}$,
- (vii) exhibit an eigenvalue spectrum of quantum dimensions given by the solutions \tilde{d}_μ of (2.24).

The Abelian property (ii) holds generally since we do not add the \mathbb{Z}_2 automorphism in the D_{2l} cases.

Within the context of CFT, the properties of defect lines are initially posited but are ultimately confirmed to be consistent and formalized as the axioms of various kinds of fusion categories. Alternatively, as we pursue here, the properties of the defects can be established in the context of integrable (defect) seams for the associated Yang-Baxter integrable A - D - E RSOS lattice models as in Section 4. The properties (i)–(vii) are then inherited by the defect lines in the continuum scaling limit. This is the approach that we adopt here.

2.7 Boundary and defect g-factors and coset quantum dimensions

For the A -type $\mathcal{M}(m, m')$ minimal models, the 1-boundary Affleck-Ludwig g-factors [29] are

$$\tilde{\mathfrak{g}}_{(r,s)} = \left(\frac{8}{mm'}\right)^{1/4} \frac{\sin \frac{r\pi}{m} \sin \frac{s\pi}{m'}}{\sqrt{\sin \frac{\pi}{m} \sin \frac{\pi}{m'}}} = \tilde{\mathfrak{g}}_{(m-r,s)} = \tilde{\mathfrak{g}}_{(r,m'-s)} = \tilde{\mathfrak{g}}_{(1,1)} \tilde{d}_{(r,s)} \quad (2.27)$$

where

$$\tilde{\mathfrak{g}}_{(1,1)} = \left(\frac{8}{mm'}\right)^{1/4} \sqrt{\sin \frac{\pi}{m} \sin \frac{\pi}{m'}}, \quad \tilde{d}_{(r,s)} = \frac{\sin \frac{r\pi}{m} \sin \frac{s\pi}{m'}}{\sin \frac{\pi}{m} \sin \frac{\pi}{m'}} = [r]_{e^{\pi i/m}} [s]_{e^{\pi i/m'}} \quad (2.28)$$

and the coset quantum dimension $\tilde{d}_{(r,s)} = \tilde{d}_{(r,1)} \tilde{d}_{(1,s)}$ gives the g-factor associated with the (r, s) defect. The 1-boundary g-factors are not directly measurable so we focus instead on 2-boundary g-factors $\tilde{\mathfrak{g}}_{(r,s)|(r',s')} = \tilde{\mathfrak{g}}_{(r,s)} \tilde{\mathfrak{g}}_{(r',s')}$ with

$$\tilde{\mathfrak{g}}_{(1,1)|(r,s)} = \tilde{\mathfrak{g}}_{(1,1)} \tilde{\mathfrak{g}}_{(r,s)} = \tilde{\mathfrak{g}}_{(1,1)|(1,1)} \tilde{d}_{(r,s)} = \sqrt{\frac{8}{mm'}} \sin \frac{r\pi}{m} \sin \frac{s\pi}{m'} = \mathcal{S}_{(r_0, s_0), (r,s)} \quad (2.29)$$

The last equality follows straightforwardly using the relation (2.6) between r_0 and s_0 .

More generally, for the (A, G) minimal models, the 2-boundary g-factors are given by [14]

$$\hat{\mathfrak{g}}_{(1,1)|(r,a)} = \hat{\mathfrak{g}}_{(1,1)} \hat{\mathfrak{g}}_{(r,a)} = \tilde{\mathfrak{g}}_{(1,1)|(1,1)} \hat{d}_{(r,a)} = \sqrt{\frac{2m'}{m}} \frac{\sin \frac{r\pi}{m}}{\sin \frac{\pi}{m'}} \Psi_1^1 \Psi_a^1, \quad \hat{d}_{(r,a)} = \sum_{s=1}^{m'-1} n_{s1}^a \tilde{d}_{(r,s)} \quad (2.30)$$

where $\Psi_1^1 = \|\psi\|^{-1}$ and $\hat{\mathfrak{g}}_{(1,1)|(1,1)} = \sqrt{\frac{2m'}{m}} \frac{\sin \frac{\pi}{m}}{\sin \frac{\pi}{m'}} \|\psi\|^{-2}$ with ψ given by (2.2). The quantum dimension $\hat{d}_{(r,a)}$ gives the g-factor associated with the (r, a) defect. These defect g-factors give a 1-dimensional representation of the coset graph fusion algebra. The boundary and defect entropies are

$$S_{(r,a)}^{\text{bdy}} = \log \hat{\mathfrak{g}}_{(r,a)}, \quad S_{(r,a)}^{\text{defect}} = \log \hat{d}_{(r,a)} \quad (2.31)$$

The g -factors are multiplicative while the entropies are additive.

Numerical g -factors can be calculated from the limits of conformal tower degeneracies. The q -series for the Virasoro characters are

$$\chi_{r,s}^{m,m'}(q) = q^{-c/24 + \Delta_{r,s}^{m,m'}} \sum_{n=0,1,2,\dots}^{\infty} d_n^{(r,s)} q^n \quad (2.32)$$

where $n = E \in \mathbb{N}_0$ is an energy level in the conformal tower with degeneracy $d_n^{(r,s)} \in \mathbb{N}_0$. Remarkably, the degeneracies $d_n^{(r,s)}$ allow for the numerical calculation of the effective central charge c_{eff} (2.5) and the 2-boundary g -factors $\tilde{g}_{(1,1)|(r,a)}$ (2.30)

$$c_{\text{eff}} = c - 24\Delta_{\min} = 1 - \frac{6}{mm'} = \lim_{n \rightarrow \infty} \frac{3}{2\pi^2 n} (\log d_n^{(r,s)})^2, \quad \text{independent of } (r, s) \quad (2.33a)$$

$$\tilde{g}_{(1,1)|(r,s)} = \lim_{n \rightarrow \infty} 2 \left(\frac{6n^3}{c_{\text{eff}}} \right)^{1/4} \exp\left(-2\pi \sqrt{\frac{nc_{\text{eff}}}{6}}\right) d_n^{(r,s)}, \quad \hat{g}_{(1,1)|(r,a)} = \sum_{s=1}^{m'-1} n_s 1^a \tilde{g}_{(1,1)|(r,s)} \quad (2.33b)$$

These two formulas generalize relations in [55, 29] respectively to allow for nonunitary theories. For unitary theories, $m' = m \pm 1$, $\Delta_{\min} = 0$ and $c_{\text{eff}} = c$. These limits are checked numerically against the analytic expressions for each theory that we study. The extrapolation of some typical sequences are shown in Figure 3.

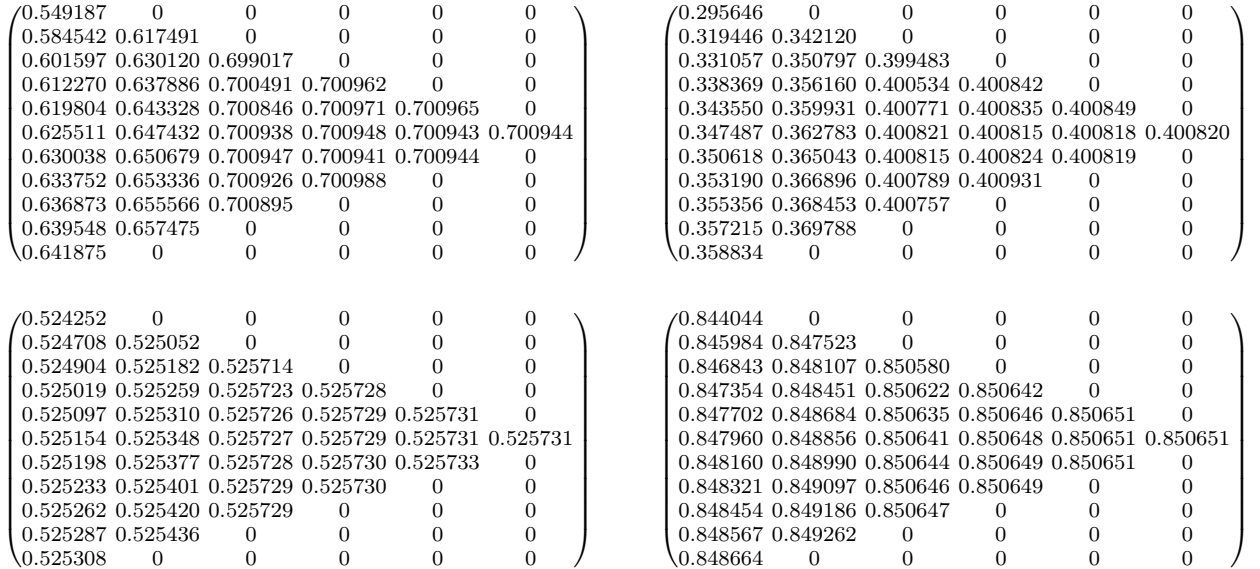


Figure 3: Vanden Broeck-Schwartz [56] extrapolations of degeneracy sequences for c_{eff} (top row) and 2-boundary g -factors (bottom row). The top row relates to (i) the central charge $c = c_{\text{eff}} = \frac{7}{10}$ of the tricritical Ising model $\mathcal{M}(4, 5)$, (ii) the effective central charge $c_{\text{eff}} = \frac{2}{5}$ of the Lee-Yang model $\mathcal{M}(2, 5)$. The bottom row relates to (iii-iv) the 2-boundary g -factors $\tilde{g}_{(1,1)|(1,1)} = 0.525731\dots$ and $\tilde{g}_{(1,1)|(1,2)} = 0.850651\dots$ of the Lee-Yang model $\mathcal{M}(2, 5)$. The values of n in the sequences (2.33) range from $n = 1000$ to $n = 11000$ in increments of $\Delta n = 1000$. The convergence of the g -factors is faster than the convergence of the effective central charges.

2.8 Asymptotic counting of coset fusion paths

The fundamental fusion matrix \tilde{N}_2 acts to move from one node of the coset fusion graph \tilde{G} to a neighbour. So the application of N fundamental fusions corresponds to an N -step fusion path on \tilde{G} . For large N , the number of such N -step fusion paths grows as \tilde{d}_2^N . It is therefore natural to look at the large- N asymptotics $\lim_{N \rightarrow \infty} (\tilde{G}/\tilde{d}_2)^N$ of the dimensions $\dim \mathcal{V}_{\mu, \mu'}^{(N)}$ of the vector spaces spanned by such N -step fusion paths from μ to μ' . The details depend (i) on the parities of m and m' , (ii) on whether \tilde{G} is bipartite or not and (iii) on the number of connected components of \tilde{G} but, ultimately, a rank-1 matrix emerges

$$\lim_{N \rightarrow \infty} \left(\frac{\tilde{G}}{\tilde{d}_2} \right)^N \propto \begin{pmatrix} \tilde{\mathfrak{g}}_{1|1} & \tilde{\mathfrak{g}}_{1|2} & \cdots & \tilde{\mathfrak{g}}_{1|n} \\ \tilde{\mathfrak{g}}_{2|1} & \tilde{\mathfrak{g}}_{2|2} & \cdots & \tilde{\mathfrak{g}}_{2|n} \\ \vdots & \vdots & \ddots & \vdots \\ \tilde{\mathfrak{g}}_{n|1} & \tilde{\mathfrak{g}}_{n|2} & \cdots & \tilde{\mathfrak{g}}_{n|n} \end{pmatrix} = \tilde{\mathfrak{g}}_{1|1} \begin{pmatrix} 1 \\ \tilde{d}_2 \\ \vdots \\ \tilde{d}_n \end{pmatrix} (1 \ \tilde{d}_2 \ \cdots \ \tilde{d}_n) = \tilde{\mathfrak{g}}_{1|1} \sum_{\mu=1}^n \tilde{d}_\mu \tilde{N}_\mu = \tilde{\mathfrak{g}}_{1|1} \mathcal{D}, \quad n = |\mathbb{K}| \quad (2.34)$$

where $\tilde{d}_1 = 1$ and $\mu = 2$ denotes the fundamental. If the coset graph \tilde{G} is bipartite, we combine the limits for the odd and even sublattices. Both the 2-boundary \mathfrak{g} -factors $\tilde{\mathfrak{g}}_{\mu|\mu'}$ and the quantum dimensions \tilde{d}_μ can be obtained from (2.34). Indeed, the quantum dimensions \tilde{d}_μ can be obtained by factoring out $\tilde{\mathfrak{g}}_{1|1}$ and solving the equations

$$\lim_{N \rightarrow \infty} \frac{\tilde{G}^N}{(\tilde{G}^N)_{1,1}} = \begin{pmatrix} 1 \\ \tilde{d}_2 \\ \vdots \\ \tilde{d}_n \end{pmatrix} (1 \ \tilde{d}_2 \ \cdots \ \tilde{d}_n) = \sum_{\mu=1}^n \tilde{d}_\mu \tilde{N}_\mu \quad (2.35)$$

The physical interpretation (see Figure 2) of these equations is that $\tilde{\mathfrak{g}}_{\mu|\mu'}$ gives the \mathfrak{g} -factor for the system with boundary condition μ on the left and μ' on the right. The boundaries μ, μ' are implemented by the action of the defects \mathcal{L}_μ on the left vacuum boundary and $\mathcal{L}_{\mu'}$ on the right vacuum boundary. The defects carry the defect \mathfrak{g} -factors given by the quantum dimensions \tilde{d}_μ and $\tilde{d}_{\mu'}$. Finally, leaving the vacuum contribution $\tilde{\mathfrak{g}}_{1|1}$ behind, the defects can propagate to the center of the cylinder where the fusion product is decomposed in accord with the fusion rules. A number of prototypical examples of this procedure are given in the examples in Section 3.2.

2.9 Relative symmetry resolved entanglement entropies

In this section, we consider relative Symmetry Resolved Entanglement Entropies or SREEs [30–36] in the framework of boundary CFT. The Hilbert spaces of the quantum Hamiltonians, corresponding to the cylinder partition functions (2.11), decompose into sectors according to the fusion rules

$$\mathcal{H}_{\mu'|\mu''} = \bigoplus_{\mu \in \mathbb{K}} \tilde{N}_{\mu\mu'\mu''} \mathcal{H}_{1|\mu} \quad (2.36)$$

where the fusion labels μ are quantum numbers. Strictly speaking, in the nonunitary cases, this is not a Hilbert space. The reduced density matrix is a block-diagonal sum over sectors

$$\rho_{\mu'|\mu''} = \bigoplus_{\mu \in \mathbb{K}} p_\mu \tilde{N}_{\mu\mu'\mu''} \rho_{1|\mu} \quad (2.37)$$

where p_μ are probabilities. SREEs arise by using the above decomposition to refine the notion of entanglement entropy. In terms of the cylinder partition functions (2.11), the Rényi entropies with n replicas are defined by

$$S_{\mu'|\mu''}^n := \frac{1}{1-n} \log \text{Tr} \rho_{\mu'|\mu''}^n(q) = \frac{1}{1-n} \log \frac{Z_{\mu'|\mu''}(q^n)}{[Z_{\mu'|\mu''}(q)]^n} \quad (2.38)$$

Although originating as an integer, n is treated as a continuous variable. Indeed, the von Neumann entanglement entropies are recovered as $\lim_{n \rightarrow 1} S_{\mu'|\mu''}^n$.

We are interested in relative SREEs $\Delta S_{\mu,\mu',\mu''}^n$, defined as

$$\begin{aligned} \Delta S_{\mu,\mu',\mu''}^n &:= \lim_{q \rightarrow 1} (S_{1|\mu}^n - S_{\mu'|\mu''}^n) = \lim_{q \rightarrow 1} \frac{1}{1-n} \left[\log \frac{Z_{1,\mu}(q^n)}{[Z_{1,\mu}(q)]^n} - \log \frac{Z_{\mu',\mu''}(q^n)}{[Z_{\mu',\mu''}(q)]^n} \right] \\ &= \lim_{q \rightarrow 1} \frac{1}{1-n} \left[\log \frac{Z_{1,\mu}(q^n)}{Z_{\mu',\mu''}(q^n)} - n \log \frac{Z_{1,\mu}(q)}{Z_{\mu',\mu''}(q)} \right] = \lim_{q \rightarrow 1} \log \frac{Z_{1,\mu}(q^n)}{Z_{\mu',\mu''}(q^n)} \end{aligned} \quad (2.39)$$

where μ appears in the decomposition of the fusion product $\mu' \times \mu''$. The relative SREEs $\Delta S_{\mu,\mu',\mu''}^n$ measure the contribution of the sector μ to the entanglement entropy $\lim_{q \rightarrow 1} S_{\mu'|\mu''}^n$. Using the asymptotic result of Affleck and Ludwig [29] (see also (4.5) of [14]) in (2.39)

$$\log Z_{\mu|\mu'} \sim -\log \tilde{q}^{\frac{c_{\text{eff}}}{24}} + \log \tilde{\mathfrak{g}}_{(1,1)|(1,1)} + \log \hat{d}_\mu \hat{d}_{\mu'}, \quad \tilde{q} \rightarrow 0 \text{ or } q \rightarrow 1 \quad (2.40)$$

now yields the desired result independent of n

$$\Delta S_{\mu,\mu',\mu''}^n = \log \frac{\hat{d}_\mu}{\hat{d}_{\mu'} \hat{d}_{\mu''}} \quad (2.41)$$

Since this result is independent of n , no ambiguity can arise from the analytic continuation in n . From (2.23), it follows that

$$1 = \sum_{\mu=1}^{|\mathbb{K}|} \tilde{N}_{\mu'\mu''\mu} \frac{\hat{d}_\mu}{\hat{d}_{\mu'} \hat{d}_{\mu''}} = \sum_{\mu=1}^{|\mathbb{K}|} \tilde{N}_{\mu'\mu''\mu} \exp(\Delta S_{\mu,\mu',\mu''}^n) \quad (2.42)$$

so the exponentials of the relative SREEs, given by the ratios of quantum dimensions, are probabilities.

3 Prototypical CFTs

Except for special cases, such as $m = 2$ or $m = 3$, the tensor product graphs $A_{m-1} \otimes G$ decompose into two disconnected graphs equivalent to the coset graph $\tilde{G} = A \otimes G / \mathbb{Z}_2$. The coset graph \tilde{G} may be bipartite or not bipartite depending on the absence or presence of loops. For $\mathcal{M}(m, m')$, we find

$$\tilde{G} = \begin{cases} \text{single non-bipartite component,} & m = 2 \text{ and } m' \text{ odd} \\ \text{single bipartite component,} & m = 3 \text{ and } m' \text{ odd or even} \\ \text{single bipartite component,} & m \geq 4 \text{ and } mm' \text{ even} \\ \text{direct sum of two non-bipartite components,} & m \geq 5 \text{ odd and } m' \text{ odd} \end{cases} \quad (3.1)$$

For $\mathcal{M}(2, m')$, the coset graph $A_1 \otimes A_{m'-1} / \mathbb{Z}_2$ is the tadpole graph $\tilde{G} = T_{(m'-1)/2}$. For $\mathcal{M}(3, m')$, the coset graph $A_2 \otimes A_{m'-1} / \mathbb{Z}_2$ is the graph $\tilde{G} = A_{m'-1}$. The general expressions for the coset graphs are given in Appendix A.

3.1 Prototypical unitary CFTs

3.1.1 Critical Ising model $\mathcal{M}(3, 4) = (A_2, A_3)$

The coset graph \tilde{G} of the Ising model $\mathcal{M}(3, 4)$ is $A_2 \otimes A_3 / \mathbb{Z}_2 = A_3$ as shown in Figure 4. Explicitly, the nimrep fusion matrices are

$$\tilde{N}_1 = I = \begin{pmatrix} 1 & 0 & 0 \\ 0 & 1 & 0 \\ 0 & 0 & 1 \end{pmatrix}, \quad \tilde{N}_2 = \tilde{G} = \begin{pmatrix} 0 & 1 & 0 \\ 1 & 0 & 1 \\ 0 & 1 & 0 \end{pmatrix}, \quad \tilde{N}_3 = \sigma = \begin{pmatrix} 0 & 0 & 1 \\ 0 & 1 & 0 \\ 1 & 0 & 0 \end{pmatrix} \quad (3.2)$$

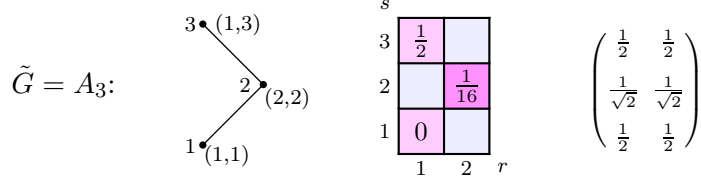


Figure 4: The bipartite coset graph $\tilde{G} = A_2 \otimes A_3/\mathbb{Z}_2 = A_3$ and Kac tables of conformal weights and 2-boundary \mathfrak{g} -factors $\mathfrak{g}_{(1,1)|(r,s)}$ for the critical Ising model $\mathcal{M}(3,4)$ with $c = \frac{1}{2}$. Under the Kac table symmetry $(1,2) \equiv (2,2)$, so the nodes $(r,s) = (1,1), (2,2), (1,3)$ are simply labelled by $s = 1, 2, 3$.

with $\tilde{N}_2^2 = I + \tilde{N}_3$, $\tilde{N}_2\tilde{N}_1 = \tilde{N}_2\tilde{N}_3 = \tilde{N}_2$, $\tilde{N}_3^2 = I$ and quantum dimensions $\tilde{d}_s = [s]_y$ where $s = 1, 2, 3$, $y = e^{\pi i/4}$ and $\sigma = \tilde{N}_3$ is the spin-reversal operator. The coset graph fusion algebra is realized as the polynomial ring

$$\mathbb{Z}[y]/\langle y^2 - 2 \rangle \quad (3.3)$$

The conformal cylinder partition functions $Z_{s|s'}(q) = Z_{s'|s}(q)$ are

$$Z_{1|s}(q) = \chi_{1,s}^{3,4}(q), \quad Z_{2|2}(q) = \chi_{1,1}^{3,4}(q) + \chi_{1,3}^{3,4}(q), \quad Z_{2|3}(q) = \chi_{1,2}^{3,4}(q), \quad Z_{3|3}(q) = \chi_{1,1}^{3,4}(q) \quad (3.4)$$

The unitary matrix \mathcal{S} that diagonalizes \tilde{G} is the modular matrix

$$\mathcal{S} = \mathcal{S}^T = \frac{1}{2} \begin{pmatrix} 1 & \sqrt{2} & 1 \\ \sqrt{2} & 0 & -\sqrt{2} \\ 1 & -\sqrt{2} & 1 \end{pmatrix}, \quad \mathcal{S}^{-1}\tilde{N}_2\mathcal{S} = \begin{pmatrix} \sqrt{2} & 0 & 0 \\ 0 & 0 & 0 \\ 0 & 0 & -\sqrt{2} \end{pmatrix}, \quad \mathcal{S}^2 = I \quad (3.5)$$

The 2-boundary \mathfrak{g} -factors $\tilde{\mathfrak{g}}_{s|s'} = \tilde{\mathfrak{g}}_s\tilde{\mathfrak{g}}_{s'}$ are

$$\tilde{\mathfrak{g}}_{1|1} = \tilde{\mathfrak{g}}_{1|3} = \mathcal{S}_{1,1} = \frac{1}{2}, \quad \tilde{\mathfrak{g}}_{2|2} = \mathcal{S}_{1,2} = \frac{1}{\sqrt{2}}, \quad \tilde{\mathfrak{g}}_{2|2} = \frac{\tilde{\mathfrak{g}}_{1|2}^2}{\tilde{\mathfrak{g}}_{1|1}} = 1 \quad (3.6)$$

The multiplicative defect \mathfrak{g} -factors \tilde{d}_s

$$\tilde{d}_s = \frac{\tilde{\mathfrak{g}}_{1|s}}{\tilde{\mathfrak{g}}_{1|1}}, \quad \tilde{d}_1 = \tilde{d}_3 = 1, \quad \tilde{d}_2 = 2 \cos \frac{\pi}{4} = \sqrt{2} = 1.414214\dots, \quad \tilde{d}_2^2 = 1 + \tilde{d}_3 \quad (3.7)$$

give a 1-dimensional representation of the coset graph fusion algebra.

In terms of the asymptotics of counting fusion paths, we find

$$\lim_{\substack{N \rightarrow \infty \\ N = \kappa \bmod 2}} \left(\frac{1}{\sqrt{2}}\right)^N \tilde{G}^N = \lim_{\substack{N \rightarrow \infty \\ N = \kappa \bmod 2}} \left(\frac{1}{\sqrt{2}}\right)^N \begin{pmatrix} 0 & 1 & 0 \\ 1 & 0 & 1 \\ 0 & 1 & 0 \end{pmatrix}^N = \mathcal{S} \begin{pmatrix} 1 & 0 & 0 \\ 0 & 0 & 0 \\ 0 & 0 & (-1)^\kappa \end{pmatrix} \mathcal{S}^{-1} = \begin{cases} \mathbf{D}_+, & N \text{ even} \\ \mathbf{D}_-, & N \text{ odd} \end{cases} \quad (3.8)$$

with

$$\mathbf{D}_+ = \frac{1}{2} \begin{pmatrix} 1 & 0 & 1 \\ 0 & 2 & 0 \\ 1 & 0 & 1 \end{pmatrix} = \frac{1}{2}(\tilde{N}_1 + \tilde{N}_3), \quad \mathbf{D}_- = \frac{1}{2} \begin{pmatrix} 0 & \sqrt{2} & 0 \\ \sqrt{2} & 0 & \sqrt{2} \\ 0 & \sqrt{2} & 0 \end{pmatrix} = \frac{1}{\sqrt{2}}\tilde{N}_2 \quad (3.9)$$

Combining the even and odd matrices, gives the rank-1 matrix

$$\mathbf{D} = \frac{1}{2}(\mathbf{D}_+ + \mathbf{D}_-) = \frac{1}{4} \begin{pmatrix} 1 & \sqrt{2} & 1 \\ \sqrt{2} & 2 & \sqrt{2} \\ 1 & \sqrt{2} & 1 \end{pmatrix} = \tilde{\mathfrak{g}}_{1|1} \begin{pmatrix} \tilde{\mathfrak{g}}_{1|1} & \tilde{\mathfrak{g}}_{1|2} & \tilde{\mathfrak{g}}_{1|3} \\ \tilde{\mathfrak{g}}_{2|1} & \tilde{\mathfrak{g}}_{2|2} & \tilde{\mathfrak{g}}_{2|3} \\ \tilde{\mathfrak{g}}_{3|1} & \tilde{\mathfrak{g}}_{3|2} & \tilde{\mathfrak{g}}_{3|3} \end{pmatrix} = \tilde{\mathfrak{g}}_{1|1}^2 \begin{pmatrix} 1 & \tilde{d}_2 & \tilde{d}_3 \\ \tilde{d}_2 & \tilde{d}_2^2 & \tilde{d}_2\tilde{d}_3 \\ \tilde{d}_3 & \tilde{d}_3\tilde{d}_2 & \tilde{d}_3^2 \end{pmatrix} = \tilde{\mathfrak{g}}_{1|1}^2 \begin{pmatrix} 1 \\ \tilde{d}_2 \\ \tilde{d}_3 \end{pmatrix} (1 \ \tilde{d}_2 \ \tilde{d}_3) \quad (3.10)$$

The boundary and defect \mathfrak{g} -factors are simply obtained by solving these equations. Notice that

$$\mathbf{D} = \tilde{\mathfrak{g}}_{1|1}^2 \sum_{s=1}^3 \tilde{d}_s \tilde{N}_s \quad (3.11)$$

3.1.2 Tricritical Ising model $\mathcal{M}(4, 5) = (A_3, A_4)$

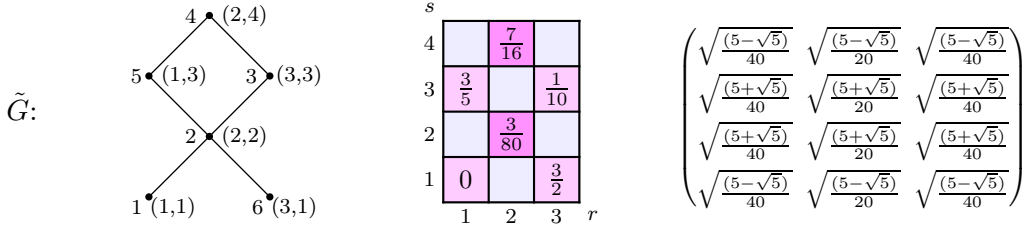


Figure 5: The bipartite coset graph $\tilde{G} = \tilde{N}_2 = A_3 \otimes A_4/\mathbb{Z}_2$ and Kac tables of conformal weights and 2-boundary \mathfrak{g} -factors $\mathfrak{g}_{(1,1)|(r,s)}$ for the tricritical Ising model $\mathcal{M}(4, 5)$ with $c = \frac{7}{10}$. Choosing the $r+s$ even sublattice, the nodes $(r, s) \in \mathbb{K} = \{(1, 1), (2, 2), (3, 3), (2, 4), (1, 3), (3, 1)\}$ are labelled by $\mu = 1, 2, \dots, 6$. The fundamental $(2, 2)$ is labelled by $\mu = 2$.

The coset graph \tilde{G} of the tricritical Ising model [57–59] $\mathcal{M}(4, 5)$ is $\tilde{G} = A_3 \otimes A_4/\mathbb{Z}_2$ as shown in Figure 5. With these choices, the explicit nimrep fusion matrices are

$$\begin{aligned} \tilde{N}_1 &= \begin{pmatrix} 1 & 0 & 0 & 0 & 0 & 0 \\ 0 & 1 & 0 & 0 & 0 & 0 \\ 0 & 0 & 1 & 0 & 0 & 0 \\ 0 & 0 & 0 & 1 & 0 & 0 \\ 0 & 0 & 0 & 0 & 1 & 0 \\ 0 & 0 & 0 & 0 & 0 & 1 \end{pmatrix}, & \tilde{N}_2 &= \begin{pmatrix} 0 & 1 & 0 & 0 & 0 & 0 \\ 1 & 0 & 1 & 0 & 1 & 1 \\ 0 & 1 & 0 & 1 & 0 & 0 \\ 0 & 0 & 1 & 0 & 1 & 0 \\ 0 & 1 & 0 & 1 & 0 & 0 \\ 0 & 1 & 0 & 0 & 0 & 0 \end{pmatrix}, & \tilde{N}_3 &= \begin{pmatrix} 0 & 0 & 1 & 0 & 0 & 0 \\ 0 & 1 & 0 & 1 & 0 & 0 \\ 1 & 0 & 0 & 0 & 1 & 0 \\ 0 & 1 & 0 & 0 & 0 & 0 \\ 0 & 0 & 1 & 0 & 0 & 1 \\ 0 & 0 & 0 & 0 & 1 & 0 \end{pmatrix} \\ \tilde{N}_4 &= \begin{pmatrix} 0 & 0 & 0 & 1 & 0 & 0 \\ 0 & 0 & 1 & 0 & 1 & 0 \\ 0 & 1 & 0 & 0 & 0 & 0 \\ 1 & 0 & 0 & 0 & 0 & 1 \\ 0 & 1 & 0 & 0 & 0 & 0 \\ 0 & 0 & 0 & 1 & 0 & 0 \end{pmatrix}, & \tilde{N}_5 &= \begin{pmatrix} 0 & 0 & 0 & 0 & 1 & 0 \\ 0 & 1 & 0 & 1 & 0 & 0 \\ 0 & 0 & 1 & 0 & 0 & 1 \\ 0 & 1 & 0 & 0 & 0 & 0 \\ 1 & 0 & 0 & 0 & 1 & 0 \\ 0 & 0 & 1 & 0 & 0 & 0 \end{pmatrix}, & \tilde{N}_6 &= \begin{pmatrix} 0 & 0 & 0 & 0 & 0 & 1 \\ 0 & 1 & 0 & 0 & 0 & 0 \\ 0 & 0 & 0 & 0 & 1 & 0 \\ 0 & 0 & 0 & 1 & 0 & 0 \\ 0 & 0 & 1 & 0 & 0 & 0 \\ 1 & 0 & 0 & 0 & 0 & 0 \end{pmatrix} \end{aligned} \quad (3.12)$$

Since $\tilde{N}_{\mu 1}^{\mu'} = \delta_{\mu, \mu'}$, the fusion matrices are linearly independent and μ labels the position of the single 1 in the first row of \tilde{N}_{μ} . The fusion matrices, along with the quantum dimensions $\tilde{d}_{(r,s)} = [r]_x [s]_y$ for $(r, s) \in \mathbb{K}$, $x = e^{\pi i/4}$ and $y = e^{\pi i/5}$, satisfy the coset graph fusion algebra. The coset graph fusion algebra is realized as the polynomial ring

$$\mathbb{Z}[x, y]/\langle x^3 - 2x, y^2 - x^2 y + y - 1 \rangle \quad (3.13)$$

The conformal cylinder partition functions $Z_{s|s'}(q) = Z_{s'|s}(q)$ are given by (2.11). The unitary matrix \mathcal{S} that diagonalizes the fusion matrices is the modular matrix

$$\mathcal{S} = \mathcal{S}^T = \frac{1}{2} \begin{pmatrix} s_1 & \sqrt{2}s_2 & s_2 & \sqrt{2}s_1 & s_2 & s_1 \\ \sqrt{2}s_2 & 0 & \sqrt{2}s_1 & 0 & -\sqrt{2}s_1 & -\sqrt{2}s_2 \\ s_2 & \sqrt{2}s_1 & -s_1 & -\sqrt{2}s_2 & -s_1 & s_2 \\ \sqrt{2}s_1 & 0 & -\sqrt{2}s_2 & 0 & \sqrt{2}s_2 & -\sqrt{2}s_1 \\ s_2 & -\sqrt{2}s_1 & -s_1 & \sqrt{2}s_2 & -s_1 & s_2 \\ s_1 & -\sqrt{2}s_2 & s_2 & -\sqrt{2}s_1 & s_2 & s_1 \end{pmatrix}, \quad \mathcal{S}^{-1} \tilde{N}_2 \mathcal{S} = \begin{pmatrix} \lambda_+ & 0 & 0 & 0 & 0 & 0 \\ 0 & 0 & 0 & 0 & 0 & 0 \\ 0 & 0 & \lambda_- & 0 & 0 & 0 \\ 0 & 0 & 0 & 0 & 0 & 0 \\ 0 & 0 & 0 & 0 & -\lambda_- & 0 \\ 0 & 0 & 0 & 0 & 0 & -\lambda_+ \end{pmatrix}, \quad \mathcal{S}^2 = I \quad (3.14)$$

where $s_1 = \frac{2}{\sqrt{5}} \sin \frac{\pi}{5}$, $s_2 = \frac{2}{\sqrt{5}} \sin \frac{2\pi}{5}$ and $\lambda_{\pm} = \sqrt{3 \pm \sqrt{5}}$. The multiplicative boundary \mathfrak{g} -factors $\tilde{\mathfrak{g}}_{s|s'} = \tilde{\mathfrak{g}}_s \tilde{\mathfrak{g}}_{s'}$ are

$$\tilde{\mathfrak{g}}_{1|1} = \tilde{\mathfrak{g}}_{1|6} = \mathcal{S}_{1,1} = \frac{1}{2} s_1, \quad \tilde{\mathfrak{g}}_{1|2} = \mathcal{S}_{1,2} = \frac{1}{\sqrt{2}} s_2, \quad \tilde{\mathfrak{g}}_{1|3} = \tilde{\mathfrak{g}}_{1|5} = \mathcal{S}_{1,3} = \frac{1}{2} s_2, \quad \tilde{\mathfrak{g}}_{1|4} = \mathcal{S}_{1,4} = \frac{1}{\sqrt{2}} s_1 \quad (3.15)$$

The multiplicative defect \mathbf{g} -factors are

$$\tilde{d}_\mu = \frac{\tilde{\mathfrak{g}}_{1|\mu}}{\tilde{\mathfrak{g}}_{1|1}} = \frac{\mathcal{S}_{1,\mu}}{\mathcal{S}_{1,1}} = \left\{ 1, \sqrt{3+\sqrt{5}}, \frac{1}{2}(1+\sqrt{5}), \sqrt{2}, \frac{1}{2}(1+\sqrt{5}), 1 \right\} \quad (3.16a)$$

$$\tilde{d}_{(1,1)} = \tilde{d}_{(3,1)} = 1, \quad \tilde{d}_{(2,2)} = \sqrt{3+\sqrt{5}}, \quad \tilde{d}_{(3,3)} = \tilde{d}_{(1,3)} = \frac{1}{2}(1+\sqrt{5}), \quad \tilde{d}_{(2,4)} = \sqrt{2} \quad (3.16b)$$

In terms of the asymptotics of counting fusion paths, we find

$$\lim_{\substack{N \rightarrow \infty \\ N = \kappa \bmod 2}} \left(\frac{1}{\lambda^+} \right)^N \tilde{G}^N = \mathcal{S} \operatorname{diag}\{1, 0, 0, 0, 0, (-1)^\kappa\} \mathcal{S}^{-1} = \begin{cases} \mathbf{D}_+, & N \text{ even} \\ \mathbf{D}_-, & N \text{ odd} \end{cases} \quad (3.17)$$

Combining the even and odd matrices, gives the rank-1 matrix

$$\mathbf{D} = \frac{1}{2} (\mathbf{D}_+ + \mathbf{D}_-) = \frac{1}{2} \begin{pmatrix} \frac{1}{20}(5-\sqrt{5}) & \frac{1}{\sqrt{10}} & \frac{1}{2\sqrt{5}} & \sqrt{\frac{1}{20}(3-\sqrt{5})} & \frac{1}{2\sqrt{5}} & \frac{1}{20}(5-\sqrt{5}) \\ \frac{1}{\sqrt{10}} & \frac{1}{10}(5+\sqrt{5}) & \sqrt{\frac{1}{20}(3+\sqrt{5})} & \frac{1}{\sqrt{5}} & \sqrt{\frac{1}{20}(3+\sqrt{5})} & \frac{1}{\sqrt{10}} \\ \frac{1}{2\sqrt{5}} & \sqrt{\frac{1}{20}(3+\sqrt{5})} & \frac{1}{20}(5+\sqrt{5}) & \frac{1}{\sqrt{10}} & \frac{1}{20}(5+\sqrt{5}) & \frac{1}{2\sqrt{5}} \\ \sqrt{\frac{1}{20}(3-\sqrt{5})} & \frac{1}{\sqrt{5}} & \frac{1}{\sqrt{10}} & \frac{1}{10}(5-\sqrt{5}) & \frac{1}{\sqrt{10}} & \sqrt{\frac{1}{20}(3-\sqrt{5})} \\ \frac{1}{2\sqrt{5}} & \sqrt{\frac{1}{20}(3+\sqrt{5})} & \frac{1}{20}(5+\sqrt{5}) & \frac{1}{\sqrt{10}} & \frac{1}{20}(5+\sqrt{5}) & \frac{1}{2\sqrt{5}} \\ \frac{1}{20}(5-\sqrt{5}) & \frac{1}{\sqrt{10}} & \frac{1}{2\sqrt{5}} & \sqrt{\frac{1}{20}(3-\sqrt{5})} & \frac{1}{2\sqrt{5}} & \frac{1}{20}(5-\sqrt{5}) \end{pmatrix} \quad (3.18)$$

The boundary and defect \mathbf{g} -factors are obtained by solving

$$\mathbf{D} = \hat{\mathfrak{g}}_{1|1} \begin{pmatrix} \hat{\mathfrak{g}}_{1|1} & \hat{\mathfrak{g}}_{1|2} & \cdots & \hat{\mathfrak{g}}_{1|6} \\ \hat{\mathfrak{g}}_{2|1} & \hat{\mathfrak{g}}_{2|2} & \cdots & \hat{\mathfrak{g}}_{2|6} \\ \vdots & \vdots & \ddots & \vdots \\ \hat{\mathfrak{g}}_{6|1} & \hat{\mathfrak{g}}_{6|2} & \cdots & \hat{\mathfrak{g}}_{6|6} \end{pmatrix} = \hat{\mathfrak{g}}_{1|1}^2 \begin{pmatrix} 1 & \hat{d}_2 & \cdots & \hat{d}_6 \\ \hat{d}_2 & \hat{d}_2^2 & \cdots & \hat{d}_2 \hat{d}_6 \\ \vdots & \vdots & \ddots & \vdots \\ \hat{d}_6 & \hat{d}_2 \hat{d}_6 & \cdots & \hat{d}_6^2 \end{pmatrix} = \hat{\mathfrak{g}}_{1|1}^2 \begin{pmatrix} 1 \\ \hat{d}_2 \\ \vdots \\ \hat{d}_6 \end{pmatrix} (1 \ \hat{d}_2 \ \cdots \ \hat{d}_6) \quad (3.19)$$

Notice that

$$\mathbf{D} = \hat{\mathfrak{g}}_{1|1}^2 \sum_{\mu=1}^6 \hat{d}_\mu \hat{N}_\mu \quad (3.20)$$

Alternatively, using $\tilde{G} = A_3 \otimes A_4 / \mathbb{Z}_2 = A_3 \otimes T_2$ with (r, s) representatives restricted by $1 \leq s \leq 2$, we could have chosen $\mathbb{K} = \{(1, 1), (1, 2), (2, 1), (2, 2), (3, 1), (3, 2)\}$. The nimrep fusion matrices would then be $\tilde{N}_{r,s} = N_r^{(A_3)} \otimes N_s^{(T_2)}$ with

$$\tilde{N}_{1,s} = \begin{pmatrix} N_s^{(T_2)} & 0 & 0 \\ 0 & N_s^{(T_2)} & 0 \\ 0 & 0 & N_s^{(T_2)} \end{pmatrix}, \quad \tilde{N}_{2,s} = \begin{pmatrix} 0 & N_s^{(T_2)} & 0 \\ N_s^{(T_2)} & 0 & N_s^{(T_2)} \\ 0 & N_s^{(T_2)} & 0 \end{pmatrix}, \quad \tilde{N}_{3,s} = \begin{pmatrix} 0 & 0 & N_s^{(T_2)} \\ 0 & N_s^{(T_2)} & 0 \\ N_s^{(T_2)} & 0 & 0 \end{pmatrix}, \quad s = 1, 2 \quad (3.21)$$

Allowing for a simultaneous permutation of the rows and columns of $\tilde{N}_{r,s}$, \mathcal{S} , \mathbf{D} and an associated reordering of the elements of \mathbb{K} , the results are identical.

3.1.3 Critical 3-state Potts model (A_4, D_4)

The coset graph of the 3-state Potts model [47, 60, 61] is $\tilde{G} = A_4 \otimes D_4 / \mathbb{Z} = T_2 \otimes D_4$ as shown in Figure 6. Explicitly, the nimrep fusion matrices are

$$\tilde{N}_{r,a} = N_r^{(T_2)} \otimes \hat{N}_a^{(D_4)}, \quad \tilde{N}_{1,a} = \begin{pmatrix} \hat{N}_a^{(D_4)} & 0 \\ 0 & \hat{N}_a^{(D_4)} \end{pmatrix}, \quad \tilde{N}_{2,a} = \begin{pmatrix} 0 & \hat{N}_a^{(D_4)} \\ \hat{N}_a^{(D_4)} & \hat{N}_a^{(D_4)} \end{pmatrix}, \quad r = 1, 2; \quad a = 1, 2, 3, 4 \quad (3.22)$$

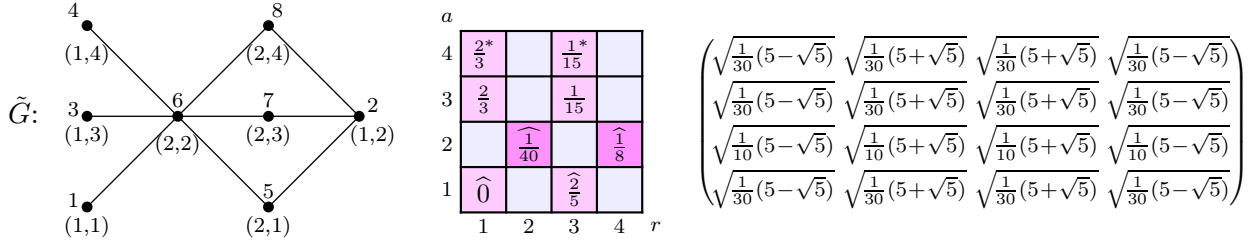


Figure 6: The bipartite coset graph $\tilde{G} = A_4 \otimes D_4 / \mathbb{Z}_2 = T_2 \otimes D_4$ and Kac tables of conformal weights and 2-boundary \mathfrak{g} -factors $\hat{\mathfrak{g}}_{(1,1)|(r,a)}$ of the critical 3-state Potts model (A_4, D_4) with $c = \frac{4}{5}$ where T_2 is the tadpole on 2 nodes. The nodes are (r, a) with $r = 1, 2$ and $a = 1, 2, 3, 4$. Alternatively, the ordered nodes $(r, a) = (1, 1), (1, 2), (1, 3), (1, 4), (2, 1), (2, 2), (2, 3), (2, 4)$ are labelled by $\mu = 1, 2, \dots, 8$. The label $a = 4$ can be replaced with $a = 3^*$ reflecting the fact that $a = 3$ and 4 are on the same sublattice and rows 3 and 4 are duplicates. The D_4 graph arises as the \mathbb{Z}_2 orbifold of the A_5 diagram. Under the (A_4, A_5) Kac table symmetry, $(2, 1) \equiv (3, 1)$, $(2, 3) \equiv (3, 3)$, $(2, 4) \equiv (3, 4)$ and $(1, 2) \equiv (4, 2)$. The extended conformal weights are $\hat{0} = 0 + 3$, $\frac{\hat{1}}{40} = \frac{1}{40} + \frac{21}{40}$, $\frac{\hat{1}}{8} = \frac{1}{8} + \frac{13}{8}$, $\frac{\hat{2}}{5} = \frac{2}{5} + \frac{7}{5}$.

The nimreps of T_2 and D_4 and the adjacency matrix (fundamental nimrep) $\tilde{G} = \tilde{N}_{2,2}$ are

$$N_r^{(T_2)} = \begin{pmatrix} 1 & 0 \\ 0 & 1 \end{pmatrix}, \begin{pmatrix} 0 & 1 \\ 1 & 1 \end{pmatrix}; \quad \hat{N}_a^{(D_4)} = \begin{pmatrix} 1 & 0 & 0 & 0 \\ 0 & 1 & 0 & 0 \\ 0 & 0 & 1 & 0 \\ 0 & 0 & 0 & 1 \end{pmatrix}, \begin{pmatrix} 0 & 1 & 0 & 0 \\ 1 & 0 & 1 & 1 \\ 0 & 1 & 0 & 0 \\ 0 & 1 & 0 & 0 \end{pmatrix}, \begin{pmatrix} 0 & 0 & 1 & 0 \\ 0 & 1 & 0 & 0 \\ 0 & 0 & 0 & 1 \\ 1 & 0 & 0 & 0 \end{pmatrix}, \begin{pmatrix} 0 & 0 & 0 & 1 \\ 0 & 1 & 0 & 0 \\ 1 & 0 & 0 & 0 \\ 0 & 0 & 1 & 0 \end{pmatrix}; \quad \tilde{G} = \begin{pmatrix} 0 & 0 & 0 & 0 & 1 & 0 & 0 \\ 0 & 0 & 0 & 0 & 1 & 0 & 1 & 1 \\ 0 & 0 & 0 & 0 & 0 & 1 & 0 & 0 \\ 0 & 0 & 0 & 0 & 0 & 1 & 0 & 0 \\ 0 & 1 & 0 & 0 & 0 & 1 & 0 & 0 \\ 1 & 0 & 1 & 1 & 1 & 0 & 1 & 1 \\ 0 & 1 & 0 & 0 & 0 & 1 & 0 & 0 \\ 0 & 1 & 0 & 0 & 0 & 1 & 0 & 0 \end{pmatrix} \quad (3.23)$$

The polynomial ring for this case will be discussed elsewhere. The Cayley table of the $T_2 \otimes D_4$ graph fusion algebra is shown in Figure 7. It is possible to add the \mathbb{Z}_2 diagram automorphism σ to the coset graph fusion algebra. In this case, the enlarged graph fusion algebra becomes noncommutative because it contains within it the noncommutative symmetric group \mathfrak{S}_3 but we do not do this here.

	11	12	13	14	21	22	23	24
11	11	12	13	14	21	22	23	24
12	12	11+13+14	12	12	22	21+23+24	22	22
13	13	12	14	11	23	22	24	21
14	14	12	11	13	24	22	21	23
21	21	22	23	24	11+21	12+22	13+23	14+24
22	22	21+23+24	22	22	12+22	11+13+14+21+23+24	12+22	12+22
23	23	22	24	21	13+23	12+22	14+24	11+21
24	24	22	21	23	14+24	12+22	11+21	13+23

Figure 7: Cayley table of the coset graph fusion algebra of the critical 3-state Potts model. We use the compact notations $ra = \tilde{N}_{r,a}$, $r = 1, 2$; $a = 1, 2, 3, 4$ with the order $(r, a) = (1, 1), (1, 2), (1, 3), (1, 4), (2, 1), (2, 2), (2, 3), (2, 4)$ labelled by $\mu = 1, 2, \dots, 8$.

The unitary matrix Ψ that diagonalizes \tilde{G} and the coset fusion matrices is [47]

$$\Psi = \mathcal{S} \otimes \Psi, \quad \mathcal{S} = \frac{2}{\sqrt{5}} \begin{pmatrix} \sin \frac{\pi}{5} & \sin \frac{2\pi}{5} \\ \sin \frac{2\pi}{5} & -\sin \frac{\pi}{5} \end{pmatrix}, \quad \Psi = \frac{1}{\sqrt{3}} \begin{pmatrix} \frac{1}{\sqrt{2}} & \frac{1}{\sqrt{2}} & 1 & 1 \\ \sqrt{\frac{3}{2}} & -\sqrt{\frac{3}{2}} & 0 & 0 \\ \frac{1}{\sqrt{2}} & \frac{1}{\sqrt{2}} & \omega & \omega^2 \\ \frac{1}{\sqrt{2}} & \frac{1}{\sqrt{2}} & \omega^2 & \omega \end{pmatrix} \quad (3.24a)$$

$$\Psi^{-1} \tilde{G} \Psi = \text{diag} \left\{ \frac{\sqrt{3}}{2}(1+\sqrt{5}), -\frac{\sqrt{3}}{2}(1+\sqrt{5}), 0, 0, -\frac{\sqrt{3}}{2}(\sqrt{5}-1), \frac{\sqrt{3}}{2}(\sqrt{5}-1), 0, 0 \right\} \quad (3.24b)$$

where $\omega = \exp(2\pi i/3)$. The 2-boundary \mathbf{g} -factors $\hat{\mathbf{g}}_{(1,1)|(r,a)}$ and defect \mathbf{g} -factors $\hat{d}_{(r,a)}$ are

$$\hat{\mathbf{g}}_{(1,1)|(r,a)} = \frac{4}{\sqrt{15}} \sin \frac{\pi}{5} \sin \frac{\pi}{6} \hat{d}_{(r,a)}, \quad \hat{d}_{(r,a)} = \{1, \sqrt{3}, 1, 1, \frac{1}{2}(1+\sqrt{5}), \frac{\sqrt{3}}{2}(1+\sqrt{5}), \frac{1}{2}(1+\sqrt{5}), \frac{1}{2}(1+\sqrt{5})\} \quad (3.25)$$

In terms of the asymptotics of counting fusion paths, we find

$$\lim_{\substack{N \rightarrow \infty \\ N = \kappa \bmod 2}} \left(\frac{1}{\lambda_+}\right)^N \tilde{G}^N = \Psi \text{diag}\{1, (-1)^\kappa, 0, 0, 0, 0, 0, 0\} \Psi^{-1} = \begin{cases} \mathbf{D}_+, & N \text{ even} \\ \mathbf{D}_-, & N \text{ odd} \end{cases} \quad (3.26)$$

with $\lambda_+ = \frac{\sqrt{3}}{2}(1+\sqrt{5})$. Combining the even and odd matrices, gives the rank-1 matrix $\mathbf{D} = \mathbf{D}_+ + \mathbf{D}_-$

$$\mathbf{D} = \begin{pmatrix} \frac{1}{30}(5-\sqrt{5}) & \frac{1}{\sqrt{45}} \\ \frac{1}{\sqrt{45}} & \frac{1}{30}(5+\sqrt{5}) \end{pmatrix} \otimes \begin{pmatrix} \frac{1}{\sqrt{3}} & \sqrt{3} & 1 & 1 \\ \sqrt{3} & 3 & \sqrt{3} & \sqrt{3} \\ 1 & \sqrt{3} & 1 & 1 \\ 1 & \sqrt{3} & 1 & 1 \end{pmatrix} \quad (3.27)$$

Using the fact that $\hat{\mathbf{g}}_{1|1} = \frac{4}{\sqrt{15}} \sin \frac{\pi}{5} \sin \frac{\pi}{6}$ and $\hat{\mathbf{g}}_{1|1}^2 = \frac{1}{30}(5-\sqrt{5})$, the 2-boundary \mathbf{g} -factors $\hat{\mathbf{g}}_{\mu|\mu'}$ and defect \mathbf{g} -factors \hat{d}_μ are obtained by solving

$$\mathbf{D} = \hat{\mathbf{g}}_{1|1} \begin{pmatrix} \hat{\mathbf{g}}_{1|1} & \hat{\mathbf{g}}_{1|2} & \dots & \hat{\mathbf{g}}_{1|8} \\ \hat{\mathbf{g}}_{2|1} & \hat{\mathbf{g}}_{2|2} & \dots & \hat{\mathbf{g}}_{2|8} \\ \vdots & \vdots & \ddots & \vdots \\ \hat{\mathbf{g}}_{8|1} & \hat{\mathbf{g}}_{8|2} & \dots & \hat{\mathbf{g}}_{8|8} \end{pmatrix} = \hat{\mathbf{g}}_{1|1}^2 \begin{pmatrix} \hat{d}_1 \\ \hat{d}_2 \\ \vdots \\ \hat{d}_8 \end{pmatrix} (1 \hat{d}_2 \dots \hat{d}_8) = \hat{\mathbf{g}}_{1|1}^2 \sum_{\mu=1}^8 \hat{d}_\mu \hat{N}_\mu \quad (3.28)$$

3.1.4 Tricritical 3-state Potts model (A_6, D_4)

The coset graph of the tricritical 3-state Potts model [62, 63] is $\tilde{G} = A_6 \otimes D_4 / \mathbb{Z} = T_3 \otimes D_4$ as shown in Figure 8. Explicitly, the nimrep fusion matrices $\tilde{N}_{r,a} = N_r^{(T_3)} \otimes \hat{N}_a^{(D_4)}$ are

$$\tilde{N}_{1,a} = \begin{pmatrix} \hat{N}_a^{(D_4)} & 0 & 0 \\ 0 & \hat{N}_a^{(D_4)} & 0 \\ 0 & 0 & \hat{N}_a^{(D_4)} \end{pmatrix}, \quad \tilde{N}_{2,a} = \begin{pmatrix} 0 & \hat{N}_a^{(D_4)} & 0 \\ \hat{N}_a^{(D_4)} & 0 & \hat{N}_a^{(D_4)} \\ 0 & \hat{N}_a^{(D_4)} & \hat{N}_a^{(D_4)} \end{pmatrix}, \quad \tilde{N}_{3,a} = \begin{pmatrix} 0 & 0 & \hat{N}_a^{(D_4)} \\ 0 & \hat{N}_a^{(D_4)} & \hat{N}_a^{(D_4)} \\ \hat{N}_a^{(D_4)} & \hat{N}_a^{(D_4)} & \hat{N}_a^{(D_4)} \end{pmatrix}, \quad r \leq 3; \quad a \leq 4 \quad (3.29)$$

The adjacency matrix (fundamental nimrep) is $\tilde{G} = \tilde{N}_{2,2}$ and the nimreps of T_3 and D_4 are

$$N_r^{(T_3)} = \begin{pmatrix} 1 & 0 & 0 \\ 0 & 1 & 0 \\ 0 & 0 & 1 \end{pmatrix}, \quad \begin{pmatrix} 0 & 1 & 0 \\ 1 & 0 & 1 \\ 0 & 1 & 1 \end{pmatrix}, \quad \begin{pmatrix} 0 & 0 & 1 \\ 0 & 1 & 1 \\ 1 & 1 & 1 \end{pmatrix}; \quad \hat{N}_a^{(D_4)} = \begin{pmatrix} 1 & 0 & 0 & 0 \\ 0 & 1 & 0 & 0 \\ 0 & 0 & 1 & 0 \\ 0 & 0 & 0 & 1 \end{pmatrix}, \quad \begin{pmatrix} 0 & 1 & 0 & 0 \\ 1 & 0 & 1 & 1 \\ 0 & 1 & 0 & 0 \\ 0 & 1 & 0 & 0 \end{pmatrix}, \quad \begin{pmatrix} 0 & 0 & 1 & 0 \\ 0 & 1 & 0 & 0 \\ 0 & 0 & 0 & 1 \\ 1 & 0 & 0 & 0 \end{pmatrix}, \quad \begin{pmatrix} 0 & 0 & 0 & 1 \\ 0 & 1 & 0 & 0 \\ 0 & 0 & 0 & 1 \\ 0 & 0 & 1 & 0 \end{pmatrix} \quad (3.30)$$

for $r = 1, 2, 3$ and $a = 1, 2, 3, 4$. The polynomial ring for this case will be discussed elsewhere.

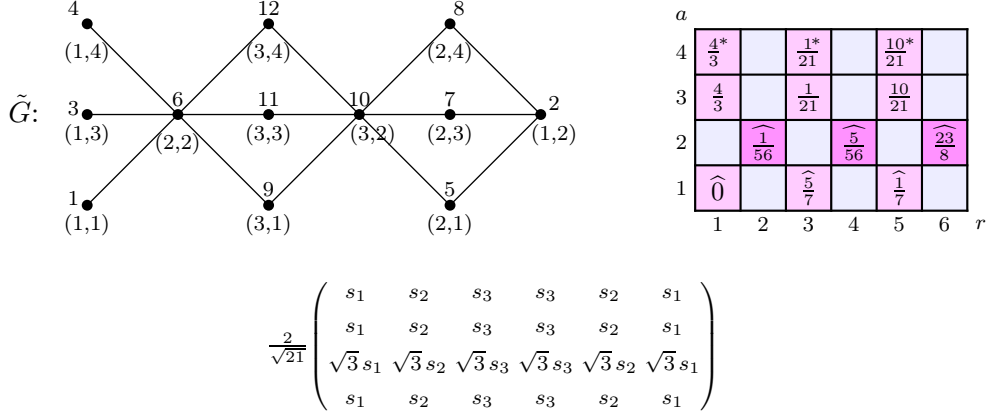


Figure 8: The bipartite coset graph $\tilde{G} = A_6 \otimes D_4 / \mathbb{Z}_2 = T_3 \otimes D_4$ and Kac tables of conformal weights and 2-boundary \mathbf{g} -factors $\hat{\mathbf{g}}_{(1,1)|(r,a)}$ of the tricritical 3-state Potts model (A_6, D_4) with $c = \frac{6}{7}$ where T_3 is the tadpole on 3 nodes and $s_r = \sin \frac{r\pi}{7}$. The nodes are (r, a) with $r = 1, 2, 3$ and $a = 1, 2, 3, 4$. Alternatively, the ordered nodes $(r, a) = (1, 1), (1, 2), (1, 3), (1, 4), (2, 1), (2, 2), (2, 3), (2, 4), (3, 1), (3, 2), (3, 3), (3, 4)$ are labelled by $\mu = 1, 2, \dots, 12$. The label $a = 4$ can be replaced with $a = 3^*$ reflecting the fact that $a = 3$ and 4 are on the same sublattice and rows 3 and 4 are duplicates. The D_4 graph arises as the \mathbb{Z}_2 orbifold of the A_5 diagram. Under the (A_6, A_5) Kac table symmetry, $(3, 2) \equiv (4, 2)$, $(2, 1) \equiv (5, 1)$, $(2, 3) \equiv (5, 3)$, $(2, 4) \equiv (5, 4)$ and $(1, 2) \equiv (6, 2)$. The extended conformal weights are $\hat{0} = 0 + 5$, $\hat{\frac{1}{56}} = \frac{1}{56} + \frac{85}{56}$, $\hat{\frac{5}{56}} = \frac{5}{56} + \frac{33}{56}$, $\hat{\frac{1}{7}} = \frac{1}{7} + \frac{22}{7}$, $\hat{\frac{3}{8}} = \frac{3}{8} + \frac{23}{8}$, $\hat{\frac{5}{7}} = \frac{5}{7} + \frac{12}{7}$.

The unitary matrix Ψ that diagonalizes \tilde{G} and the coset fusion matrices is

$$\Psi = \mathcal{S} \otimes \Psi, \quad \mathcal{S} = \mathcal{S}^T = \frac{2}{\sqrt{7}} \begin{pmatrix} \sin \frac{2\pi}{7} & -\sin \frac{3\pi}{7} & \sin \frac{\pi}{7} \\ -\sin \frac{3\pi}{7} & -\sin \frac{\pi}{7} & \sin \frac{2\pi}{7} \\ \sin \frac{\pi}{7} & \sin \frac{2\pi}{7} & \sin \frac{3\pi}{7} \end{pmatrix}, \quad \Psi = \frac{1}{\sqrt{3}} \begin{pmatrix} \frac{1}{\sqrt{2}} & \frac{1}{\sqrt{2}} & 1 & 1 \\ \sqrt{\frac{3}{2}} & -\sqrt{\frac{3}{2}} & 0 & 0 \\ \frac{1}{\sqrt{2}} & \frac{1}{\sqrt{2}} & \omega & \omega^2 \\ \frac{1}{\sqrt{2}} & \frac{1}{\sqrt{2}} & \omega^2 & \omega \end{pmatrix} \quad (3.31a)$$

$$\Psi^{-1} \tilde{G} \Psi = 2\sqrt{3} \text{diag} \left\{ -\cos \frac{2\pi}{7}, \cos \frac{2\pi}{7}, 0, 0, \cos \frac{3\pi}{7}, -\cos \frac{3\pi}{7}, 0, 0, \cos \frac{\pi}{7}, -\cos \frac{\pi}{7}, 0, 0 \right\} \quad (3.31b)$$

where $\omega = \exp(2\pi i/3)$. The 2-boundary \mathbf{g} -factors $\hat{\mathbf{g}}_{(1,1)|(r,a)}$ and defect \mathbf{g} -factors $\hat{d}_{(r,a)}$ are

$$\hat{\mathbf{g}}_{(1,1)|(r,a)} = \frac{2}{\sqrt{21}} \sin \frac{\pi}{6} \sin \frac{\pi}{7} \tilde{d}_{(r,a)}, \quad \hat{d}_{(r,a)} = s_1^{-1} \{s_1, \sqrt{3} s_1, s_1, s_1, s_2, \sqrt{3} s_2, s_2, s_2, s_3, \sqrt{3} s_3, s_3, s_3\} \quad (3.32)$$

In terms of the asymptotic counting of fusion paths, we find

$$\lim_{\substack{N \rightarrow \infty \\ N = \kappa \bmod 2}} \left(\frac{1}{\lambda_+} \right)^N \tilde{G}^N = \Psi \text{diag} \{0, 0, 0, 0, 0, 0, 0, 0, 1, (-1)^\kappa, 0, 0\} \Psi^{-1} = \begin{cases} \mathbf{D}_+, & N \text{ even} \\ \mathbf{D}_-, & N \text{ odd} \end{cases} \quad (3.33)$$

with $\lambda_+ = \cos \frac{\pi}{7}$. Combining the even and odd matrices, gives the rank-1 matrix $\mathbf{D} = \mathbf{D}_+ + \mathbf{D}_-$

$$\mathbf{D} = \hat{\mathbf{g}}_{1|1}^2 \begin{pmatrix} 1 \\ s_2 \\ s_1 \\ s_3 \\ s_1 \end{pmatrix} (1 \frac{s_2}{s_1} \frac{s_3}{s_1}) \otimes \begin{pmatrix} 1 \\ \sqrt{3} \\ 1 \\ 1 \end{pmatrix} (1 \sqrt{3} 1 1) \quad (3.34)$$

Using the fact that $\hat{\mathbf{g}}_{1|1} = \frac{2}{\sqrt{21}} s_1$ and $\hat{\mathbf{g}}_{1|1}^2 = \frac{4}{21} s_1^2$, the 2-boundary \mathbf{g} -factors $\hat{\mathbf{g}}_{\mu|\mu'}$ and defect \mathbf{g} -factors

\hat{d}_μ are obtained from

$$D = \hat{\mathfrak{g}}_{1|1} \begin{pmatrix} \hat{\mathfrak{g}}_{1|1} & \hat{\mathfrak{g}}_{1|2} & \cdots & \hat{\mathfrak{g}}_{1|12} \\ \hat{\mathfrak{g}}_{2|1} & \hat{\mathfrak{g}}_{2|2} & \cdots & \hat{\mathfrak{g}}_{2|12} \\ \vdots & \vdots & \ddots & \vdots \\ \hat{\mathfrak{g}}_{12|1} & \hat{\mathfrak{g}}_{12|2} & \cdots & \hat{\mathfrak{g}}_{12|12} \end{pmatrix} = \hat{\mathfrak{g}}_{1|1}^2 \begin{pmatrix} 1 \\ \hat{d}_2 \\ \vdots \\ \hat{d}_{12} \end{pmatrix} (1 \hat{d}_2 \cdots \hat{d}_{12}) = \hat{\mathfrak{g}}_{1|1}^2 \sum_{\mu=1}^{12} \hat{d}_\mu \hat{N}_\mu \quad (3.35)$$

It is possible to add the \mathbb{Z}_2 diagram automorphism σ to the coset graph fusion algebra. In this case, the enlarged graph fusion algebra becomes noncommutative because it contains within it the noncommutative symmetric group \mathbb{S}_3 but we do not do this here.

3.2 Prototypical nonunitary CFTs

3.2.1 Critical Lee-Yang model $\mathcal{M}(2, 5) = (A_1, A_4)$

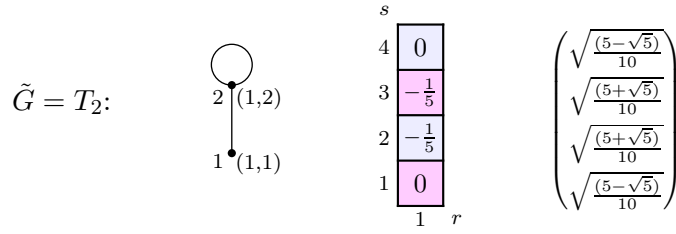


Figure 9: The non-bipartite coset graph $\tilde{G} = A_1 \otimes A_4 / \mathbb{Z}_2 = T_2$ and Kac tables of conformal weights and 2-boundary \mathfrak{g} -factors $\mathfrak{g}_{(1,1)|(r,s)}$ for the Lee-Yang model $\mathcal{M}(2, 5)$ with $c = -\frac{22}{5}$ and $c_{\text{eff}} = \frac{2}{5}$. T_2 is the tadpole on 2 nodes resulting from the \mathbb{Z}_2 folding of A_4 . The nodes $(r, s) = (1, 1), (1, 2)$ are labelled by $\mu = 1, 2$. The groundstate is $(r_0, s_0) = (1, 2)$.

The coset graph \tilde{G} of the Lee-Yang model [64–68] $\mathcal{M}(2, 5)$ is $A_1 \otimes A_4 / \mathbb{Z}_2 = T_2$ as shown in Figure 9. Explicitly, the nimrep fusion matrices are

$$\tilde{N}_1 = I = \begin{pmatrix} 1 & 0 \\ 0 & 1 \end{pmatrix}, \quad \tilde{N}_2 = \tilde{G} = \begin{pmatrix} 0 & 1 \\ 1 & 1 \end{pmatrix} \quad (3.36)$$

with $\tilde{N}_2^2 = I + \tilde{N}_2$ and quantum dimensions $\tilde{d}_1 = 1$, $\tilde{d}_2 = 2 \cos \frac{\pi}{5} = [2]_x$ where $x = e^{\pi i/5}$. The coset graph fusion algebra is realized as the polynomial ring

$$\mathbb{Z}[y] / \langle y^2 - y - 1 \rangle \quad (3.37)$$

The conformal cylinder partition functions $Z_{s|s'}(q) = Z_{(1,s)|(1,s')}(q)$ are

$$Z_{1|1}(q) = \chi_{1,1}^{2,5}(q), \quad Z_{1|2}(q) = \chi_{1,2}^{2,5}(q), \quad Z_{2|2}(q) = \chi_{1,1}^{2,5}(q) + \chi_{1,2}^{2,5}(q) \quad (3.38)$$

The unitary matrix \mathcal{S} that diagonalizes \tilde{G} is the modular matrix

$$\mathcal{S} = \mathcal{S}^T = \frac{2}{\sqrt{5}} \begin{pmatrix} \sin \frac{\pi}{5} & \sin \frac{2\pi}{5} \\ \sin \frac{2\pi}{5} & -\sin \frac{\pi}{5} \end{pmatrix}, \quad \mathcal{S}^{-1} \tilde{N}_2 \mathcal{S} = \begin{pmatrix} 2 \cos \frac{\pi}{5} & 0 \\ 0 & 2 \cos \frac{2\pi}{5} \end{pmatrix} = \begin{pmatrix} \frac{1}{2}(1+\sqrt{5}) & 0 \\ 0 & \frac{1}{2}(1-\sqrt{5}) \end{pmatrix}, \quad \mathcal{S}^2 = I \quad (3.39)$$

The 2-boundary \mathfrak{g} -factors $\tilde{\mathfrak{g}}_{s|s'} = \tilde{\mathfrak{g}}_s \tilde{\mathfrak{g}}_{s'}$ are

$$\tilde{\mathfrak{g}}_{1|1} = \mathcal{S}_{1,1} = \sqrt{\frac{5-\sqrt{5}}{10}} = \frac{2}{\sqrt{5}} \sin \frac{\pi}{5} = 0.525731 \dots, \quad \tilde{\mathfrak{g}}_{1|2} = \mathcal{S}_{1,2} = \sqrt{\frac{5+\sqrt{5}}{10}} = \frac{2}{\sqrt{5}} \sin \frac{2\pi}{5} = 0.850651 \dots \quad (3.40)$$

The defect \tilde{d}_s g-factors are

$$\tilde{d}_1 = 1, \quad \tilde{d}_2 = \frac{\tilde{\mathfrak{g}}_{1|2}}{\tilde{\mathfrak{g}}_{1|1}} = 2 \cos \frac{\pi}{5} = 1.61803\dots, \quad \tilde{d}_2^2 = 1 + \tilde{d}_2 \quad (3.41)$$

In terms of the asymptotics of counting fusion paths, we find the rank-1 matrix

$$\mathbf{D} = \lim_{N \rightarrow \infty} (2 \cos \frac{\pi}{5})^{-N} \begin{pmatrix} 0 & 1 \\ 1 & 1 \end{pmatrix}^N = \mathcal{S} \begin{pmatrix} 1 & 0 \\ 0 & 0 \end{pmatrix} \mathcal{S}^{-1} = \begin{pmatrix} \frac{1}{10}(5-\sqrt{5}) & \frac{1}{\sqrt{5}} \\ \frac{1}{\sqrt{5}} & \frac{1}{10}(5+\sqrt{5}) \end{pmatrix} = \tilde{\mathfrak{g}}_{1|1} \begin{pmatrix} \tilde{\mathfrak{g}}_{1|1} & \tilde{\mathfrak{g}}_{1|2} \\ \tilde{\mathfrak{g}}_{2|1} & \tilde{\mathfrak{g}}_{2|2} \end{pmatrix} = \tilde{\mathfrak{g}}_{1|1}^2 \begin{pmatrix} 1 & \tilde{d}_2 \\ \tilde{d}_2 & \tilde{d}_2^2 \end{pmatrix} \quad (3.42)$$

This is just the asymptotics of Fibonacci numbers. The boundary and defect g-factors are simply obtained by solving these equations. Notice that

$$\mathbf{D} = \tilde{\mathfrak{g}}_{1|1}^2 \sum_{s=1}^2 \tilde{d}_s \tilde{N}_s \quad (3.43)$$

3.2.2 Critical $\mathcal{M}(2,7) = (A_1, A_6)$ model

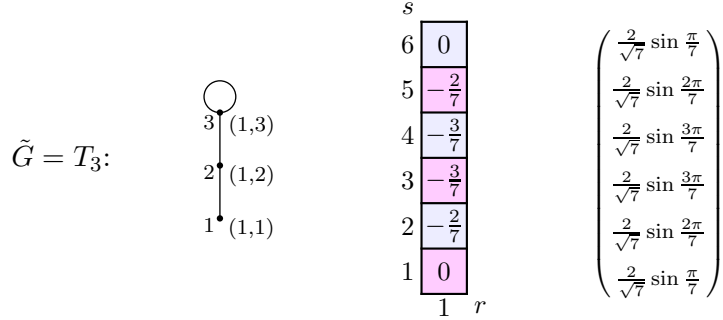


Figure 10: The non-bipartite coset graph $\tilde{G} = A_1 \otimes A_6 / \mathbb{Z}_2 = T_3$ and Kac tables of conformal weights and 2-boundary g-factors $\mathfrak{g}_{(1,1)|(r,s)}$ for the $\mathcal{M}(2,7)$ model with $c = -\frac{68}{7}$ and $c_{\text{eff}} = \frac{4}{7}$. T_3 is the tadpole on 3 nodes. The tadpole results from the \mathbb{Z}_2 folding of A_6 . The nodes $(r, s) = (1, 1), (1, 2), (1, 3)$ are labelled by $s = 1, 2, 3$. The groundstate is $(r_0, s_0) = (1, 3)$.

The coset graph \tilde{G} of the $\mathcal{M}(2,7)$ model is $A_1 \otimes A_6 / \mathbb{Z}_2 = T_3$ as shown in Figure 10. Explicitly, the nimrep fusion matrices are

$$\tilde{N}_1 = I = \begin{pmatrix} 1 & 0 & 0 \\ 0 & 1 & 0 \\ 0 & 0 & 1 \end{pmatrix}, \quad \tilde{N}_2 = \tilde{G} = \begin{pmatrix} 0 & 1 & 0 \\ 1 & 0 & 1 \\ 0 & 1 & 1 \end{pmatrix}, \quad \tilde{N}_3 = \begin{pmatrix} 0 & 0 & 1 \\ 0 & 1 & 1 \\ 1 & 1 & 1 \end{pmatrix} \quad (3.44)$$

with $\tilde{N}_2^2 = I + \tilde{N}_3$, $\tilde{N}_2 \tilde{N}_3 = \tilde{N}_2 + \tilde{N}_3$, $\tilde{N}_3^2 = I + \tilde{N}_2 + \tilde{N}_3$ and quantum dimensions $\tilde{d}_1 = 1$, $\tilde{d}_2 = 2 \cos \frac{\pi}{7} = [2]_x$, $\tilde{d}_3 = 1 + 2 \cos \frac{2\pi}{7} = [3]_x$ where $x = e^{\pi i/7}$. The coset graph fusion algebra is realized as the polynomial ring

$$\mathbb{Z}[y] / \langle y^3 - y^2 - 2y + 1 \rangle \quad (3.45)$$

The conformal cylinder partition functions $Z_{s|s'}(q) = Z_{(1,s)|(1,s')}(q)$ are

$$\begin{aligned} Z_{1|1}(q) &= \chi_{1,1}^{2,7}(q), & Z_{1|2}(q) &= \chi_{1,2}^{2,7}(q), & Z_{1|3}(q) &= \chi_{1,3}^{2,7}(q), & Z_{2|2}(q) &= \chi_{1,1}^{2,7}(q) + \chi_{1,3}^{2,7}(q) \\ Z_{2|3}(q) &= \chi_{1,2}^{2,7}(q) + \chi_{1,3}^{2,7}(q), & Z_{3|3}(q) &= \chi_{1,1}^{2,7}(q) + \chi_{1,2}^{2,7}(q) + \chi_{1,3}^{2,7}(q) \end{aligned} \quad (3.46)$$

The unitary matrix \mathcal{S} that diagonalizes \tilde{G} is the modular matrix

$$\mathcal{S} = \mathcal{S}^T = \frac{2}{\sqrt{7}} \begin{pmatrix} \sin \frac{2\pi}{7} & -\sin \frac{3\pi}{7} & \sin \frac{\pi}{7} \\ -\sin \frac{3\pi}{7} & -\sin \frac{\pi}{7} & \sin \frac{2\pi}{7} \\ \sin \frac{\pi}{7} & \sin \frac{2\pi}{7} & \sin \frac{3\pi}{7} \end{pmatrix}, \quad \mathcal{S}^{-1} \tilde{N}_2 \mathcal{S} = \begin{pmatrix} 2 \cos \frac{5\pi}{7} & 0 & 0 \\ 0 & 2 \cos \frac{3\pi}{7} & 0 \\ 0 & 0 & 2 \cos \frac{\pi}{7} \end{pmatrix}, \quad \mathcal{S}^2 = I \quad (3.47)$$

Since $s = 3$ is the groundstate, the 2-boundary \mathfrak{g} -factors $\tilde{\mathfrak{g}}_{s|s'}$ are

$$\tilde{\mathfrak{g}}_{3|s} = \mathcal{S}_{3,s} = \frac{2}{\sqrt{7}} \sin \frac{s\pi}{7} = 0.327985\dots, 0.591009\dots, 0.736976\dots \quad (3.48)$$

The defect \mathfrak{g} -factors \tilde{d}_s

$$\tilde{d}_1 = 1, \quad \tilde{d}_2 = \frac{\tilde{\mathfrak{g}}_{1|2}}{\tilde{\mathfrak{g}}_{1|1}} = 2 \cos \frac{\pi}{7} = 1.80194\dots, \quad \tilde{d}_3 = \frac{\tilde{\mathfrak{g}}_{1|3}}{\tilde{\mathfrak{g}}_{1|1}} = 1 + 2 \cos \frac{2\pi}{7} = 2.24698\dots \quad (3.49)$$

give a 1-dimensional representation of the coset fusion algebra corresponding to the largest eigenvalues of the fusion matrices.

In terms of the asymptotic counting of fusion paths, we find the rank-1 matrix

$$\mathbf{D} = \lim_{N \rightarrow \infty} (2 \cos \frac{\pi}{7})^{-N} \begin{pmatrix} 0 & 1 & 0 \\ 1 & 0 & 1 \\ 0 & 1 & 1 \end{pmatrix}^N = \mathcal{S} \begin{pmatrix} 1 & 0 & 0 \\ 0 & 0 & 0 \\ 0 & 0 & 0 \end{pmatrix} \mathcal{S}^{-1} = \tilde{\mathfrak{g}}_{1|1} \begin{pmatrix} \tilde{\mathfrak{g}}_{1|1} & \tilde{\mathfrak{g}}_{1|2} & \tilde{\mathfrak{g}}_{1|3} \\ \tilde{\mathfrak{g}}_{2|1} & \tilde{\mathfrak{g}}_{2|2} & \tilde{\mathfrak{g}}_{2|3} \\ \tilde{\mathfrak{g}}_{3|1} & \tilde{\mathfrak{g}}_{3|2} & \tilde{\mathfrak{g}}_{3|3} \end{pmatrix} = \tilde{\mathfrak{g}}_{1|1}^2 \begin{pmatrix} 1 \\ \tilde{d}_2 \\ \tilde{d}_3 \end{pmatrix} (1 \ \tilde{d}_2 \ \tilde{d}_3) \quad (3.50)$$

Notice that

$$\mathbf{D} = \tilde{\mathfrak{g}}_{1|1}^2 \sum_{s=1}^3 \tilde{d}_s \tilde{N}_s \quad (3.51)$$

3.2.3 Critical $\mathcal{M}(3, 5) = (A_2, A_4)$ model

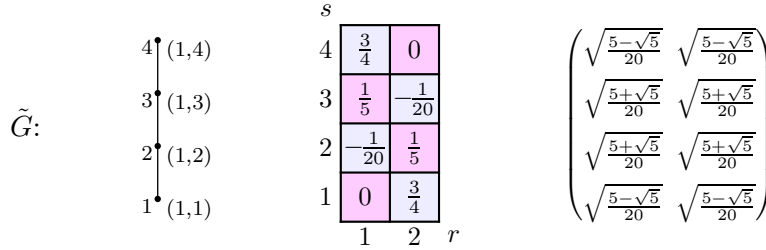


Figure 11: The bipartite coset graph $\tilde{G} = A_4$ and Kac tables of conformal weights and 2-boundary $\tilde{\mathfrak{g}}$ -factors $\mathfrak{g}_{(1,1)|(r,s)}$ for the $\mathcal{M}(3, 5)$ model with $c = -\frac{3}{5}$ and $c_{\text{eff}} = \frac{3}{5}$. The nodes $(r, s) = (1, 1), (1, 2), (1, 3), (1, 4)$ are labelled by $s = 1, 2, 3, 4$. The groundstate is $(r_0, s_0) = (1, 2)$.

The coset graph \tilde{G} of the $\mathcal{M}(3, 5)$ model is A_4 as shown in Figure 11. Explicitly, the nimrep fusion matrices are

$$\tilde{N}_1 = I, \quad \tilde{N}_2 = \begin{pmatrix} 0 & 1 & 0 & 0 \\ 1 & 0 & 1 & 0 \\ 0 & 1 & 0 & 1 \\ 0 & 0 & 1 & 0 \end{pmatrix}, \quad \tilde{N}_3 = \begin{pmatrix} 0 & 0 & 1 & 0 \\ 0 & 1 & 0 & 1 \\ 1 & 0 & 1 & 0 \\ 0 & 1 & 0 & 0 \end{pmatrix}, \quad \tilde{N}_4 = \begin{pmatrix} 0 & 0 & 0 & 1 \\ 0 & 0 & 1 & 0 \\ 0 & 1 & 0 & 0 \\ 1 & 0 & 0 & 0 \end{pmatrix} \quad (3.52)$$

with $\tilde{N}_2^2 = I + \tilde{N}_3$, $\tilde{N}_2 \tilde{N}_3 = \tilde{N}_2 + \tilde{N}_4$, $\tilde{N}_2 \tilde{N}_4 = \tilde{N}_3$, $\tilde{N}_3^2 = \tilde{N}_1 + \tilde{N}_3$, $\tilde{N}_3 \tilde{N}_4 = \tilde{N}_2$, $\tilde{N}_4^2 = I$. The fusion matrices, along with the quantum dimensions $\tilde{d}_{(r,s)} = [r]_x [s]_y$ for $(r, s) \in \mathbb{K}$, $x = e^{\pi i/3}$ and $y = e^{\pi i/5}$, satisfy the coset graph fusion algebra. The coset graph fusion algebra is realized as the polynomial ring

$$\mathbb{Z}[x, y] / \langle x^2 - 1, y^2 - xy - 1 \rangle \quad (3.53)$$

The conformal cylinder partition functions $Z_{s|s'}(q) = Z_{s'|s}(q) = Z_{(1,s)|(1,s')}(q)$ are

$$\begin{aligned} Z_{1|s}(q) &= \chi_{1,s}^{3,5}(q), & Z_{2|2}(q) &= \chi_{1,1}^{3,5}(q) + \chi_{1,3}^{3,5}(q), & Z_{2|3}(q) &= \chi_{1,2}^{3,5}(q) + \chi_{1,4}^{3,5}(q), \\ Z_{2|4}(q) &= \chi_{1,3}^{3,5}(q), & Z_{3|3}(q) &= \chi_{1,1}^{3,5}(q) + \chi_{1,3}^{3,5}(q), & Z_{3|4}(q) &= \chi_{1,2}^{3,5}(q), & Z_{4|4}(q) &= \chi_{1,1}^{3,5}(q) \end{aligned} \quad (3.54)$$

The unitary matrix \mathcal{S} that diagonalizes \tilde{G} is the modular matrix

$$\mathcal{S} = \mathcal{S}^T = \sqrt{\frac{2}{5}} \begin{pmatrix} \sin \frac{2\pi}{5} & \sin \frac{\pi}{5} & -\sin \frac{\pi}{5} & -\sin \frac{2\pi}{5} \\ \sin \frac{\pi}{5} & \sin \frac{2\pi}{5} & \sin \frac{2\pi}{5} & \sin \frac{\pi}{5} \\ -\sin \frac{\pi}{5} & \sin \frac{2\pi}{5} & -\sin \frac{2\pi}{5} & \sin \frac{\pi}{5} \\ -\sin \frac{2\pi}{5} & \sin \frac{\pi}{5} & \sin \frac{\pi}{5} & -\sin \frac{2\pi}{5} \end{pmatrix}, \quad \mathcal{S}^{-1} \tilde{N}_2 \mathcal{S} = \begin{pmatrix} 2 \cos \frac{2\pi}{5} & 0 & 0 & 0 \\ 0 & 2 \cos \frac{\pi}{5} & 0 & 0 \\ 0 & 0 & -2 \cos \frac{\pi}{5} & 0 \\ 0 & 0 & 0 & -2 \cos \frac{2\pi}{5} \end{pmatrix} \quad (3.55)$$

with $\mathcal{S}^2 = I$. Since $s = 2$ is the groundstate, the 2-boundary \mathfrak{g} -factors $\tilde{\mathfrak{g}}_{s|s'} = \tilde{\mathfrak{g}}_s \tilde{\mathfrak{g}}_{s'}$ are

$$\tilde{\mathfrak{g}}_{1|s} = \mathcal{S}_{2,s} = \sqrt{\frac{2}{5}} \sin \frac{s\pi}{5} = 0.371748\dots, 0.601501\dots, 0.601501\dots, 0.371748\dots \quad (3.56)$$

The defect \mathfrak{g} -factors \tilde{d}_μ giving a 1-dimensional representation of the coset graph fusion algebra are

$$\tilde{d}_1 = \tilde{d}_4 = 1, \quad \tilde{d}_2 = \tilde{d}_3 = \frac{\tilde{\mathfrak{g}}_{1|2}}{\tilde{\mathfrak{g}}_{1|1}} = 2 \cos \frac{\pi}{5} = 1.61803\dots \quad (3.57)$$

In terms of the asymptotics of counting fusion paths, we find

$$\lim_{\substack{N \rightarrow \infty \\ N = \kappa \bmod 2}} (2 \cos \frac{\pi}{5})^{-N} \begin{pmatrix} 0 & 1 & 0 & 0 \\ 1 & 0 & 1 & 0 \\ 0 & 1 & 0 & 1 \\ 0 & 0 & 1 & 0 \end{pmatrix}^N = \mathcal{S} \begin{pmatrix} 0 & 0 & 0 & 0 \\ 0 & 1 & 0 & 0 \\ 0 & 0 & (-1)^\kappa & 0 \\ 0 & 0 & 0 & 0 \end{pmatrix} \mathcal{S}^{-1} = \begin{cases} \mathbf{D}_+, & N \text{ even} \\ \mathbf{D}_-, & N \text{ odd} \end{cases} \quad (3.58)$$

with

$$\mathbf{D}_+ = \begin{pmatrix} \frac{5-\sqrt{5}}{10} & 0 & \frac{1}{\sqrt{5}} & 0 \\ 0 & \frac{5-\sqrt{5}}{10} & 0 & \frac{1}{\sqrt{5}} \\ \frac{1}{\sqrt{5}} & 0 & \frac{5+\sqrt{5}}{10} & 0 \\ 0 & \frac{1}{\sqrt{5}} & 0 & \frac{5+\sqrt{5}}{10} \end{pmatrix} = \frac{5-\sqrt{5}}{10} \tilde{N}_1 + \frac{1}{\sqrt{5}} \tilde{N}_3, \quad \mathbf{D}_- = \begin{pmatrix} 0 & \frac{1}{\sqrt{5}} & 0 & \frac{5-\sqrt{5}}{10} \\ \frac{1}{\sqrt{5}} & 0 & \frac{5+\sqrt{5}}{10} & 0 \\ 0 & \frac{5+\sqrt{5}}{10} & 0 & \frac{1}{\sqrt{5}} \\ \frac{5-\sqrt{5}}{10} & 0 & \frac{1}{\sqrt{5}} & 0 \end{pmatrix} = \frac{5-\sqrt{5}}{10} \tilde{N}_4 + \frac{1}{\sqrt{5}} \tilde{N}_2 \quad (3.59)$$

Combining the even and odd matrices, gives the rank-1 matrix

$$\mathbf{D} = \frac{1}{2}(\mathbf{D}_+ + \mathbf{D}_-) = \tilde{\mathfrak{g}}_{1|1} \begin{pmatrix} \tilde{\mathfrak{g}}_{1|1} & \tilde{\mathfrak{g}}_{1|2} & \tilde{\mathfrak{g}}_{1|3} & \tilde{\mathfrak{g}}_{1|4} \\ \tilde{\mathfrak{g}}_{2|1} & \tilde{\mathfrak{g}}_{2|2} & \tilde{\mathfrak{g}}_{2|3} & \tilde{\mathfrak{g}}_{2|4} \\ \tilde{\mathfrak{g}}_{3|1} & \tilde{\mathfrak{g}}_{3|2} & \tilde{\mathfrak{g}}_{3|3} & \tilde{\mathfrak{g}}_{3|4} \\ \tilde{\mathfrak{g}}_{4|1} & \tilde{\mathfrak{g}}_{4|2} & \tilde{\mathfrak{g}}_{4|3} & \tilde{\mathfrak{g}}_{4|4} \end{pmatrix} = \tilde{\mathfrak{g}}_{1|1}^2 \begin{pmatrix} 1 \\ \tilde{d}_2 \\ \tilde{d}_3 \\ \tilde{d}_4 \end{pmatrix} (1 \ \tilde{d}_2 \ \tilde{d}_3 \ \tilde{d}_4) \quad (3.60)$$

The boundary and defect \mathfrak{g} -factors are simply obtained by solving these equations. Notice that

$$\mathbf{D} = \tilde{\mathfrak{g}}_{1|1}^2 \sum_{s=1}^4 \tilde{d}_s \tilde{N}_s \quad (3.61)$$

3.2.4 Critical $\mathcal{M}(5, 7) = (A_4, A_6)$ model

The coset graph of the $\mathcal{M}(5, 7)$ model is $\tilde{G} = \tilde{G}_0 \oplus \tilde{G}_0$ where \tilde{G}_0 is shown in Figure 12. Explicitly, the nimrep fusion matrices are

$$\tilde{\mathcal{N}}_\mu = \begin{cases} \begin{pmatrix} \tilde{N}_\mu & 0 \\ 0 & \tilde{N}_\mu \end{pmatrix}, & \mu = 1, 2, \dots, 6 \quad (r+s \text{ even}) \\ \begin{pmatrix} 0 & \tilde{N}_\mu \\ \tilde{N}_\mu & 0 \end{pmatrix}, & \mu = 7, 8, \dots, 12 \quad (r+s \text{ odd}) \end{cases} \quad (3.62)$$

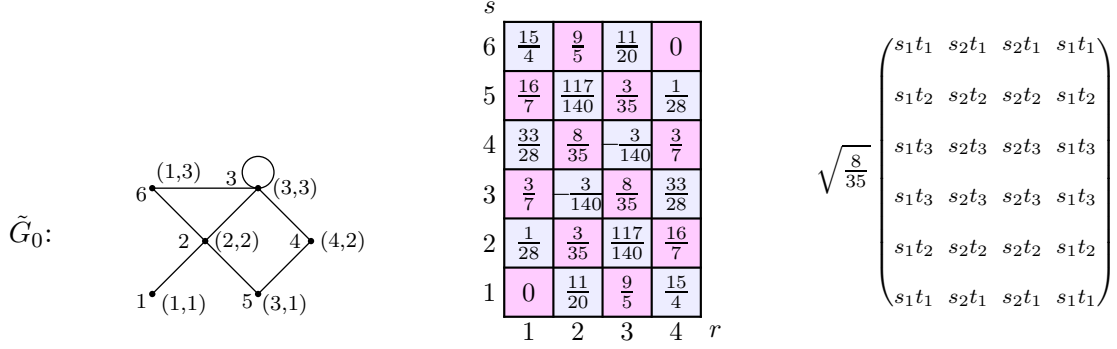


Figure 12: The non-bipartite coset graph is $\tilde{G} = \tilde{G}_0 \oplus \tilde{G}_0$ where \tilde{G}_0 is shown. Also shown are the Kac tables of conformal weights and 2-boundary $\tilde{\mathbf{g}}$ -factors $\mathbf{g}_{(2,3)|(r,s)}$ for the $\mathcal{M}(5,7)$ model with $c = \frac{11}{35}$ and $c_{\text{eff}} = \frac{29}{35}$. Restricting to the lower-half of the Kac table, $s_r = \sin \frac{r\pi}{5}$, $r = 1, 2, 3, 4$ and $t_s = \sin \frac{s\pi}{7}$, $s = 1, 2, 3$. The nodes $(r, s) = (1, 1), (2, 2), (3, 3), (4, 2), (3, 1), (1, 3), (4, 1), (3, 2), (2, 3), (1, 2), (2, 1), (4, 3) \in \mathbb{K}$ are labelled by $\mu = 1, 2, \dots, 12$. The groundstate $\mu = 9$ is $(r_0, s_0) = (2, 3)$.

where, with the basis ordering of \mathbb{K} as in Figure 12,

$$\tilde{N}_\mu|_{\mu=1,2,\dots,6} = \begin{pmatrix} 1 & 0 & 0 & 0 & 0 & 0 \\ 0 & 1 & 0 & 0 & 0 & 0 \\ 0 & 0 & 1 & 0 & 0 & 0 \\ 0 & 0 & 0 & 1 & 0 & 0 \\ 0 & 0 & 0 & 0 & 1 & 0 \\ 0 & 0 & 0 & 0 & 0 & 1 \end{pmatrix}, \begin{pmatrix} 0 & 1 & 0 & 0 & 0 & 0 \\ 1 & 0 & 1 & 0 & 1 & 1 \\ 0 & 1 & 1 & 1 & 0 & 1 \\ 0 & 0 & 1 & 0 & 1 & 0 \\ 0 & 1 & 0 & 1 & 0 & 0 \\ 0 & 1 & 1 & 0 & 0 & 0 \end{pmatrix}, \begin{pmatrix} 0 & 0 & 1 & 0 & 0 & 0 \\ 0 & 1 & 1 & 1 & 0 & 1 \\ 1 & 1 & 1 & 1 & 1 & 1 \\ 0 & 1 & 1 & 0 & 0 & 0 \\ 0 & 0 & 1 & 0 & 0 & 1 \\ 0 & 1 & 1 & 0 & 1 & 0 \end{pmatrix}, \begin{pmatrix} 0 & 0 & 0 & 1 & 0 & 0 \\ 0 & 0 & 1 & 0 & 1 & 0 \\ 0 & 1 & 1 & 0 & 0 & 0 \\ 1 & 0 & 0 & 0 & 0 & 1 \\ 0 & 1 & 0 & 0 & 0 & 0 \\ 0 & 0 & 0 & 1 & 0 & 1 \end{pmatrix}, \begin{pmatrix} 0 & 0 & 0 & 0 & 1 & 0 \\ 0 & 1 & 0 & 1 & 0 & 0 \\ 0 & 0 & 1 & 0 & 0 & 1 \\ 0 & 1 & 0 & 0 & 0 & 0 \\ 0 & 1 & 0 & 0 & 0 & 0 \\ 0 & 0 & 1 & 0 & 0 & 0 \end{pmatrix}, \begin{pmatrix} 0 & 0 & 0 & 0 & 0 & 1 \\ 0 & 1 & 1 & 0 & 0 & 0 \\ 0 & 1 & 1 & 0 & 1 & 0 \\ 0 & 0 & 0 & 1 & 0 & 1 \\ 0 & 0 & 1 & 0 & 1 & 0 \\ 1 & 0 & 0 & 1 & 0 & 1 \end{pmatrix} \quad (3.63)$$

The fusion matrices, along with the quantum dimensions $\tilde{d}_{(r,s)} = [r]_x [s]_y$ for $(r, s) \in \mathbb{K}$, $x = e^{\pi i/5}$ and $y = e^{\pi i/7}$, satisfy the coset graph fusion algebra. The coset graph fusion algebra is realized as the polynomial ring

$$\mathbb{Z}[x, y] / \langle x^4 - 3x^2 + 1, y^3 - x^3 y^2 + 2xy^2 - 2y + x^3 - 2x \rangle \quad (3.64)$$

The $\mathcal{M}(5,7)$ modular matrix that diagonalizes the fusion rules is

$$\mathcal{S} = \mathcal{S}^T = \begin{pmatrix} -S_0 & S_0 \\ S_0 & S_0 \end{pmatrix}, \quad S_0 = \sqrt{\frac{8}{35}} \begin{pmatrix} -s_2 t_2 & -s_1 t_3 & s_1 t_1 & s_2 t_3 & s_1 t_2 & -s_2 t_1 \\ -s_1 t_3 & -s_2 t_1 & s_2 t_2 & -s_1 t_1 & -s_2 t_3 & s_1 t_2 \\ s_1 t_1 & s_2 t_2 & s_2 t_3 & s_1 t_2 & s_2 t_1 & s_1 t_3 \\ s_2 t_3 & -s_1 t_1 & s_1 t_2 & s_2 t_1 & -s_1 t_3 & -s_2 t_2 \\ s_1 t_2 & -s_2 t_3 & s_2 t_1 & -s_1 t_3 & s_2 t_2 & s_1 t_1 \\ -s_2 t_1 & s_1 t_2 & s_1 t_3 & -s_2 t_2 & s_1 t_1 & -s_2 t_3 \end{pmatrix} \quad (3.65a)$$

$$\begin{pmatrix} -S_0 & S_0 \\ S_0 & S_0 \end{pmatrix} \begin{pmatrix} \tilde{N}_2 & 0 \\ 0 & \tilde{N}_2 \end{pmatrix} \begin{pmatrix} -S_0 & S_0 \\ S_0 & S_0 \end{pmatrix} = \begin{pmatrix} 2S_0 \tilde{N}_2 S_0 & 0 \\ 0 & 2S_0 \tilde{N}_2 S_0 \end{pmatrix}, \quad 2S_0 \tilde{N}_2 S_0 = \text{diag}\{\lambda_\mu\}_{\mu=1,2,\dots,6} \quad (3.65b)$$

$$s_r = \sin \frac{r\pi}{5}, \quad t_s = \sin \frac{s\pi}{7}, \quad S_0^2 = \frac{1}{2}I, \quad \mathcal{S}^2 = I, \quad \lambda_\mu = \lambda_{\mu+6} = \lambda_{r,s} = 4 \cos \frac{2\pi r}{5} \cos \frac{2\pi s}{7} \quad (3.65c)$$

Since the groundstate is $\mu = 9$ corresponding to $(r_0, s_0) = (2, 3)$, the 2-boundary $\tilde{\mathbf{g}}$ -factors $\tilde{\mathbf{g}}_{\mu|\mu'} = \tilde{\mathbf{g}}_\mu \tilde{\mathbf{g}}_{\mu'}$ are

$$\tilde{\mathbf{g}}_{\mu|\mu'} = \frac{\tilde{\mathbf{g}}_{1|\mu} \tilde{\mathbf{g}}_{1|\mu'}}{\tilde{\mathbf{g}}_{1|1}}, \quad \mu, \mu' = 1, 2, \dots, 12; \quad \tilde{\mathbf{g}}_{1|\mu} = \mathcal{S}_{9,\mu} = \sqrt{\frac{8}{35}} \sin \frac{r\pi}{5} \sin \frac{s\pi}{7}, \quad (r, s) \in \mathbb{K} \quad (3.66)$$

The defect \tilde{d}_μ giving a 1-dimensional representation of the coset graph fusion algebra are

$$\tilde{d}_\mu = \frac{\tilde{\mathbf{g}}_{1|\mu}}{\tilde{\mathbf{g}}_{1|1}} = \frac{\sin \frac{r\pi}{5} \sin \frac{s\pi}{7}}{\sin \frac{\pi}{5} \sin \frac{\pi}{7}}, \quad \mu = 1, 2, \dots, 12 \quad (3.67)$$

In terms of the asymptotics of counting fusion paths, we find the rank-1 matrix

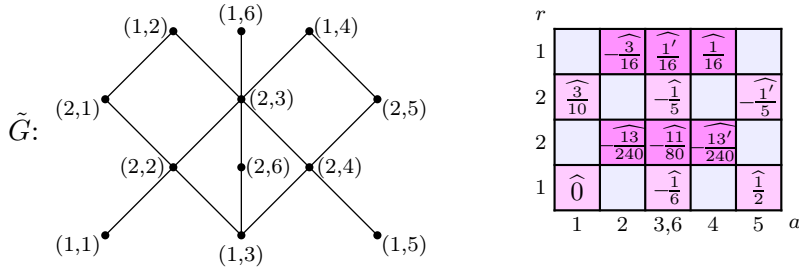
$$\mathbf{D} = \lim_{N \rightarrow \infty} \lambda_{2,3}^{-N} \tilde{N}_2^N = S_0 \text{diag}\{0, 0, 1, 0, 0, 0\} S_0^{-1} = \tilde{\mathbf{g}}_{1|1} \begin{pmatrix} \tilde{\mathbf{g}}_{1|1} & \tilde{\mathbf{g}}_{1|2} & \cdots & \tilde{\mathbf{g}}_{1|6} \\ \tilde{\mathbf{g}}_{2|1} & \tilde{\mathbf{g}}_{2|2} & \cdots & \tilde{\mathbf{g}}_{2|6} \\ \vdots & \vdots & \ddots & \vdots \\ \tilde{\mathbf{g}}_{6|1} & \tilde{\mathbf{g}}_{6|2} & \cdots & \tilde{\mathbf{g}}_{6|6} \end{pmatrix} = \tilde{\mathbf{g}}_{1|1}^2 \begin{pmatrix} 1 \\ \tilde{d}_2 \\ \vdots \\ \tilde{d}_6 \end{pmatrix} (1 \tilde{d}_2 \cdots \tilde{d}_6) \quad (3.68)$$

The boundary and defect \mathbf{g} -factors are simply obtained by solving these equations. Since the fusion matrices \tilde{N}_μ form a basis for the matrix powers of \tilde{N}_2 and $\tilde{N}_{\mu}^{\mu'} = \delta_{\mu, \mu'}$, reading off the first row of (3.68) gives

$$\mathbf{D} = \tilde{\mathbf{g}}_{1|1}^2 \begin{pmatrix} 1 \\ \tilde{d}_2 \\ \vdots \\ \tilde{d}_6 \end{pmatrix} (1 \tilde{d}_2 \cdots \tilde{d}_6) = \tilde{\mathbf{g}}_{1|1}^2 \sum_{\mu=1}^6 \tilde{d}_\mu \tilde{N}_\mu \quad (3.69)$$

consistent with the fact that the quantum dimensions \tilde{d}_μ satisfy the coset graph fusion algebra.

3.2.5 Critical (A_4, E_6) model



$$\sqrt{\frac{5-\sqrt{5}}{40}} \begin{pmatrix} \frac{1}{2}(1+\sqrt{5}) & \sqrt{2+\sqrt{3}} & \sqrt{2} & \sqrt{2+\sqrt{3}} & & \\ & \frac{1}{2}(1+\sqrt{5})\sqrt{2+\sqrt{3}} & \frac{1}{2}(1+\sqrt{5})(1+\sqrt{3}) & & & \\ & & \frac{1}{\sqrt{2}}(1+\sqrt{5}) & & & \\ & & & \frac{1}{2}(1+\sqrt{5})\sqrt{2+\sqrt{3}} & & \\ & & & & 1+\sqrt{3} & \\ & & & & & 1 \end{pmatrix}$$

Figure 13: The bipartite coset graph $\tilde{G} = A_4 \otimes E_6 / \mathbb{Z}_2 = T_2 \otimes E_6$ and Kac tables of conformal weights and 2-boundary \mathbf{g} -factors $\hat{\mathbf{g}}_{(1,1)|(r,a)}$ of the critical (A_4, E_6) model with $c = -\frac{39}{10}$ and $c_{\text{eff}} = \frac{9}{10}$ where T_2 is the tadpole on 2 nodes. The nodes are (r, a) with $r = 1, 2$ and $a = 1, 2, \dots, 6$. Alternatively, the ordered nodes $(r, a) = (1, 1), (1, 2), (1, 3), (1, 4), (1, 5), (1, 6), (2, 1), (2, 2), (2, 3), (2, 4), (2, 5), (2, 6)$ are labelled by $\mu = 1, 2, \dots, 12$. The E_6 graph intertwines with A_{11} [69, 70]. The extended conformal weights are $\hat{0} = 0 + 2$, $-\hat{\frac{3}{16}} = -\frac{3}{16} + \frac{55}{48} + \frac{49}{16}$, $-\hat{\frac{1}{6}} = -\frac{1}{6} + \frac{1}{2} + 2 + \frac{13}{3}$, $\hat{\frac{1}{16}} = \frac{1}{16} + \frac{55}{48} + \frac{93}{16}$, $\hat{\frac{1}{2}} = \frac{1}{2} + \frac{15}{2}$, $\hat{\frac{1}{16}} = \frac{1}{16} + \frac{49}{16}$; $\hat{\frac{3}{10}} = \frac{3}{10} + \frac{13}{10}$, $-\hat{\frac{13}{240}} = -\frac{13}{240} + \frac{49}{80} + \frac{69}{80}$, $-\hat{\frac{1}{5}} = -\frac{1}{5} + \frac{2}{15} + \frac{3}{10} + \frac{49}{30}$, $-\hat{\frac{13'}{240}} = -\frac{13}{240} - \frac{11}{80} + \frac{209}{80}$, $-\hat{\frac{1}{5}} = -\frac{1'}{5} + \frac{19}{5}$, $-\hat{\frac{11}{80}} = -\frac{11}{80} + \frac{69}{80}$.

The coset graph of the critical (A_4, E_6) model is $\tilde{G} = A_4 \otimes E_6 / \mathbb{Z} = T_2 \otimes E_6$ as shown in Figure 13. Explicitly, the nimrep fusion matrices are

$$\tilde{N}_{r,a} = N_r^{(T_2)} \otimes \hat{N}_a^{(E_6)}, \quad \tilde{N}_{1,a} = \begin{pmatrix} \hat{N}_a^{(E_6)} & 0 \\ 0 & \hat{N}_a^{(E_6)} \end{pmatrix}, \quad \tilde{N}_{2,a} = \begin{pmatrix} 0 & \hat{N}_a^{(E_6)} \\ \hat{N}_a^{(E_6)} & \hat{N}_a^{(E_6)} \end{pmatrix}, \quad r = 1, 2; \quad a = 1, 2, \dots, 6 \quad (3.70)$$

The nimreps of T_2 are given in (3.36) and the nimreps of E_6 are

$$\hat{N}_a^{(E_6)} = \begin{pmatrix} 1 & 0 & 0 & 0 & 0 & 0 \\ 0 & 1 & 0 & 0 & 0 & 0 \\ 0 & 0 & 1 & 0 & 0 & 0 \\ 0 & 0 & 0 & 1 & 0 & 0 \\ 0 & 0 & 0 & 0 & 1 & 0 \\ 0 & 0 & 0 & 0 & 0 & 1 \end{pmatrix}, \begin{pmatrix} 0 & 1 & 0 & 0 & 0 & 0 \\ 1 & 0 & 1 & 0 & 0 & 0 \\ 0 & 1 & 0 & 1 & 0 & 1 \\ 0 & 0 & 1 & 0 & 1 & 0 \\ 0 & 0 & 0 & 1 & 0 & 1 \\ 0 & 0 & 0 & 1 & 0 & 0 \end{pmatrix}, \begin{pmatrix} 0 & 0 & 1 & 0 & 0 & 0 \\ 0 & 1 & 0 & 1 & 0 & 1 \\ 1 & 0 & 2 & 0 & 1 & 0 \\ 0 & 1 & 0 & 1 & 0 & 1 \\ 0 & 0 & 1 & 0 & 0 & 0 \\ 0 & 1 & 0 & 1 & 0 & 0 \end{pmatrix}, \begin{pmatrix} 0 & 0 & 0 & 1 & 0 & 0 \\ 0 & 0 & 1 & 0 & 1 & 0 \\ 0 & 1 & 0 & 1 & 0 & 1 \\ 1 & 0 & 1 & 0 & 0 & 0 \\ 0 & 1 & 0 & 0 & 0 & 0 \\ 0 & 0 & 1 & 0 & 0 & 0 \end{pmatrix}, \begin{pmatrix} 0 & 0 & 0 & 0 & 1 & 0 \\ 0 & 0 & 0 & 1 & 0 & 0 \\ 0 & 0 & 1 & 0 & 0 & 0 \\ 0 & 1 & 0 & 0 & 0 & 0 \\ 1 & 0 & 0 & 0 & 0 & 0 \\ 0 & 0 & 0 & 0 & 1 & 0 \end{pmatrix}, \begin{pmatrix} 0 & 0 & 0 & 0 & 0 & 1 \\ 0 & 0 & 1 & 0 & 0 & 0 \\ 0 & 0 & 1 & 0 & 0 & 0 \\ 0 & 1 & 0 & 1 & 0 & 0 \\ 0 & 0 & 1 & 0 & 0 & 0 \\ 0 & 0 & 0 & 0 & 1 & 0 \end{pmatrix} \quad (3.71)$$

The unitary matrix Ψ that diagonalizes \tilde{G} and the coset graph fusion matrices is

$$\Psi = S \otimes \Psi, \quad S = \frac{2}{\sqrt{5}} \begin{pmatrix} \sin \frac{\pi}{5} & \sin \frac{2\pi}{5} \\ \sin \frac{2\pi}{5} & -\sin \frac{\pi}{5} \end{pmatrix}, \quad \Psi^T = \Psi^{-1} = \begin{pmatrix} \sqrt{\frac{3-\sqrt{3}}{24}} & \sqrt{\frac{3+\sqrt{3}}{24}} & \sqrt{\frac{3+\sqrt{3}}{12}} & \sqrt{\frac{3+\sqrt{3}}{24}} & \sqrt{\frac{3-\sqrt{3}}{24}} & \sqrt{\frac{3-\sqrt{3}}{24}} \\ \frac{1}{2} & \frac{1}{2} & 0 & -\frac{1}{2} & -\frac{1}{2} & 0 \\ \sqrt{\frac{3+\sqrt{3}}{24}} & \sqrt{\frac{3+\sqrt{3}}{24}} & -\sqrt{\frac{3-\sqrt{3}}{12}} & \sqrt{\frac{3-\sqrt{3}}{24}} & \sqrt{\frac{3+\sqrt{3}}{24}} & -\sqrt{\frac{3+\sqrt{3}}{24}} \\ \sqrt{\frac{3+\sqrt{3}}{24}} & -\sqrt{\frac{3-\sqrt{3}}{24}} & -\sqrt{\frac{3-\sqrt{3}}{12}} & -\sqrt{\frac{3-\sqrt{3}}{24}} & \sqrt{\frac{3+\sqrt{3}}{24}} & \sqrt{\frac{3+\sqrt{3}}{24}} \\ \frac{1}{2} & -\frac{1}{2} & 0 & \frac{1}{2} & -\frac{1}{2} & 0 \\ \sqrt{\frac{3-\sqrt{3}}{24}} & -\sqrt{\frac{3-\sqrt{3}}{24}} & \sqrt{\frac{3+\sqrt{3}}{12}} & -\sqrt{\frac{3+\sqrt{3}}{24}} & \sqrt{\frac{3-\sqrt{3}}{24}} & -\sqrt{\frac{3-\sqrt{3}}{24}} \end{pmatrix} \quad (3.72)$$

$$\Psi^{-1} \tilde{G} \Psi = \text{diag}\{\lambda_{r,a}\}, \quad \lambda_{1,a} = 4 \cos \frac{\pi}{5} \cos \frac{a\pi}{12}, \quad \lambda_{2,a} = 4 \cos \frac{3\pi}{5} \cos \frac{a\pi}{12}, \quad a \in \text{Exp}(E_6) \quad (3.73)$$

where $\text{Exp}(E_6) = \{1, 4, 5, 7, 8, 11\}$. The 2-boundary \mathfrak{g} -factors $\hat{\mathfrak{g}}_{(1,1)|(r,a)}$ and defect \mathfrak{g} -factors $\hat{d}_{(r,a)}$ are

$$\hat{\mathfrak{g}}_{(1,1)|(r,a)} = \sqrt{\frac{5-\sqrt{5}}{40}} \tilde{d}_{(r,a)}, \quad \hat{d}_{(r,a)} = \left(\frac{1+\sqrt{5}}{2}\right)^{r-1} \left\{ [1]_x, [2]_x, [3]_x, [2]_x, [1]_x, \frac{[3]_x}{[2]_x} \right\}, \quad x = e^{\pi i/12} \quad (3.74)$$

where $\hat{\mathfrak{g}}_{(1,1)|(1,1)} = \sqrt{\frac{5-\sqrt{5}}{40}}$.

In terms of the asymptotics of counting fusion paths, we find

$$\lim_{\substack{N \rightarrow \infty \\ N = \kappa \bmod 2}} \left(\frac{1}{\lambda_+}\right)^N \tilde{G}^N = \Psi \text{diag}\{1, 0, 0, 0, 0, (-1)^\kappa, 0, 0, 0, 0, 0, 0\} \Psi^{-1} = \begin{cases} \mathbf{D}_+, & N \text{ even} \\ \mathbf{D}_-, & N \text{ odd} \end{cases} \quad (3.75)$$

with $\lambda_+ = \frac{(1+\sqrt{3})(1+\sqrt{5})}{2\sqrt{2}}$. Combining the even and odd matrices, gives the rank-1 matrix $\mathbf{D} = \mathbf{D}_+ + \mathbf{D}_-$

$$\mathbf{D} = \begin{pmatrix} \frac{1}{10}(5-\sqrt{5}) & & & & & \\ & \frac{1}{\sqrt{5}} & & & & \\ & & \frac{1}{10}(5+\sqrt{5}) & & & \\ & & & & & \\ & & & & & \\ & & & & & \end{pmatrix} \otimes \begin{pmatrix} \frac{3-\sqrt{3}}{12} & \frac{1}{2\sqrt{6}} & \frac{1}{2\sqrt{3}} & \frac{1}{2\sqrt{6}} & \frac{3-\sqrt{3}}{12} & \sqrt{\frac{2-\sqrt{3}}{12}} \\ \frac{1}{2\sqrt{6}} & \frac{3+\sqrt{3}}{12} & \sqrt{\frac{2+\sqrt{3}}{12}} & \frac{3+\sqrt{3}}{12} & \frac{1}{2\sqrt{6}} & \frac{1}{2\sqrt{3}} \\ \frac{1}{2\sqrt{3}} & \sqrt{\frac{2+\sqrt{3}}{12}} & \frac{3+\sqrt{3}}{6} & \sqrt{\frac{2+\sqrt{3}}{12}} & \frac{1}{2\sqrt{3}} & \frac{1}{\sqrt{6}} \\ \frac{1}{2\sqrt{6}} & \frac{3+\sqrt{3}}{12} & \sqrt{\frac{2+\sqrt{3}}{12}} & \frac{3+\sqrt{3}}{12} & \frac{1}{2\sqrt{6}} & \frac{1}{2\sqrt{3}} \\ \frac{3-\sqrt{3}}{12} & \frac{1}{2\sqrt{6}} & \frac{1}{2\sqrt{3}} & \frac{1}{2\sqrt{6}} & \frac{3-\sqrt{3}}{12} & \sqrt{\frac{2-\sqrt{3}}{12}} \\ \sqrt{\frac{2-\sqrt{3}}{12}} & \frac{1}{2\sqrt{3}} & \frac{1}{\sqrt{6}} & \frac{1}{2\sqrt{3}} & \sqrt{\frac{2-\sqrt{3}}{12}} & \frac{3-\sqrt{3}}{6} \end{pmatrix} \quad (3.76)$$

Using the fact that $8\|\psi\|^{-2} \hat{\mathfrak{g}}_{1|1}^2 = \frac{1}{120}(3-\sqrt{3})(5-\sqrt{5})$ where ψ is the Perron-Frobenius eigenvector given by (2.2), the 2-boundary \mathfrak{g} -factors $\hat{\mathfrak{g}}_{\mu|\mu'}$ and defect \mathfrak{g} -factors \hat{d}_μ are given by

$$\mathbf{D} = 8\|\psi\|^{-2} \hat{\mathfrak{g}}_{1|1} \begin{pmatrix} \hat{\mathfrak{g}}_{1|1} & \hat{\mathfrak{g}}_{1|2} & \cdots & \hat{\mathfrak{g}}_{1|12} \\ \hat{\mathfrak{g}}_{2|1} & \hat{\mathfrak{g}}_{2|2} & \cdots & \hat{\mathfrak{g}}_{2|12} \\ \vdots & \vdots & \ddots & \vdots \\ \hat{\mathfrak{g}}_{12|1} & \hat{\mathfrak{g}}_{12|2} & \cdots & \hat{\mathfrak{g}}_{12|12} \end{pmatrix} = 8\|\psi\|^{-2} \hat{\mathfrak{g}}_{1|1}^2 \begin{pmatrix} 1 \\ \hat{d}_2 \\ \vdots \\ \hat{d}_{12} \end{pmatrix} (1 \hat{d}_2 \dots \hat{d}_{12}) = 8\|\psi\|^{-2} \hat{\mathfrak{g}}_{1|1}^2 \sum_{\mu=1}^{12} \hat{d}_\mu \tilde{N}_\mu \quad (3.77)$$

4 A-D-E RSOS Lattice Models

In this section, we consider the *A-D-E* RSOS lattice models [39–43] with Coxeter numbers (m, m') and crossing parameter $\lambda = \frac{(m'-m)\pi}{m'}$. Starting in 1984, the first such models were built on the *A*-type Dynkin diagrams and solved off-criticality by Andrews, Baxter and Forrester [39, 40]. The full family of critical *A-D-E* lattice models was subsequently introduced and studied by Pasquier [41–43]. These 2-dimensional lattice models on the square lattice are Yang-Baxter integrable [38] so they are exactly solvable. The unitary and nonunitary (A, G) minimal CFTs are obtained from these lattice models in the continuum scaling limit. In particular, the CFT defect lines \mathcal{L}_μ emerge as the continuum scaling limits of *integrable seams* [19, 20] implemented on the lattice as special column transfer matrices.

4.1 A-D-E lattice models and their *T*- and *Y*-systems

The face weights of the unitary and nonunitary critical *A-D-E* RSOS lattice models are

$$\begin{array}{|c|c|} \hline d & c \\ \hline u & \\ \hline a & b \\ \hline \end{array} = W \left(\begin{array}{c|c} d & c \\ \hline a & b \\ \hline \end{array} \middle| u \right) = \frac{\sin(\lambda - u)}{\sin \lambda} \delta_{a,c} + \frac{g_c \sin u}{g_a \sin \lambda} \frac{\sqrt{\psi_a} \sqrt{\psi_c}}{\psi_b} \delta_{b,d} \quad (4.1)$$

for $|a-b| = |b-c| = |c-d| = |d-a| = 1$ but vanish otherwise. The spectral parameter is u , the crossing parameter is $\lambda = \frac{\pi(m'-m)}{m'}$ with $m'-m \in \text{Exp}(G)$, g_a are arbitrary gauge factors and here ψ_a are the components of the eigenvector of G corresponding to the eigenvalue $2 \cos \lambda$. We will work in the symmetric gauge with $g_a = 1$. Some care needs to be taken with the principal branch square roots $\sqrt{z} = e^{\frac{1}{2} \log z}$ since, for nonunitary cases, some ψ_a are negative and it is not generally true that $\sqrt{\psi_a \psi_c} = \sqrt{\psi_a} \sqrt{\psi_c}$. These face weights can be written in terms of the generators of the Temperley-Lieb algebra and satisfy the Yang-Baxter equation as shown in Appendix B. With $g_a = 1$, the braid limits of the allowed *A-D-E* face weights are

$$\begin{array}{|c|c|} \hline d & c \\ \hline -i\infty & \\ \hline a & b \\ \hline \end{array} = B \left(\begin{array}{c|c} d & c \\ \hline a & b \\ \hline \end{array} \right) = \lim_{u \rightarrow -i\infty} \frac{x^{-\frac{1}{2}}}{i\rho(u)} W \left(\begin{array}{c|c} d & c \\ \hline a & b \\ \hline \end{array} \middle| u \right) = -i \left(x^{-\frac{1}{2}} \delta_{ac} - x^{\frac{1}{2}} \frac{\sqrt{\psi_a} \sqrt{\psi_c}}{\psi_b} \delta_{bd} \right) \quad (4.2a)$$

$$\begin{array}{|c|c|} \hline d & c \\ \hline i\infty & \\ \hline a & b \\ \hline \end{array} = \overline{B} \left(\begin{array}{c|c} d & c \\ \hline a & b \\ \hline \end{array} \right) = \lim_{u \rightarrow i\infty} \frac{i x^{\frac{1}{2}}}{\rho(u)} W \left(\begin{array}{c|c} d & c \\ \hline a & b \\ \hline \end{array} \middle| u \right) = i \left(x^{\frac{1}{2}} \delta_{ac} - x^{-\frac{1}{2}} \frac{\sqrt{\psi_a} \sqrt{\psi_c}}{\psi_b} \delta_{bd} \right) \quad (4.2b)$$

where $x = e^{i\lambda}$, $\rho(u) = \sin(\lambda - u) / \sin \lambda$ and bars denote complex conjugation. In the continuum scaling limit, these braid limits relate to the left and right chiral halves of the theory related to each other by complex conjugation (see Figure 14).

Let us consider a cylinder with boundary conditions (r, b) on the left and (r', c) on the right. The double row transfer matrix [44] with N faces is

$$\mathbf{D}_{(r,b)|(r',c)}^{(N)}(u) = \begin{array}{c} \begin{array}{|c|c|c|c|c|c|} \hline b & b & b_2 & b_3 & \dots & b_{N-1} & c \\ \hline \lambda-u & \lambda-u & \dots & \dots & \dots & \lambda-u \\ \hline u & u & \dots & \dots & \dots & u \\ \hline b & b & a_2 & a_3 & \dots & a_{N-1} & c \\ \hline \end{array} \\ \begin{array}{|c|c|} \hline b & c \\ \hline \end{array} \end{array} \quad r, r' \in A; \quad b, c \in G \quad (4.3)$$

where the internal heights are summed over. The triangle boundary weights, dependent on a parameter ξ , are specified in [45]. As shown in [44], these matrices form a 1-parameter family of commuting double row transfer matrices $[\mathbf{D}_{(r,b)|(r',c)}^{(N)}(u), \mathbf{D}_{(r,b)|(r',c)}^{(N)}(v)] = 0$.

The vertical single column transfer matrix is

$$\mathbf{T}^{(2,1)}(\xi) = \begin{array}{c} \begin{array}{cccccc} b_1 & b_2 & \cdots & b_M & b_1 \\ \hline u+\xi & \lambda-u+\xi & u+\xi & \lambda-u+\xi & u+\xi & \lambda-u+\xi \\ \hline a_1 & a_2 & \cdots & a_M & a_1 \end{array} \\ \cdots \end{array} \quad (4.4)$$

with periodicity $a_{M+1} = a_1$, $b_{M+1} = b_1$. For display convenience, we have rotated the transfer matrix by 90 degrees anticlockwise. For this fundamental r -type integrable seam, the parameter ξ plays the role of the spectral parameter and u and $\lambda-u$ are alternating inhomogeneities. Using the local Yang-Baxter equations, it follows that the column transfer matrices form a commuting family $[\mathbf{T}(\xi), \mathbf{T}(\xi')] = 0$. The braid limits $\xi \rightarrow \pm i\infty$ of these face weights are given by (4.2) independent of the inhomogeneities u and $\lambda-u$. It follows that the fundamental s -type integrable seams

$$\mathbf{n}_2 = \mathbf{B} = \mathbf{T}^{(1,2)} = \lim_{\xi \rightarrow -i\infty} \left(\frac{i x^{\frac{1}{2}}}{\rho(\xi)} \right)^M \mathbf{T}^{(2,1)}(\xi) = \begin{array}{c} \begin{array}{cccccc} b_1 & b_2 & \cdots & b_N & b_1 \\ \hline -i\infty & -i\infty & -i\infty & -i\infty & -i\infty & -i\infty \\ \hline a_1 & a_2 & \cdots & a_N & a_1 \end{array} \\ \cdots \end{array} \quad (4.5)$$

$$\bar{\mathbf{n}}_2 = \bar{\mathbf{B}} = \bar{\mathbf{T}}^{(1,2)} = \lim_{\xi \rightarrow i\infty} \left(\frac{x^{-\frac{1}{2}}}{i\rho(\xi)} \right)^M \mathbf{T}^{(2,1)}(\xi) = \begin{array}{c} \begin{array}{cccccc} b_1 & b_2 & \cdots & b_N & b_1 \\ \hline i\infty & i\infty & i\infty & i\infty & i\infty & i\infty \\ \hline a_1 & a_2 & \cdots & a_N & a_1 \end{array} \\ \cdots \end{array} \quad (4.6)$$

precisely coincide with the torus Ocneanu integrable seams \mathbf{n}_2 and $\bar{\mathbf{n}}_2$ of [19, 20]. It therefore also follows that \mathbf{n}_2 and $\bar{\mathbf{n}}_2$ separately satisfy the graph fusion algebra (2.8) with the Verlinde structure constants

$$\mathbf{n}_1 = \bar{\mathbf{n}}_1 = \mathbf{I}, \quad \mathbf{n}_2 = \mathbf{B}, \quad \bar{\mathbf{n}}_2 = \bar{\mathbf{B}}, \quad \mathbf{n}_i \mathbf{n}_j = \sum_{k=1}^{m'-1} N_{ij}^k \mathbf{n}_k, \quad \bar{\mathbf{n}}_i \bar{\mathbf{n}}_j = \sum_{k=1}^{m'-1} N_{ij}^k \bar{\mathbf{n}}_k \quad (4.7)$$

Compound (r, s) integrable seams

$$\mathbf{T}^{(r,s)}(u) = \mathbf{T}^{(r,1)}(u) \mathbf{T}^{(1,s)}, \quad \bar{\mathbf{T}}^{(r,s)}(u) = \mathbf{T}^{(r,1)}(u) \bar{\mathbf{T}}^{(1,s)}, \quad r, s = 1, 2, \dots, m'-1 \quad (4.8)$$

can be constructed using fusion or recursively using known fusion functional equations [7, 8] and their braid limits [19, 20]

$$\mathbf{T}_0^{(r,1)} \mathbf{T}_{r-1}^{(2,1)} = f_{r-1} \mathbf{T}_0^{(r-1,1)} + f_{r-2} \mathbf{T}_0^{(r+1,1)}, \quad \mathbf{T}_0^{(0,1)} = \mathbf{T}_0^{(m',1)} = \mathbf{0}, \quad \mathbf{T}_0^{(1,1)} = f_{-1} \mathbf{I}, \quad \mathbf{T}_0^{(m'-1,1)} = f_{m'-2} \boldsymbol{\sigma} \quad (4.9)$$

$$\mathbf{T}^{(1,s)} \mathbf{T}^{(1,2)} = \mathbf{T}^{(1,s-1)} + \mathbf{T}^{(1,s+1)}, \quad \mathbf{T}^{(1,0)} = \mathbf{T}^{(1,m')} = \mathbf{0}, \quad \mathbf{T}^{(1,1)} = \mathbf{I}, \quad \mathbf{T}^{(1,m'-1)} = \boldsymbol{\sigma} \quad (4.10)$$

where 2 denotes the fundamental, the dependence on the inhomogeneities $u, \lambda-u$ is suppressed, $\boldsymbol{\sigma}$ is the \mathbb{Z}_2 height reversal operator and

$$\mathbf{T}_q^{(r,1)} = \mathbf{T}^{(r,1)}(\xi + q\lambda), \quad \mathbf{T}_0^{(r,1)} = \boldsymbol{\sigma} \mathbf{T}_r^{(m'-r,1)}, \quad f_r = \left(\frac{\sin(\xi+u+r\lambda) \sin(\xi-u+(r+1)\lambda)}{\sin^2 \lambda} \right)^{M/2} \quad (4.11)$$

The r -type T - and Y -systems [8] are

$$\frac{\mathbf{T}_0^{(r,1)} \mathbf{T}_1^{(r,1)}}{f_{-1} f_{r-1}} = \mathbf{I} + \frac{\mathbf{T}_1^{(r-1,1)} \mathbf{T}_0^{(r+1,1)}}{f_{-1} f_{r-1}} \equiv \mathbf{I} + \mathbf{Y}_0^r, \quad r = 1, 2, \dots, m-1 \quad (4.12)$$

$$\mathbf{Y}_0^r \mathbf{Y}_1^r = (\mathbf{I} + \mathbf{Y}_1^{r-1})(\mathbf{I} + \mathbf{Y}_0^{r+1}), \quad r = 1, 2, \dots, m-2 \quad (4.13)$$

with $\mathbf{Y}_q^r = \mathbf{Y}^r(\xi + q\lambda)$. These functional equations were originally established [7, 8] for unitary cases ($m' - m = 1$) without inhomogeneities but can be established for unitary and nonunitary $A(m, m')$ models with inhomogeneities by the same methods. The f functions remove the non-universal bulk free energies. In obtaining conformal defects in the continuum scaling limit, it suffices to consider the isotropic case with homogeneities $u = \lambda - u = \frac{\lambda}{2}$. The s -type integrable seams are topological on the lattice [71] whereas the r -type integrable seams are not.

The continuum scaling limit of the RSOS lattice models yields the associated CFT. More precisely, the scaling limit is $a \rightarrow 0$, $M, N \rightarrow \infty$, $aM \rightarrow L$, $aN \rightarrow R$ where a is the lattice spacing, L and R are continuous coordinates and $M/N \rightarrow L/R$ is the aspect ratio. Within the CFT, the transfer matrices $\mathbf{T}^{(r,1)}(u)$ are replaced [72] by a set $\mathbf{T}^r(u)$ of operator valued functions of the complex spectral parameter $u \in \mathbb{C}$. The operators $\mathbf{T}^r(u)$ satisfy [72] precisely the same T - and Y -systems of functional equations as the lattice transfer matrices $\mathbf{T}^{(r,1)}(u)$. So the conformal topological defects \mathcal{L}_r and \mathcal{L}_s are operators corresponding to specializations of $\mathbf{T}^r(u)$ in the bulk and braid limits respectively as we explain in the next subsection.

4.2 Braid and bulk scaling limits of integrable seams

For the finite-size s -type transfer matrices $\mathbf{T}^{(1,s)}$, s is a good quantum number so the eigenvalues fall into sectors labelled by s or equivalently the braid limit eigenvalues $\tilde{d}_{(1,s)} = 2 \cos \frac{s\pi}{m}$. For the finite-size r -type transfer matrices $\mathbf{T}^{(r,1)}$, r is not a quantum number. In this case, r only becomes a quantum number in the continuum scaling limit, that is, first the scaling limit must be taken with $\xi = \frac{\lambda}{2} + \frac{\lambda}{\pi} ix$ and $x \sim \mp \log M$ with $M \rightarrow \infty$ followed by the limit $x \rightarrow \pm\infty$. Since ultimately $\xi \rightarrow \pm i\infty$, the bulk limits are constants independent of the inhomogeneities. The r and s scaling regimes are shown schematically in Figure 14. Considering the A cases, replacing r with j and taking the bulk (r -type scaling) limit of the eigenvalues of the T - and Y -systems (4.12) and (4.13) using (3.2) of [8] gives the recurrence relations

$$d_j d_2 = d_{j-1} + d_{j+1}, \quad d_j^2 = 1 + d_{j-1} d_{j+1} = 1 + \varepsilon_j, \quad j = 1, 2, \dots, m-1 \quad (4.14)$$

$$\varepsilon_j^2 = d_{j-1}^2 d_{j+1}^2 = (1 + \varepsilon_{j-1})(1 + \varepsilon_{j+1}), \quad j = 1, 2, \dots, m-2 \quad (4.15)$$

where the generalized r -type quantum dimension d_j is the scaling limit of $\mathbf{T}_0^{(j,1)}(u)$ in (4.9) and ε_j is the bulk limit of \mathbf{Y}_0^j in (4.13). The index j indicates the fusion level so $j = 1$ is the identity, $j = 2$ is the spin- $\frac{1}{2}$ fundamental, $j = 3$ is spin-1 and so on. The solutions of these equations are given by

$$d_j = d_{j,r}^m = \frac{\sin j\tau}{\sin \tau}, \quad \varepsilon_j = \varepsilon_{j,r}^m = \frac{\sin(j-1)\tau \sin(j+1)\tau}{\sin^2 \tau}, \quad \tau = \frac{r\pi}{m}, \quad r = 1, 2, \dots, m-1 \quad (4.16)$$

where r is a Coxeter exponent of A_{m-1} . These solutions imply $d_{j,r}^m = \pm 1$ for $j = m-1$. The fundamental quantum dimensions are $d_{2,r}^m = \tilde{d}_{(1,r)} = 2 \cos \frac{r\pi}{m}$. Restricting to the upper half plane, the latter recurrence is also in accord with the bulk asymptotics of the TBA pseudoenergies $\varepsilon_j(x)$ given, in the unitary cases, by (3.92) of [73]

$$\varepsilon_j(-\infty)^2 = (1 + \varepsilon_{j-1}(-\infty))(1 + \varepsilon_{j+1}(-\infty)), \quad j = 1, 2, \dots, m-2 \quad (4.17)$$

with $\varepsilon_j = \varepsilon_j(-\infty)$. This equation for the bulk asymptotics of the TBA pseudoenergies is universal independent of the boundary conditions and topology. The quantum dimensions $d_{j,r}^m$ and the analogs $d_{j,s}^{m'}$ for the s -type integrable seams, where s is a Coxeter exponent of $A_{m'-1}$, are good quantum numbers of the CFT.

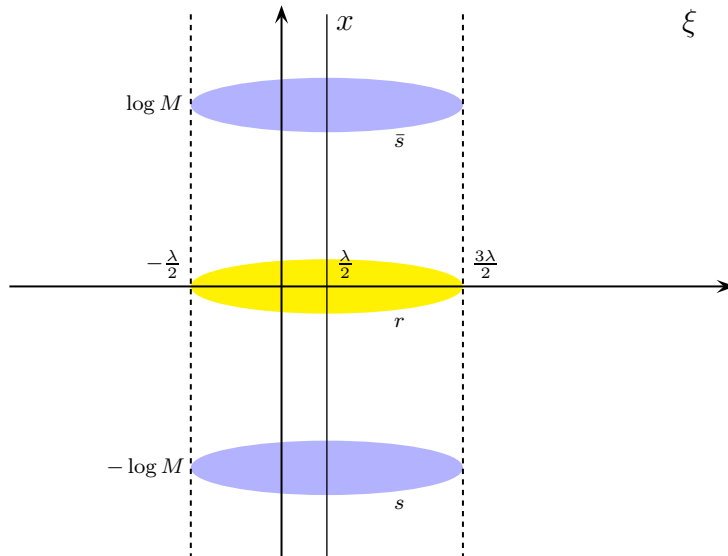


Figure 14: The complex plane of the spectral parameter ξ showing the fundamental ($j = 2$) analyticity strip $-\frac{\lambda}{2} < \text{re } \xi < \frac{3\lambda}{2}$. The scaling regimes for large M are shown for r (shaded yellow), s and \bar{s} (both shaded blue). The s , \bar{s} scaling regimes are related by complex conjugation and are at a distance $\mp \log M$ from the real axis. For A -type models with diagonal modular invariants $\bar{s} = s$. Similar analyticity strips are related to each fusion level $j = 2, 3, \dots, m' - 2$. For the ground state eigenenergy and $j = 2$, the zeros are dense on the dashed lines between the s and \bar{s} scaling regimes. The spectral parameter is written as $\xi = \frac{\lambda}{2} + \frac{\lambda}{\pi} i x$ and the braid limits are $x \rightarrow \mp \infty$. The lower/upper half planes relate to the left/right chiral halves of the associated CFT in the scaling limit. The r scaling regime is reached by first taking the continuum scaling limit $x \sim \mp \log M$ with M large thus moving to the s scaling regime in the upper/lower half-plane, followed by taking the limit $x \rightarrow \pm \infty$ thus moving to the real axis. In [8] this is called the “bulk limit”. The braid and bulk limits in the upper half planes are directly related to the plateaux asymptotics at $x = \pm \infty$ in the Thermodynamic Bethe Ansatz (TBA). The r scaling regime, centered on the real axis, is common to both left and right chiral halves of the CFT. The integers r, s, \bar{s} are good quantum numbers for the CFT in the continuum scaling limit.

4.3 Dilogarithm identities

In this section we show that the basic conformal data (central charges and conformal weights) can be expressed in terms of the generalized quantum dimensions $d_{j,r}^m$ and $d_{j,s}^{m'}$.

The unitary and nonunitary A - D - E lattice models are exactly solvable by the methods of Klümper and Pearce [57, 58, 8, 74]. For nonunitary models the details will be given in a separate paper. However, the details of these calculations for the (nonunitary) Lee-Yang model $\mathcal{M}(2, 5)$ are given in [68]. Yang-Baxter integrability means that it is possible to calculate the effective central charges and conformal weights in terms of dilogarithms [55, 75, 76]. For the central charges, this was first carried out in [7]. For the conformal dimensions, this involves analytic continuations of the dilogarithms and was first carried out in [57, 58, 8]. In the current context, these considerations lead to the following formulas

valid for all (m, m') and for all unitary and nonunitary A - D - E models:

$$c_{\text{eff}}^{m,m'} = \frac{1}{m'-m} \Theta_{1,1}^{m,m'} \quad (4.18a)$$

$$\Delta_{r,s}^{m,m'} = \frac{1}{4}(r-s)(r-s+m'-m) - \frac{m'-m}{24} \left[\Theta_{r,s}^{m,m'} - \Theta_{1,1}^{m,m'} \right] \quad (4.18b)$$

$$\Theta_{r,s}^{m,m'} = \frac{6}{\pi^2} \left[\sum_{j=1}^{m'-2} L_+(\varepsilon_{j,s}^{m'}) - \sum_{j=1}^{m-2} L_+(\varepsilon_{j,r}^m) \right], \quad \varepsilon_{j,t}^m = \frac{\sin(j-1)\frac{t\pi}{m} \sin(j+1)\frac{t\pi}{m}}{\sin^2 \frac{t\pi}{m}} \quad (4.18c)$$

where the sums over dilogarithms relate to the braid and bulk limits in the strips labelled by the fusion level j . The standard Rogers dilogarithms are given by

$$L(x) = -\frac{1}{2} \int_0^x \left[\frac{\log(1-t)}{t} + \frac{\log t}{1-t} \right] dt, \quad L_+(x) = \frac{1}{2} \int_0^x \left[\frac{\log(1+t)}{t} - \frac{\log t}{1+t} \right] dt, \quad 0 \leq x \leq 1 \quad (4.19)$$

For our purposes, we analytic continue the dilogarithm functions to the real line using

$$L_+(x) = \begin{cases} L\left(\frac{x}{1+x}\right), & x \geq 0 \\ -L(-x), & x < 0 \end{cases} \quad L(x) = \begin{cases} \frac{\pi^2}{3} - L\left(\frac{1}{x}\right), & x > 1 \\ L\left(\frac{1}{1-x}\right) - \frac{\pi^2}{6}, & x < 0 \end{cases} \quad (4.20)$$

Notice that, as required, the formula for $c_{\text{eff}}^{m,m'} = 1 - \frac{6}{mm'}$ is in fact symmetric in m and m' .

For the analytic continuation [75] of $L(x)$, we have

$$L_+(\varepsilon_j) = \begin{cases} L\left(\frac{\varepsilon_j}{1+\varepsilon_j}\right) = L\left(1 - \frac{1}{d_j^2}\right) = \frac{\pi^2}{6} - L\left(\frac{1}{d_j^2}\right) = L(d_j^2) - \frac{\pi^2}{6}, & \varepsilon_j \geq 0 \\ -L(-\varepsilon_j) = -L(-d_{j-1}d_{j+1}) = -L(1-d_j^2) = L(d_j^2) - \frac{\pi^2}{6}, & \varepsilon_j < 0 \end{cases} \quad (4.21)$$

where we use (4.20) and the identity $L(x) + L(1-x) = \frac{\pi^2}{6}$. This leads to formulas, equivalent to (4.18), where $L_+(x)$ is replaced with $L(x)$ and squares of the quantum dimensions appear

$$c_{\text{eff}}^{m,m'} = \frac{1}{m'-m} \theta_{1,1}^{m,m'} - 1 \quad (4.22a)$$

$$\Delta_{r,s}^{m,m'} = \frac{1}{4}(r-s)(r-s+m'-m) - \frac{m'-m}{24} \left[\theta_{r,s}^{m,m'} - \theta_{1,1}^{m,m'} \right] \quad (4.22b)$$

$$\theta_{r,s}^{m,m'} = \frac{6}{\pi^2} \left[\sum_{j=1}^{m'-2} L((d_{j,s}^{m'})^2) - \sum_{j=1}^{m-2} L((d_{j,r}^m)^2) \right], \quad d_{j,t}^m = \frac{\sin \frac{jt\pi}{m}}{\sin \frac{t\pi}{m}} \quad (4.22c)$$

These identities precisely coincide with Corollary 3.8 of [75] after systematically making the replacement $L((d_{j,t}^m)^2) = \frac{\pi^2}{3} - L((d_{j,t}^m)^{-2})$.

The results (4.18) imply the master dilogarithm identities

$$1 - \frac{6}{mm'} = \frac{1}{m'-m} \Theta_{1,1}^{m,m'}, \quad \Theta_{r,s}^{m,m'} - \Theta_{1,1}^{m,m'} = \frac{6(m'-m+mm'(r-s)+ms^2-m'r^2)}{mm'} \quad (4.23)$$

We call these master dilogarithm identities because they hold on the dense set $\frac{m'-m}{m'} \in (0, 1)$. In fact, using the logarithmic limit of Rasmussen [77], we find the further identities

$$c_{\log, \text{eff}}^{p,p'} = \lim_{k \rightarrow \infty} c_{\text{eff}}^{kp, kp'} = 1, \quad \Delta_{\log, r, s}^{p,p'} = \lim_{k \rightarrow \infty} \Delta_{r, s}^{kp, kp'} = \Delta_{r, s}^{p, p'} = \frac{(rp' - sp)^2 - (p' - p)^2}{4pp'}, \quad r, s, k \in \mathbb{N}_{>0} \quad (4.24)$$

for the effective central charges and infinitely extended set of conformal weights of the logarithmic minimal models $\mathcal{LM}(p, p')$ [52–54]. In the latter formula, $\Delta_{r, s}^{kp, kp'}$ stands for the dilogarithm terms on the RHS of (4.18b) with $m = kp$, $m' = kp'$ and p, p' coprime. The limit $k \rightarrow \infty$ is only needed to extend the range of r and s . Note that the RHS of (4.18b) makes sense even when m and m' have a common factor k .

4.4 Construction of integrable seams on the lattice

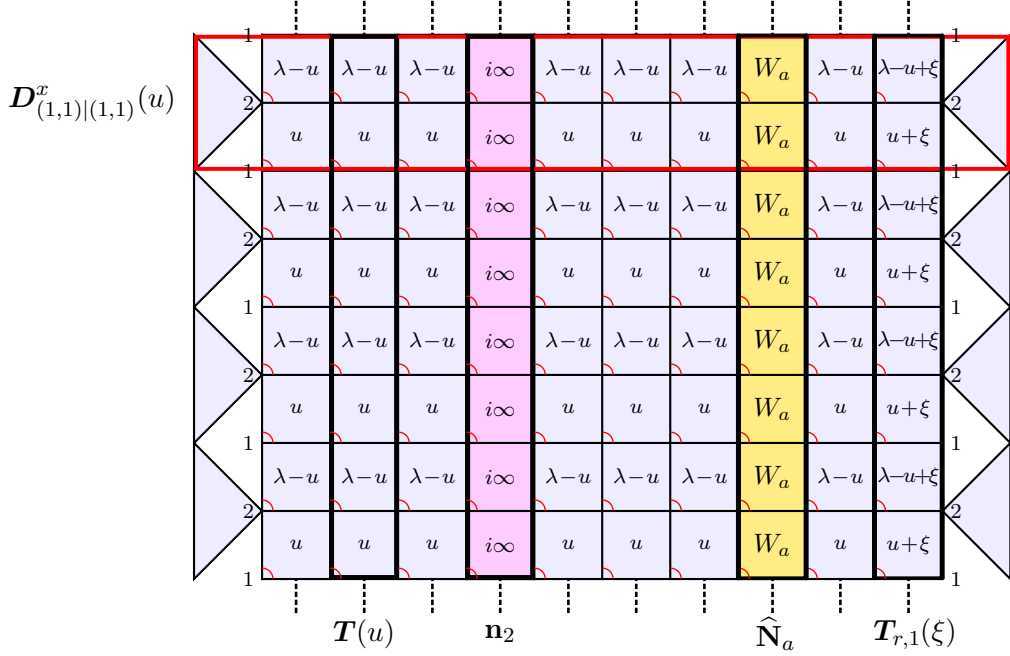


Figure 15: An $N \times M$ lattice on the cylinder with $(N, M) = (10, 8)$ showing (i) the column/seam transfer matrices $\mathbf{T}(u)$, $\mathbf{n}_2 = \mathbf{B}$, $\widehat{\mathbf{N}}_a$ and $\mathbf{T}_{r,1}(\xi)$ as explained in [19, 20] and (ii) the resulting double row transfer matrix $D^x_{(1,1)|(1,1)}(u)$ (outlined in red) with $(1, 2)$, $(1, a)$ and $(2, 1)$ seam segments. The labels W_a indicate that special face weights are assigned to the faces of the $(1, a)$ segment. The integrable seams commute with each other and $\mathbf{T}(u)$ so they can both be pushed to the left or right boundary.

Integrable seams for RSOS models on the lattice were first implemented in [78–80] and studied more recently in [81–83]. On the cylinder with symmetry algebra Vir , there are three relevant types of integrable seam, namely, (i) Verlinde \mathbf{n}_s , (ii) Pasquier $\widehat{\mathbf{N}}_a$ and (iii) \mathbb{Z}_2 automorphism seams σ . In contrast, on the torus with symmetry algebra $\text{Vir} \otimes \text{Vir}$, there are additionally (iv) compound Ocneanu integrable seams $\widehat{\mathbf{P}}_{ab} = \widehat{\mathbf{N}}_a \widehat{\mathbf{N}}_b$ where bars denote complex conjugation (left-right chiral conjugation). The Ocneanu integrable seams also exist on the cylinder but they can be reduced to Pasquier $\widehat{\mathbf{N}}_a$ type seams.

The construction of various vertical integrable seams on the cylinder, as shown in Figure 15, precisely coincides with the construction of Ocneanu integrable seams on the torus as explained in detail in [19, 20]. We therefore forego giving further details of the construction here. We observe, however, that the various integrable seams satisfy (i) the Verlinde fusion algebra [27], (ii) the Pasquier graph fusion algebra [28], (iii) the internal symmetry (Dynkin graph) automorphism group and (iv) the Ocneanu graph fusion algebra [25]. Among the A - D - E minimal models, only the D_{2l} models require the \mathbb{Z}_2 automorphism to be added separately to the fusion algebra. Explicitly, we observe that the various integrable seams satisfy the Verlinde fusion algebra, the Pasquier graph fusion algebra and the

Oceanu graph fusion algebra for arbitrary systems sizes M

$$\mathbf{n}_i \mathbf{n}_j = \sum_{k \in A_{m'-1}} N_{ij}^k \mathbf{n}_k, \quad 1 \leq i, j \leq m'-1; \quad \widehat{\mathbf{N}}_a \widehat{\mathbf{N}}_b = \sum_{c \in G} \widehat{N}_{ab}^c \widehat{\mathbf{N}}_c, \quad a, b \in G \quad (4.25a)$$

$$\widehat{\mathbf{P}}_\eta \widehat{\mathbf{P}}_\mu = \sum_{\nu=1}^{|\widetilde{G}|} \widetilde{N}_{\eta\mu}^\nu \widehat{\mathbf{P}}_\nu, \quad 1 \leq \eta, \mu \leq |\widetilde{G}| \quad (4.25b)$$

where \widetilde{G} is the Oceanu graph and $\widehat{\mathbf{P}}_\eta = \widehat{\mathbf{P}}_{ab}$ denotes the Oceanu seams. The integrable seams \mathbf{n}_j are given as Chebyshev polynomials $\mathbf{n}_j = U_{j-1}(\frac{1}{2}\mathbf{n}_2)$ of the second kind in the fundamental \mathbf{n}_2 . The integrable seams $\widehat{\mathbf{N}}_a$ are given as linear combinations of the \mathbf{n}_j . So, by construction, all these integrable seams commute with each other and with the transfer matrix $\mathbf{T}(u)$.

4.5 Conformal defects as limits of integrable lattice seams

In this section we first focus on A type theories. The conformal defects $\mathcal{L}_{r,s}$ are then obtained as the continuum (braid and bulk) scaling limits of the finite lattice integrable seams $\mathbf{T}^{(r,s)} = \mathbf{T}^{(r,1)}\mathbf{T}^{(1,s)}$ as in Section 4.2.

Since the integrable seams of Section 4.2 are simultaneously diagonalizable, we conclude that the conformal r -type defects satisfy

$$\mathcal{L}_{(r,1)}^2 = \mathcal{I} + \mathcal{L}_{(r-1,1)}\mathcal{L}_{(r+1,1)}, \quad \mathcal{L}_{(r,1)}\mathcal{L}_{(2,1)} = \mathcal{L}_{(r-1,1)} + \mathcal{L}_{(r+1,1)}, \quad \mathcal{L}_{(m-1,1)}\mathcal{L}_{(r,1)} = \mathcal{L}_{(m-r,1)} \quad (4.26)$$

where \mathcal{I} is the identity defect and the involution $\mathcal{L}_{(m-1,1)}$ is a height reversal operator. Similarly, the continuum scaling limit of the integrable braid seams satisfy

$$\mathcal{L}_{(1,s)}\mathcal{L}_{(1,2)} = \mathcal{L}_{(1,s-1)} + \mathcal{L}_{(1,s+1)}, \quad \mathcal{L}_{(1,m'-1)}\mathcal{L}_{(1,s)} = \mathcal{L}_{(1,m'-s)} \quad (4.27)$$

where the involution $\mathcal{L}_{(1,m'-1)}$ emerges from the height reversal operator. Taking the bulk and braid limits respectively of $\sigma \mathbf{T}^{(1,1)}$ gives $\mathcal{L}_{(m-1,1)}$ and $\mathcal{L}_{(1,m'-1)}$ with the product $\mathcal{L}_{(m-1,m'-1)} = \mathcal{L}_{(m-1,1)}\mathcal{L}_{(1,m'-1)} = \mathcal{I}$. So the Kac symmetry follows

$$\mathcal{L}_{(m-r,m'-s)} = \mathcal{L}_{(m-r,1)}\mathcal{L}_{(1,m'-s)} = \mathcal{L}_{(r,1)}\mathcal{L}_{(m-1,1)}\mathcal{L}_{(1,m'-1)}\mathcal{L}_{(1,s)} = \mathcal{L}_{(r,1)}\mathcal{L}_{(1,s)} = \mathcal{L}_{(r,s)} \quad (4.28)$$

These arguments follow the more detailed arguments found in [26]. Consequently, we deduce that the line defects $\mathcal{L}_\mu = \mathcal{L}_{(r,s)} = \mathcal{L}_{(r,1)}\mathcal{L}_{(1,s)}$ with $(r, s) \in \mathbb{K}$ satisfy the coset graph fusion algebra

$$\mathcal{L}_\mu \mathcal{L}_{\mu'} = \sum_{\mu''=1}^{|\mathbb{K}|} \widetilde{N}_{\mu\mu'}^{\mu''} \mathcal{L}_{\mu''} \quad (4.29)$$

The algebraic properties of the defect lines $\widehat{\mathcal{L}}_a$ and $\widehat{\mathcal{L}}_{(r,a)}$ follow from the existence and properties of rectangular intertwiners C [69, 70] satisfying

$$AC = CG \quad (4.30)$$

4.6 Boundary conditions on the lattice

The nonzero a -type right-boundary weights $|a\rangle$ are constructed [45] by fusing braid seams to the vacuum boundary

$$\begin{aligned}
 & \begin{array}{c} \text{Diagram 1: A square with a vertical seam on the left and a horizontal seam on the top, with a blue loop on the right side.} \\ \text{Diagram 2: A square with a vertical seam on the left and a horizontal seam on the top, with a blue loop on the left side.} \end{array} = \begin{array}{c} \text{Diagram 3: A square with a vertical seam on the left and a horizontal seam on the top, with a blue loop on the right side.} \\ \text{Diagram 4: A square with a vertical seam on the left and a horizontal seam on the top, with a blue loop on the left side.} \end{array} \\
 & \begin{array}{c} a' \quad b \quad b \\ \text{Diagram 5: A square with a vertical seam on the left and a horizontal seam on the top, with a blue loop on the right side.} \\ c \quad i\infty \quad i\infty \\ a \quad b \quad b \end{array} = \delta_{a,a'} \begin{array}{c} a' \\ \text{Diagram 6: A triangle with a vertical seam on the left and a horizontal seam on the top, with a blue loop on the right side.} \\ c \\ a \end{array} \\
 & \begin{array}{c} a \quad b \quad a \quad a \\ \text{Diagram 7: A square with a vertical seam on the left and a horizontal seam on the top, with a blue loop on the right side.} \\ c \quad i\infty \quad i\infty \\ a \quad b \quad a \quad a \end{array} = \begin{array}{c} a \\ \text{Diagram 8: A triangle with a vertical seam on the left and a horizontal seam on the top, with a blue loop on the right side.} \\ c \\ a \end{array} \quad (4.35a) \\
 & |1\rangle = 2 \begin{array}{c} 1 \\ \text{Diagram 9: A triangle with a vertical seam on the left and a horizontal seam on the top, with a blue loop on the right side.} \\ 1 \end{array} = \sqrt{\frac{\psi_2}{\psi_1}}, \quad |a\rangle = b \begin{array}{c} a \\ \text{Diagram 10: A square with a vertical seam on the left and a horizontal seam on the top, with a blue loop on the right side.} \\ b \\ a \end{array} = b \begin{array}{c} a \quad a_{n-1} \quad \dots \quad a_3 \quad 2 \quad 1 \quad 1 \\ \text{Diagram 11: A square with a vertical seam on the left and a horizontal seam on the top, with a blue loop on the right side.} \\ i\infty \quad i\infty \quad i\infty \quad i\infty \quad i\infty \\ i\infty \quad i\infty \quad i\infty \quad i\infty \quad i\infty \\ a \quad a_{n-1} \quad \dots \quad a_3 \quad 2 \quad 1 \quad 1 \end{array} = \sqrt{\frac{\psi_b}{\psi_a}}, \quad G_{ab} = 1 \quad (4.35b)
 \end{aligned}$$

Internal heights are summed out. From (4.35a), it follows that the boundary weights $|a\rangle$ are independent of the choice of path $(a, a_{n-1}, \dots, a_3, 2, 1)$ from a to 1 on G and that the upper and lower paths are identical and can be chosen to be the shortest path on G from a to 1. The 2-column braid matrix \widehat{B} , as in (4.37), is the $N = 2$ periodic braid seam acting on the Hilbert space spanned by the cyclic paths of length 2

$$\mathcal{H}_B = \text{span}(\{(1, 2, 1), (2, 1, 2), (2, 3, 2), \dots\}), \quad \dim \mathcal{H}_B = 2 \text{ (# edges of } G) \quad (4.36)$$

Consequently, for type I theories, it satisfies [19, 20] the Pasquier graph fusion algebra

$$\widehat{B}_1 = I, \quad \widehat{B}_2 = \widehat{B}, \quad \widehat{B}\widehat{B}_b = \sum_{c \in G} G_{bc} \widehat{B}_c, \quad \widehat{B}_a \widehat{B}_b = \sum_{c \in G} \widehat{N}_{ab}^c \widehat{B}_c, \quad \widehat{B}_{(a_1, a_2, a_1)}^{(b_1, b_2, b_1)} = \begin{array}{c} a_1 \quad b_1 \\ \text{Diagram 12: A square with a vertical seam on the left and a horizontal seam on the top, with a blue loop on the right side.} \\ i\infty \\ a_2 \\ i\infty \\ a_1 \quad b_1 \end{array} \quad (4.37)$$

Setting $|a\rangle = \widehat{B}_a|1\rangle$ and acting on the vacuum $|1\rangle$, it follows that

$$\widehat{B}|b\rangle = \sum_{c \in G} G_{bc}|c\rangle, \quad \widehat{B}_a|b\rangle = \sum_{c \in G} \widehat{N}_{ab}^c|c\rangle \quad (4.38)$$

More generally, for all type I and II A - D - E lattice models, the nonzero right s -type boundary weights $|s\rangle = B_s|1\rangle$ are defined recursively by

$$B_1 = I, \quad B_2 = B = \widehat{B}, \quad BB_s = B_{s-1} + B_{s+1}, \quad B_s B_{s'} = \sum_{s'' \in A_{m'-1}} N_{ss'}^{s''} B_{s''} \quad (4.39a)$$

$$|1\rangle = |1\rangle, \quad |2\rangle = |2\rangle, \quad B|s\rangle = |s-1\rangle + |s+1\rangle, \quad B_s|s'\rangle = \sum_{s'' \in A_{m'-1}} N_{ss'}^{s''}|s''\rangle \quad (4.39b)$$

These are the relations of the Verlinde fusion algebra with $B_s = U_{s-1}(\frac{1}{2}B)$ where $U_n(z)$ are the Chebyshev polynomials of the second kind. The solution to this recursion is

$$|s\rangle = \sum_{a \in G} C_{sa}|a\rangle, \quad C_{sa} = n_s 1^a, \quad s = 1, 2, \dots, |G| \quad (4.40)$$

where C_{sa} are the entries of the rectangular fundamental intertwiner C [69, 70]. For the A_L lattice models, B_L is the \mathbb{Z}_2 automorphism $B_L|s\rangle = |L+1-s\rangle$ and the s -type boundary conditions are

$$\{|s\rangle : s \in A_L\} \quad (4.41)$$

For the D_L lattice models, the s -type boundary conditions are

$$\{|1\rangle, |2\rangle, \dots, |L-2\rangle, |L-1\rangle+|L\rangle, |L-2\rangle, \dots, |2\rangle, |1\rangle\} \quad (4.42)$$

If L is even, then $B_s = B_{2L-2-s}$ and the \mathbb{Z}_2 automorphism needs to be added separately. If L is odd, then $\sigma = B_{2L-3}$ is the \mathbb{Z}_2 automorphism with the action to interchange the nodes $L-1$ and L and $B_s = \sigma B_{2L-2-s}$. For the E_6 , E_7 and E_8 lattice models, the s -type boundary conditions $|s\rangle$ are all given by (4.40) but, for E_7 , $|G|$ is replaced with 10. Actually, (4.40) can be inverted giving

$$E_{6,7,8} : \quad |a\rangle = \sum_{s=1}^L C_{as}^{-1} |s\rangle, \quad L = 6, 7, 8 \quad (4.43)$$

where C^{-1} is the inverse of the top $L \times L$ square block of C in (4.31). Alternatively, the s -type boundary conditions can be constructed directly using the Wenzl-Jones projectors [84, 85].

Actually, the vertical integrable seams can be taken to be general Ocneanu seams [19, 20] with independent commuting left- and right-chiral components B_s and $\overline{B}_{s'}$ (or \widehat{B}_a and \widehat{B}_b in type I cases) related by complex conjugation. However, acting on the right boundary with B_s or \overline{B}_s produces the same real boundary $|s\rangle$. This is the ‘‘gluing condition’’ $(B_s - \overline{B}_s)|1\rangle = 0$. So any \overline{B}_s seam can, without loss of generality, be replaced with a B_s seam. Since this can be lifted to the action of the integrable defect seam \mathbf{B}_s acting on the vacuum state, it guarantees that there is only one copy of Vir on the cylinder in the continuum scaling limit. The consequent reduction of the torus Ocneanu graph fusion algebras are consistent with the graph fusion algebras on the cylinder.

4.7 Boundary conditions and fusion rules for double row transfer matrices

In this section we fix $r = r' = 1$. The 1-parameter family of commuting double row transfer matrices (4.3) are normal and so they are simultaneously unitarily similar to diagonal matrices which we denote by $\mathbf{\Lambda}_{(1,b)|(1,c)}^{(N)}(u)$. The fusion rules for the finite-size $(1, s') \times (1, s'')$ and $(1, b) \times (1, c)$ double row transfer matrices are then respectively

$$\begin{aligned} D_{(1,s')|(1,s'')}^{(N)}(u) &\sim \bigoplus_s N_{ss's''} D_{(1,1)|(1,s)}^{(N)}(u) \sim \bigoplus_s N_{ss's''} \mathbf{\Lambda}_{(1,1)|(1,s)}^{(N)}(u), & G \text{ is type I or II} \\ D_{(1,b)|(1,c)}^{(N)}(u) &\sim \begin{cases} \bigoplus_s n_{sb}^c D_{(1,1)|(1,s)}^{(N)}(u) \sim \bigoplus_s n_{sb}^c \mathbf{\Lambda}_{(1,1)|(1,s)}^{(N)}(u), & G \text{ is type I or II} \\ \bigoplus_{a \in G} \widehat{N}_{ab}^c D_{(1,1)|(1,a)}^{(N)}(u) \sim \bigoplus_{a \in G} \widehat{N}_{ab}^c \mathbf{\Lambda}_{(1,1)|(1,a)}^{(N)}(u), & G \text{ is type I} \end{cases} \end{aligned} \quad (4.44b)$$

where \sim denotes equivalence up to similarity transformations.

The direct sum decompositions are a mathematical consequence of the following facts:

- (i) the boundary states are created by acting with the integrable defect seams on the vacuum boundary states on the left and right

$$\langle(1, a)| = \langle(1, 1)|\widehat{\mathbf{N}}_a, \quad |(1, b)\rangle = \widehat{\mathbf{N}}_b|(1, 1)\rangle \quad (4.45)$$

For the vacuum state on the lattice, the heights along the left and right edges alternate between heights 1 and 2.

- (ii) The seams $\widehat{\mathbf{N}}_a$ are topological, propagate freely and commute with each other.
- (iii) The integrable seams $\widehat{\mathbf{N}}_a = \widehat{\mathbf{N}}_{(1,a)}$ satisfy the graph algebra fusion rules.

This means that, as in Figure 2, the left seam can propagate from the left boundary to the right boundary where it is decomposed according to the fusion rules for seams. Essentially, this implements the local operator product expansion.

For A type theories, the spectra of the double row transfer matrices in the (s, s') sector is given by finitized Virasoro characters

$$Z_{s,s'}^{(N)}(q) = \text{Tr } \mathbf{D}_{(1,s)|(1,s')}^{(N)}(u) = \sum_{\substack{s''=|s-s'|+1 \\ s+s'+s''=1 \bmod 2}}^{s_{\max}} Z_s^{(N)}(q), \quad Z_s^{(N)}(q) = \text{Tr } \mathbf{D}_{(1,1)|(1,s)}^{(N)}(u) = \chi_{1,s}^{(N)}(q) \quad (4.46)$$

where the modular parameter is $q = \exp(-\frac{2\pi}{N} \sin \frac{\pi u}{\lambda})$. Taking the braid limit in (4.44), it also follows that

$$\mathbf{D}_{(1,s)|(1,s')}^{(N)}(\pm i\infty) \sim \bigoplus_{\substack{s''=|s-s'|+1 \\ s+s'+s''=1 \bmod 2}}^{s_{\max}} \mathbf{D}_{(1,1)|(1,s'')}^{(N)}(\pm i\infty) \sim \bigoplus_{\substack{s''=|s-s'|+1 \\ s+s'+s''=1 \bmod 2}}^{s_{\max}} \mathbf{\Lambda}_{(1,1)|(1,s'')}^{(N)}(\pm i\infty) \quad (4.47)$$

where the diagonal matrices $\mathbf{\Lambda}_{(1,1)|(1,s'')}^{(N)}(\pm i\infty)$ are multiples of the identity with the single eigenvalue $2 \cos s''\lambda$.

The proof of these direct sum decompositions (4.44) follows from properties of the boundary weights presented in the previous subsection. Since there is no simple correspondence between r -type integrable seams on the lattice and the topological r -type conformal defects that emerge in the continuum scaling limit, these simple arguments break down for r -type boundary conditions.

5 Conclusion

In this paper we considered the unitary and nonunitary (A, G) coset minimal CFTs with $G = A, D, E$. For these theories, we defined coset graph fusion algebras based on universal coset graphs $A \otimes G/\mathbb{Z}_2$. Representations of this algebra include (i) the fusion matrices (nimreps), (ii) the coset quantum dimensions and (iii) the topological defects of the associated CFT. Indeed, we argued that much of the CFT data is encoded by these coset graphs and the associated generalized quantum dimensions $d_{j,r}^m$ and $d_{j,s}^{m'}$. More specifically, the coset fusion graphs were shown to encode (i) the fusion matrices (nimreps), (ii) the Affleck-Ludwig boundary and defect \mathfrak{g} -factors and entropies, (iii) the relative Symmetry Resolved Entanglement Entropies (SREEs) and (iv) the central charges and conformal weights through analytically continued dilogarithm functions of the factorized quantum dimensions. We presented numerous prototypical examples applying these considerations to unitary and nonunitary cases for both diagonal and non-diagonal theories.

Separately, working on the cylinder, we constructed Yang-Baxter integrable seams on the lattice as mutually commuting column transfer matrices and argued that, in the continuum scaling limit, these produce the various kinds of topological line defects $\widehat{\mathcal{L}}_{(r,a)} = \mathcal{L}_{(r,1)}\widehat{\mathcal{L}}_{(1,a)}$ of the associated minimal CFTs satisfying either the Verlinde, graph fusion or Ocneanu graph fusion algebras. Due to a lattice “gluing condition”, the action of the integrable seam $\overline{\mathbf{B}}_s$ on the vacuum state reproduces \mathbf{B}_s thus ensuring there is just a single copy of Vir on the cylinder in the continuum scaling limit. Lastly, we observed throughout that, remarkably due to integrability, many of the known CFT structures already exist at the level of the lattice model.

Acknowledgments

We thank Jørgen Rasmussen and Andreas Klümper for helpful discussions. The research of JH was supported by the Commonwealth through an Australian Government Research Training Program Scholarship [DOI: <https://doi.org/10.82133/C42F-K220>].

A Coset graphs and coset nimreps

Coset graphs are constructed mathematically by combining the standard constructs of tensor product graphs and quotient graphs from graph theory (see for example [46]) as explained in this appendix. Recall that a graph G is defined as a set of nodes V with a set of edges E consisting of a set of pairs of nodes of G specifying node adjacency. We assume doubly-directed edges (also called undirected edges) and allow for loops such that a node forms an edge or is connected to itself. A graph is uniquely represented by its adjacency matrix.

Given two graphs G and G' , the nodes of the tensor product (or Kronecker product) graph $G \otimes G'$ are the pairs (a, a') where $a \in G$ and $a' \in G'$. There is an edge between the nodes (a, a') and (b, b') on $G \otimes G'$ if (a, b) is an edge of G and (a', b') is an edge of G' . The adjacency matrix of $G \otimes G'$ is just the tensor product of the adjacency matrices of G and G' . The tensor product of matrices is associative. It is also commutative up to relabelling, that is, a simultaneous permutation of the rows and columns.

Given an equivalence relation $a \equiv b$ between the nodes of a graph G , the graph can be partitioned into equivalence classes. Recall that nodes a and b belong to the same equivalence class $C_j \subset G$ if and only if $a \equiv b$ with $\cup_j C_j = G$. The nodes of the quotient graph $Q := G/R$, where R is the equivalence operation, are the equivalence classes C_j . Two equivalence classes C_j and C_k are adjacent in Q if some node in C_j is adjacent to some node in C_k on the original graph G . This process effectively “glues together” sets of nodes and edges from the original graph thereby simplifying its structure by representing groups of the original nodes with single nodes in the quotient graph. A simple example is the quotient of A_{m-1} with m odd under the \mathbb{Z}_2 equivalence relation $r \equiv m-r$. This quotient folds the A_{m-1} diagram to yield $A_{m-1}/\mathbb{Z}_2 = T_{(m-1)/2}$. Note that the folding of A diagrams to form T diagrams leads to the loops of the tadpole diagrams.

In the context of our (A, G) coset graphs, we first take the tensor product $A \otimes G$ where A and G are restricted to the Dynkin diagrams with the standard labelling of the nodes as in Figure 1. The coset graph $A \otimes G/\mathbb{Z}_2$ is subsequently constructed by taking the quotient of $A \otimes G$ with respect to the \mathbb{Z}_2 equivalence under the Kac table symmetry

$$(r, s) \equiv (m-r, m'-s), \quad G = A \tag{A.1}$$

$$(r, a) \equiv (m-r, a), \quad G \neq A \tag{A.2}$$

Importantly, we find that the coset graphs always factorize in terms of tadpoles

$$A \otimes G/\mathbb{Z}_2 = \begin{cases} A_{m-1} \otimes A_{m'-1}/\mathbb{Z}_2 = T_{(m-1)/2} \otimes A_{m'-1}, & G = A, m \text{ odd} \\ A_{m-1} \otimes A_{m'-1}/\mathbb{Z}_2 = A_{m-1} \otimes T_{(m'-1)/2}, & G = A, m' \text{ odd} \\ A_{m-1} \otimes G/\mathbb{Z}_2 = T_{(m-1)/2} \otimes G, & G = D \text{ or } E, m \text{ odd} \end{cases} \tag{A.3}$$

where this list exhausts all distinct cases.

The A - D - E diagrams in Figure 1 have distinguished nodes corresponding to the identity and fundamental labelled by $a = 1, 2$ respectively. The coset identity node of the (A, G) coset graphs is $(r, a) = (1, 1)$. The coset fundamental is the unique coset node adjacent to $(1, 1)$. This is $(r, a) = (2, 2)$ if $m > 3$ and $(r, a) = (1, 2)$ otherwise. In the latter case with $m \leq 3$, the coset graph is a linear graph,

namely, $A_{m'-1}$ ($m = 3$) or $T_{(m'-1)/2}$ ($m = 2$). It follows that the coset graph fusion matrices (nimreps) relevant to the cylinder are

$$\tilde{N}_{r,s} = \begin{cases} N_r^{(T_{\frac{1}{2}(m-1)})} \otimes N_s^{(A_{m'-1})}, & (A_{m-1}, A_{m'-1}), m \text{ odd} \\ N_r^{(A_{m-1})} \otimes N_s^{(T_{\frac{1}{2}(m'-1)})}, & (A_{m-1}, A_{m'-1}), m' \text{ odd} \\ N_r^{(T_{\frac{1}{2}(m-1)})} \otimes n_s^{(G)}, & (A_{m-1}, G), G \text{ is type I or II}, m \text{ odd} \end{cases} \quad (\text{A.4})$$

$$\tilde{N}_{r,a} = N_r^{(T_{\frac{1}{2}(m-1)})} \otimes \hat{N}_a^{(G)}, \quad (A_{m-1}, G), G \text{ is type I}, m \text{ odd} \quad (\text{A.5})$$

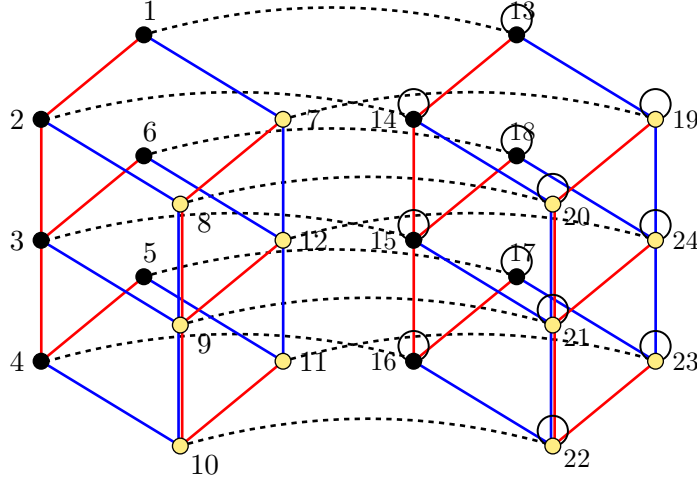


Figure 16: The coset Ocneanu fusion graph is given by the Cartesian product $A_4 \times \text{Oc}(E_6)/\mathbb{Z}_2 = T_2 \times \text{Oc}(E_6)$ with 24 vertices $\{\hat{\mathbf{P}}_\mu\}_{\mu=1}^{24} = \{\hat{\mathbf{P}}_{a,b}, \tau \hat{\mathbf{P}}_{a,b}\}_{a \in E_6; b=1,2}$ where $\tau \hat{\mathbf{P}}_\mu = \hat{\mathbf{P}}_{\mu+12}$ for $\mu = 1, 2, \dots, 12$. The solid red/blue lines show the action of the Ocneanu fundamentals $\hat{\mathbf{P}}_{2,1} = \hat{\mathbf{P}}_2$ and $\hat{\mathbf{P}}_{1,2} = \hat{\mathbf{P}}_7$. The dashed black lines and solid black loops show the action of r -type fundamental $\tau = \mathbf{N}_2 = \hat{\mathbf{P}}_{13}$ satisfying $\tau^2 = I + \tau$ with $\tau = T_2 \otimes I$.

On the torus, there are left- and right-chiral copies of the Virasoro algebra and the coset graph fusion matrices (nimreps) are replaced by coset Ocneanu graph fusion matrices. For (A, A) cases, the coset Ocneanu graph fusion matrices coincide with the cylinder coset graph fusion matrices. For the (A, G) cases, the coset Ocneanu nimreps are

$$\tilde{P}_{r,\eta} = N_r^{(T_{\frac{1}{2}(m-1)})} \otimes \hat{P}_\eta^{(G)}, \quad (A_{m-1}, G), G \text{ is type I}, m \text{ odd} \quad (\text{A.6})$$

where $\hat{P}_\eta^{(G)}$ are the known nimreps associated for the A - D - E Ocneanu graphs. As an example, the coset Ocneanu fusion graph of (A_4, E_6) is shown in Figure 16.

B Yang-Baxter equation for critical A - D - E models

The Yang-Baxter equation for critical A - D - E lattice models can be proved diagrammatically [86, 87]. The local face transfer operator associated with the face weights (4.1) can be written in terms of the Temperley-Lieb (TL) generators e_j as

$$X_j(u) = \sin(\lambda - u)I + \sin u e_j \quad (\text{B.1})$$

or diagrammatically by

$$X_j(u) = d \begin{array}{c} \text{---} c \text{---} \\ | \\ \text{---} u \text{---} \\ | \\ \text{---} a \text{---} \\ | \\ j \quad j+1 \end{array} b = \sin(\lambda - u) \delta_{a,c} \begin{array}{c} \text{---} c \text{---} \\ | \\ \text{---} \text{---} \\ | \\ \text{---} a \text{---} \\ | \\ j \quad j+1 \end{array} b + \sin u \delta_{b,d} \begin{array}{c} \text{---} c \text{---} \\ | \\ \text{---} \text{---} \\ | \\ \text{---} a \text{---} \\ | \\ j \quad j+1 \end{array} b \quad (\text{B.2})$$

where the first face is the identity I and the second face is the operator e_j for $j = 1, 2, \dots, n-1$. The face transfer matrices (B.1) automatically satisfies the Yang-Baxter equations if the generators e_j satisfy the Temperley-Lieb algebra

$$e_j^2 = 2 \cos \lambda e_j, \quad e_j e_{j \pm 1} e_j = e_j, \quad e_j e_k = e_k e_j, \quad |j - k| \geq 2 \quad (\text{B.3})$$

The Temperley-Lieb generators factor into triangles

$$\begin{array}{c} a \\ \text{---} \\ | \\ \text{---} b \end{array} = h'_{ab} G_{ab}, \quad h'_{ab} = \tilde{g}_a \frac{\psi_a}{\psi_b} \quad (\text{B.4a})$$

$$\begin{array}{c} b \\ \text{---} \\ | \\ \text{---} a \end{array} = h_{ab} G_{ab}, \quad h_{ab} = \tilde{g}_a^{-1} \quad (\text{B.4b})$$

where G is the adjacency matrix, h_{ab} and h'_{ab} are triangle weights, ψ_a are the components of the eigenvector corresponding to the eigenvalue $2 \cos \lambda$ of G with $\lambda = \frac{(m'-m)\pi}{m'}$ and \tilde{g}_a are arbitrary gauge factors. For symmetry, it is better to choose $\tilde{g}_a = g_a / \sqrt{\psi_a}$ as in (4.1) with $g_a = 1$. The first TL relation follows from

$$\begin{array}{c} \text{---} c \text{---} \\ | \\ \text{---} b \text{---} \\ | \\ \text{---} d \text{---} \\ | \\ \text{---} b \text{---} \\ | \\ \text{---} b \text{---} \\ | \\ \text{---} a \text{---} \\ | \\ j \quad j+1 \end{array} = 2 \cos \lambda \begin{array}{c} \text{---} c \text{---} \\ | \\ \text{---} \text{---} \\ | \\ \text{---} a \text{---} \\ | \\ j \quad j+1 \end{array} \quad (\text{B.5a})$$

$$\begin{array}{c} b \\ \text{---} \\ | \\ \text{---} d \text{---} \\ | \\ \text{---} b \end{array} = \sum_d G_{bd} h'_{db} h_{db} = \sum_d G_{bd} \frac{\psi_d}{\psi_b} = 2 \cos \lambda, \quad \lambda = \frac{(m'-m)\pi}{m'}, \quad m' - m \in \text{Exp}(G) \quad (\text{B.5b})$$

where the weight of the central square is determined by the eigenvalue equation $\sum_d G_{bd} \psi_d = 2 \cos \lambda \psi_b$. The second TL relations follow from

$$\begin{array}{c} \text{---} d \text{---} \\ | \\ \text{---} b \text{---} \\ | \\ \text{---} c \text{---} \\ | \\ \text{---} b \text{---} \\ | \\ \text{---} a \text{---} \\ | \\ j \quad j+1 \quad j+2 \end{array} = \begin{array}{c} \text{---} d \text{---} \\ | \\ \text{---} \text{---} \\ | \\ \text{---} a \text{---} \\ | \\ j \quad j+1 \quad j+2 \end{array} \quad (\text{B.6a})$$

$$\begin{array}{c} b \\ \text{---} \\ | \\ \text{---} c \text{---} \\ | \\ \text{---} b \end{array} = h_{bc} h'_{bc} h_{cb} h'_{cb} G_{bc} = \frac{\psi_c \psi_b}{\psi_b \psi_c} G_{bc} = G_{bc} = 1 \quad (\text{B.6b})$$

where the scalar weight is 1 since b and c are allowed neighbours. The third TL relation is trivial.

References

- [1] J. Fröhlich, J. Fuchs, I. Runkel, C. Schweigert, *Defect Lines, Dualities and Generalised Orbifolds*, in *XVIIth International Congress on Mathematical Physics, 3-8 August 2009, Prague*, P. Exner, ed., pp. 608–613, 2010. [arXiv:0909.5013 \[math-ph\]](#).
- [2] D. Gaiotto, A. Kapustin, N. Seiberg, B. Willett, *Generalized global symmetries*, *J. High Energy Phys.* (2015) 172, [arXiv:1412.5148 \[hep-th\]](#).
- [3] L. Bhardwaj and Y. Tachikawa, *On finite symmetries and their gauging in two dimensions*, *J. High Energy Phys.* (2018) 189, [arXiv:1704.02330 \[hep-th\]](#).
- [4] V.A. Fateev, A.B. Zamolodchikov, *Parafermionic Currents in the Two-Dimensional Conformal Quantum Field Theory and Selfdual Critical Points in $Z(n)$ Invariant Statistical Systems*, *Sov. Phys. JETP* **62** (1985) 215–225.
- [5] I. Affleck, *Critical behaviour of $SU(n)$ quantum chains and topological non-linear σ -models*, *Nucl. Phys.* **B305** (1988) 582–596.
- [6] I. Affleck, D. Gepner, H.J. Schulz, T. Ziman, *Critical behaviour of spin- s Heisenberg antiferromagnetic chains: analytic and numerical results*, *J. Phys.* **A22** (1989) 511–529.
- [7] V.V. Bazhanov, N.Yu. Reshetikhin, *Critical RSOS models and conformal field theory*, *Int. J. Mod. Phys.* **A4** (1989) 115–142.
- [8] A. Klümper, P.A. Pearce, *Conformal weights of RSOS lattice models and their fusion hierarchies*, *Physica* **A183** (1992) 304–350.
- [9] J. Fuchs, I. Runkel, C. Schweigert, *TFT construction of RCFT correlators I: partition functions*, *Nucl. Phys.* **B646** no. 3, (2002) 353–497, [arXiv:hep-th/0204148 \[hep-th\]](#).
- [10] A.A. Belavin, A.M. Polyakov, A.B. Zamolodchikov, *Infinite conformal symmetry in two-dimensional quantum field theory*, *Nucl. Phys.* **B241** (1984) 333–380.
- [11] P. Goddard, A. Kent, and D. Olive, *Virasoro algebras and coset space models*, *Phys. Lett.* **B152** (1985) 88–92.
- [12] P. Di Francesco, P. Mathieu, D. Sénéchal, *Conformal Field Theory*, Springer (1997).
- [13] G. Moore, N. Seiberg, *Classical and quantum conformal field theory*, *Commun. Math. Phys.* **123** (1989) 177–254.
- [14] R.E. Behrend, P.A. Pearce, V.B. Petkova, J.-B. Zuber, *Boundary conditions in rational conformal field theories*, *Nucl. Phys.* **B579** (2000) 707–773.
- [15] P. Goddard, A. Kent, D. Olive, *Virasoro algebras and coset space models*, *Phys. Lett.* **B152** (1985) 88–92.
- [16] A. Cappelli, C. Itzykson, J. B. Zuber. *The A-D-E classification of minimal and $A_1^{(1)}$ conformal invariant theories*, *Commun. Math. Phys.* **113** (1987) 1–26.
- [17] V.B. Petkova, J.-B. Zuber, *Generalised twisted partition functions*, *Physics Letters* **B504** (2001) 157–164; *Conformal field theories, graphs and quantum algebras*, *MathPhys Odyssey 2001: Integrable Models and Beyond*, 415–435.

- [18] V.B. Petkova, J.-B. Zuber, *The many faces of Ocneanu cells*, Nucl. Phys. **B603** (2001) 449–496.
- [19] P.A. Pearce, J.Rasmussen, *Ocneanu algebra of seams: Critical unitary E_6 RSOS lattice model*, Matrix Annals, [arXiv:hep-th/2409.06236](https://arxiv.org/abs/2409.06236) (2025).
- [20] P.A. Pearce, J.Rasmussen, *Ocneanu algebra of seams: Critical unitary A-D-E RSOS lattice models*, in preparation (2025).
- [21] A.M. Läuchli, *Operator content of real-space entanglement spectra at conformal critical points*, [arXiv:/1303.0741](https://arxiv.org/abs/1303.0741) (2013).
- [22] K. Ohmori, Y. Tachikawa, *Physics at the entangling surface*, J. Stat. Mech. **1504** (2015) P04010.
- [23] J. Cardy, E. Tonni, *Entanglement hamiltonians in two-dimensional conformal field theory*, J. Stat. Mech. **1612** (12) (2016) 123103.
- [24] B. Haghighat, Y. Sun, *Topological defect lines in bosonized parafermionic CFTs*, Adv. Theor. Math. Phys. **28** (2024) 1987–2023.
- [25] A. Ocneanu, *Paths on Coxeter Diagrams: From Platonic Solids and Singularities to Minimal Models and Subfactors*, in Lectures on Operator Theory, Fields Institute, Waterloo, Ontario, April 26–30, 1995, (Notes taken by S. Goto) Fields Institute Monographs, AMS 1999, Rajarama Bhat et al, eds; *Quantum symmetries for $SU(3)$ CFT Models*, Lectures at Bariloche Summer School, Argentina, Jan 2000, AMS Contemporary Mathematics, R. Coquereaux, A. Garcia and R. Trincherro, eds; *The classification of subgroups of quantum $SU(N)$* , Bariloche, 2000: <https://www.cpt.univ-mrs.fr/~coque/Bariloche2000/Bariloche2000/Bariloche2000.html>
- [26] M. Sinha, T.S. Tavares, A. Roy, H. Saleur, *Integrability and lattice discretizations of all topological defect lines in minimal CFTs*, [arXiv:/2509.04257](https://arxiv.org/abs/2509.04257) (2025).
- [27] E. Verlinde, *Fusion rules and modular transformations in 2D conformal field theory*, Nucl. Phys. **B300** (1988) 360–376.
- [28] V. Pasquier, *These d’Etat*, Orsay (1988).
- [29] I. Affleck, A.W.W. Ludwig, *Universal noninteger “ground-state degeneracy” in critical quantum systems*, Phys. Rev. Lett. **67** (1991) 161–164.
- [30] G. Di Giulio, R. Meyer, C. Northe, H. Scheppach, S. Zhao, *On the boundary conformal field theory approach to symmetry-resolved entanglement*, SciPost Physics Core, **6** (3) (2023) 049.
- [31] C. Northe, *Entanglement resolution with respect to conformal symmetry*, Phys. Rev. Lett. **131** (2023) 151601.
- [32] Y. Kusuki, S. Murciano, H. Ooguri, S. Pal, *Symmetry-resolved entanglement entropy, spectra and boundary conformal field theory*, Journal of High Energy Physics, 2023 (11) (2023) 216.
- [33] A. Das, J. Molina-Vilaplana, P. Saura-Bastida, *Generalized symmetry resolution of entanglement in conformal field theory for twisted and anyonic sectors*, Phys. Rev. **D110** (12) (2024) 125005.
- [34] J. Heymann, T. Quella, *Revisiting the symmetry-resolved entanglement for non-invertible symmetries in $1+1d$ conformal field theories*, to appear (2024).

- [35] Y. Choi, B.C. Raychaudhuri, Y. Zheng, *Noninvertible symmetry-resolved Affleck-Ludwig-Cardy formula and entanglement entropy from the boundary tube algebra*, Phys. Rev. Lett. **133** (25) (2024) 251602.
- [36] P. Saura-Bastida, A. Das, G. Sierra, J. Molina-Vilaplana, *Categorical-symmetry resolved entanglement in conformal field theory*, Phys. Rev. **D109** (10) (2024) 105026.
- [37] A. Bhattacharyya, S. Ghosh, S. Pal, J. Santara, *On the resolution of categorical symmetries in (non-) unitary rational CFTs*, [arXiv:/2511.16363](https://arxiv.org/abs/2511.16363) (2025).
- [38] R.J. Baxter, *Exactly Solved Models in Statistical Mechanics*, Academic Press (1982).
- [39] G.E. Andrews, R.J. Baxter, P.J. Forrester, *Eight-vertex SOS model and generalized Rogers-Ramanujan-type identities*, J. Stat. Phys. **35** (1984) 193–266.
- [40] P.J. Forrester, R.J. Baxter, *Further exact solutions of the eight-vertex SOS model and generalizations of the Rogers-Ramanujan identities*, J. Stat. Phys. **38** (1985) 435–472.
- [41] V. Pasquier, *Two-dimensional critical systems labelled by Dynkin diagrams*, Nucl. Phys. **B285** (1987) 162–172.
- [42] V. Pasquier, *Operator content of the ADE lattice models*, J. Phys. A: Math. Gen. **20** (1987) 5707–5717.
- [43] V. Pasquier, *Lattice derivation of modular invariant partition functions on the torus*, J. Phys. A: Math. Gen. **20** (1987) L1229–L1237.
- [44] R.E. Behrend, P.A. Pearce, D. L. O’Brien, *Interaction-round-a-face models with fixed boundary conditions: The ABF fusion hierarchy*, J. Stat. Phys. **84** (1996) 1–48.
- [45] R.E. Behrend, P.A. Pearce, *Integrable and conformal boundary conditions for $\widehat{\mathfrak{sl}}(2)$ A-D-E lattice models and unitary minimal conformal field theories*, J. Stat. Phys. **102** (2001) 577–640.
- [46] C. Godsil, G. Royle, *Algebraic Graph Theory*, Springer-Verlag, New York (2001).
- [47] R.E. Behrend, P.A. Pearce, J.-B. Zuber, *Integrable boundaries, conformal boundary conditions and A-D-E fusion rules*, J. Phys. A: Math. Gen. **31** (1998) L763–L770.
- [48] A. Kitaev, J. Preskill, *Topological entanglement entropy*, Phys. Rev. Lett. **96** 110404 (2006).
- [49] L. Fiedler, P. Naaijken, T.J. Osborne, *Jones index, secret sharing and total quantum dimension*, New J. Phys. **19** (2017) 023039 pp1-24.
- [50] P. Di Francesco, J.-B. Zuber, *Fusion potentials. I*, J. Phys. A **26** (1993) 1441
- [51] J. Fyfield, *Infinite dimensional Lie algebras: characters and fusion*, Bachelor of Advanced Science Honours Thesis; Supervisor: J. Rasmussen, University of Queensland (2018).
- [52] P.A. Pearce, J. Rasmussen, J.-B. Zuber, *Logarithmic minimal models*, J. Stat. Mech. (2006) P11017.
- [53] P.A. Pearce, J. Rasmussen, *Coset graphs in bulk and boundary logarithmic minimal models*, Nucl. Phys. **B846** (2011) 616–649.
- [54] A. Morin-Duchesne, P.A. Pearce, J. Rasmussen, *Fusion hierarchies, T-systems, and Y-systems of logarithmic minimal models*, J. Stat. Mech. (2014) P05012.

- [55] W. Nahm, A. Recknagel, M. Terhoeven, *Dilogarithm identities in conformal field theory*, Mod. Phys. Lett. **08** (1993) 1835–1847.
- [56] J.-M. Vanden Broeck, L.W. Schwartz, *A one-parameter family of sequence transformations*, SIAM J. on Math. Anal. **10** (1979) 658–666.
- [57] P.A. Pearce, A. Klümper, *Finite-size corrections and scaling dimensions of solvable lattice models: An analytic method*, Phys. Rev. Lett. **66** (1991) 974–977.
- [58] A. Klümper, P.A. Pearce, *Analytic calculation of scaling dimensions: Tricritical hard squares and critical hard hexagons*, J. Stat. Phys. **64** (1991) 13–76.
- [59] M. Lässig, G. Mussardo, L.L. Cardy, *The scaling region of the tricritical Ising model in two dimensions*, Nucl. Phys. **B348** (1991) 591–618.
- [60] S. Dasmahapatra, R. Kedem, M.M. McCoy, E. Melzer, *Virasoro characters from Bethe equations for the critical ferromagnetic three-state Potts model*, J. Stat. Phys. **74** (1994) 239–274.
- [61] M. Sinha, L. Grans-Samuelsson, A. Roy, H. Saleur, *Lattice realizations of topological defects in the critical $(1+1)$ -d three-state Potts model*, J. High Energy Phys. **225** (2024) 1–55.
- [62] D. O’Brien, P.A. Pearce, *Lattice realizations of unitary minimal modular invariant partition functions*, J. Phys. A **28** (1995) 4891–4905.
- [63] S. Iino, *Boundary CFT and tensor network approach to surface critical phenomena of the tricritical 3-state Potts model*, J. Stat. Phys. **182** (2021) 56.
- [64] T.D. Lee and C.N. Yang, *Statistical theory of equations of state and phase transitions. I. Theory of condensation; II. Lattice gas and Ising model*, Phys. Rev. **87** (1952) 404; 410.
- [65] V.V. Bazhanov, S.L. Lukyanov, A.B. Zamolodchikov, *Quantum field theories in finite volume: Excited state energies*, Nucl. Phys. **B489** (1997) 497–531.
- [66] P. Dorey, A.J. Pocklington, R. Tateo, G. Watts, *TBA and TCSA with boundaries and excited states*, Nucl. Phys. **B525** (1998) 641–663.
- [67] P. Dorey, I. Runkel, R. Tateo and G. Watts, *g -function flow in perturbed boundary conformal field theories*, Nucl. Phys. **B578** (2000) 85–122.
- [68] Z. Bajnok, O. el Deeb, P.A. Pearce, *Finite-volume spectra of the Lee-Yang model*, JHEP **04** (2015) 073 pp 1–42.
- [69] A. Ocneanu, *Quantized groups, string algebras and Galois theory for algebras in operator algebras and applications*, Lond. Math. Soc. Lecture Series **136** (1988) 119–170.
- [70] P.A. Pearce, Y.-K. Zhou, *Intertwiners and A-D-E lattice models*, Int. J. Mod. Phys. **B7** (1993) 3649–3705.
- [71] D. Aasen, P. Fendley, R.S.K. Mong, *Topological defects on the lattice: Dualities and degeneracies*, [arXiv:/2008.08598](https://arxiv.org/abs/2008.08598) (2020).
- [72] V.V. Bazhanov, S.L. Lukyanov, A.B. Zamolodchikov, *Integrable structure of conformal field theory, quantum KdV theory and thermodynamic Bethe ansatz*, Commun. Math. Phys. **177** (1996) 381–398; *Integrable structure of conformal field theory II. Q-operator and DDV equation*, Commun. Math. Phys. **190** (1997) 247–278;

- Integrable structure of conformal field theory III. The Yang-Baxter relation*, Commun. Math. Phys. **200** (1999) 297–324;
Quantum field theories in finite volume: Excited state energies, Nucl. Phys. **B489** (1997) 487–531.
- [73] G. Feverati, P.A. Pearce, N.S Witte, *Physical combinatorics quasiparticles*, J. Stat. Mech. (2009) P10013.
- [74] Y. Zhou, W. Sun, *Solving the fusion hierarchies of D and E lattice models*, Nucl. Phys. **B504** (1997) 719–737.
- [75] A.N. Kirillov, *Dilogarithm identities, partitions, and spectra in conformal field theory, Part I*, Algebra i Analiz **6** (1994) 152–175; [arXiv:hep-th/9212150](https://arxiv.org/abs/hep-th/9212150) (1992).
- [76] A.N. Kirillov, *Dilogarithm identities*, Prog. Theor. Phys. Supplement, **118** (1995) 61–142.
- [77] J. Rasmussen, *Logarithmic limits of minimal models*, Nucl. Phys. **B701** (2004) 516–528;
- [78] C.H. Otto Chui, C. Mercat, W.P. Orrick, P.A. Pearce, *Integrable lattice realizations of conformal twisted boundary conditions*, Phys. Lett. **B517** (2001) 429–435.
- [79] C.H. Otto Chui, C. Mercat, P.A. Pearce, *Integrable boundaries and universal TBA functional equations*, MathPhys Odyssey 2001: Integrable Models and Beyond, 391–413.
- [80] C.H. Otto Chui, C. Mercat, P.A. Pearce, *Integrable and conformal twisted boundary conditions for $sl(2)$ A-D-E lattice models*, J. Phys. A: Math. Gen. **36** (2003) 2623–2662.
- [81] J. Belletête, A.M. Gainutdinov, J.L Jacobsen, H. Saleur, T.S. Tavares, *Topological defects in periodic RSOS models and anyonic chains*, [arXiv:2003.11293 \[math-ph\]](https://arxiv.org/abs/2003.11293);
Topological defects in lattice models and affine Temperley-Lieb algebra, Commun. Math. Phys. **400** (2023) 1203–1254.
- [82] T.S. Tavares, M. Sinha, L. Grans-Samuelsson, A. Roy, H. Saleur, *Integrable RG flows on topological defect lines in 2D conformal field theories*, [arXiv:2408.08241 \[hep-th\]](https://arxiv.org/abs/2408.08241) (2024).
- [83] M. Sinha, F. Yan, L. Grans-Samuelsson, A. Roy, H. Saleur, *Lattice realizations of topological defects in the critical $(1+1)$ -d three state Potts model*, J. High Energy Phys, **07** (2024) 225.
- [84] H. Wenzl, *On sequences of projections*, C. R. Math. Rep. Acad. Sci. Canada, **9**(1), 5–9 (1987).
- [85] V.F.R. Jones, *A polynomial invariant for knots via von Neumann algebras*, In Fields Medallists’ lectures, Volume 5, World Sci. Ser. 20th Century Math. 448–458, World Sci. Publ., River Edge, NJ (1997).
- [86] R.J. Baxter, A.L. Owczarek, *A class of interaction-round-a-face models and its equivalence with an ice-type model*, J. Stat. Phys. **49** (1987) 1093–1115.
- [87] J. Gill, *Towards logarithmic D-type models*, University of Melbourne Master of Science Thesis, supervised by Paul Pearce (2015).